Transonic Wing and Control Surface Loads Modelling for Aeroservoelastic Analysis

Lancelot, P.M.G.J.

DOI
10.4233/uuid:e37566e8-cb46-4f90-863d-9cfe0b634507

Publication date
2023

Document Version
Final published version

Citation (APA)
Lancelot, P. M. G. J. (2023). *Transonic Wing and Control Surface Loads Modelling for Aeroservoelastic Analysis*. [Dissertation (TU Delft), Delft University of Technology]. https://doi.org/10.4233/uuid:e37566e8-cb46-4f90-863d-9cfe0b634507

Transonic Wing and Control Surface Loads Modelling for Aeroservoelastic Analysis

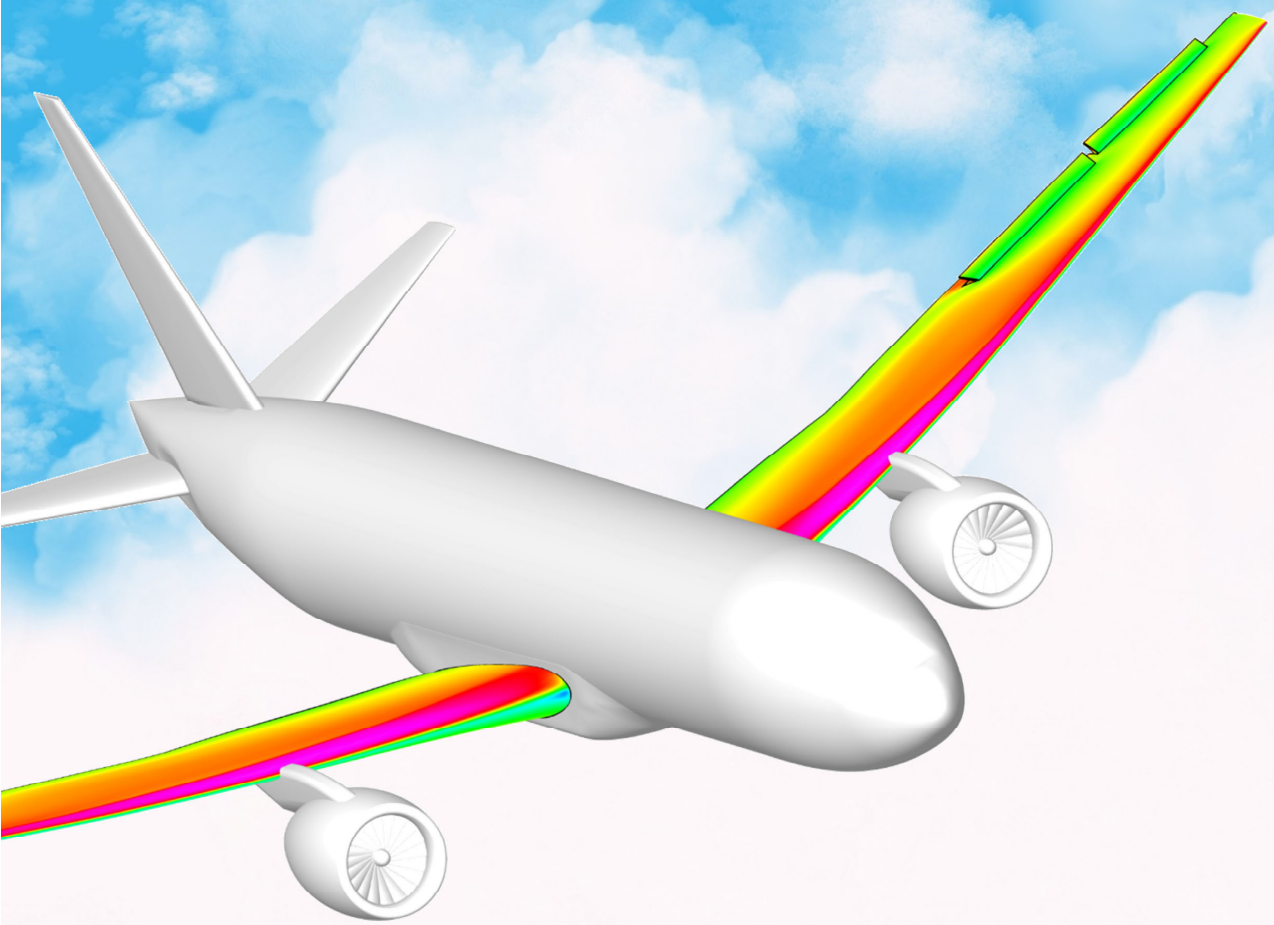

Paul Lancelot

Transonic Wing and Control Surface Loads Modelling for Aeroservoelastic Analysis

Transonic Wing and Control Surface Loads Modelling for Aeroservoelastic Analysis

Dissertation

for the purpose of obtaining the degree of doctor
at Delft University of Technology,
by the authority of the Rector Magnificus, Prof. dr. ir. T.H.J.J. van der Hagen,
chair of the Board for Doctorates,
to be defended publicly on
Monday 8 May 2023 at 15:00 o'clock

by

Paul LANCELOT

Diplôme d'Ingénieur, spécialité Mécanique et Conception des Systèmes
École Polytechnique de l'Université de Tours, France

born in Rennes, France

This dissertation has been approved by the promotors.

Composition of doctoral committee:

Rector Magnificus,	chairperson
Prof. dr. C. Bisagni	Delft University of Technology, promotor
Dr. ir. R. De Breuker	Delft University of Technology, promotor

Independent members:

Prof. dr. R. Botez	École de Technologie Supérieure, Canada
Prof. dr. M. Karpel	Technion - Israel Institute of Technology, Israel
Prof. dr. Ing. R. Radespiel	Technische Universität Braunschweig, Germany
Prof. dr. ir. L. Veldhuis	Delft University of Technology
Prof. dr. ir. R. Benedictus	Delft University of Technology, reserve member

Other members:

Dr. ir. J. Dillinger	DLR - Institut für Aeroelastik, Germany

Keywords: Aeroelasticity, control surfaces, transonic aerodynamics, structural optimisation, load alleviation, model identification

Printed by: Repromat, France

Front & Back: Designed by Paul Lancelot. Clouds image by vector_corp on Freepik.com

ISBN 978-94-6366-679-4

An electronic version of this dissertation is available at
http://repository.tudelft.nl/.

PREFACE

Writing these lines is something I had hoped to do for quite some years because it means that my dissertation is almost completed and ready to be defended.

First of all, I would like to thank Roeland De Breuker and Chiara Bisagni for being my promotors for many more years than initially written on the PhD agreement, for helping me carry through my research and for their feedback and advice on the dissertation. I would like to thank Prof. dr. Ruxandra Botez, Prof. dr. Moti Karpel, Prof. dr. Rolf Radespiel, Prof. dr. Leo Veldhuis, Prof. dr. Rinze Benedictus and Dr. Johannes Dillinger for accepting to be in my doctoral committee and for their valuable feedback on my dissertation.

Additionally, Roeland, I will be forever grateful that you allowed me to join the ASCM group, to work on the gust generator and then embark on, for several years, aircraft and aeroelasticity projects. Most importantly, your constant optimism and your enthusiasm towards aviation (especially for FlightRadar24) helped me complete this work.

My stay in Delft would not have been possible without Laura Chant for all the help regarding administrative matters and for the spirit she brought to the ASCM group. Jan Hol, for forwarding my open application to Roeland back in the summer of 2013, for allowing the gust generator to be built on the ASCM budget and helping me with the HPC on which many results of this dissertation have been computed. I wish to thank Gemma van der Windt for her help in preparing the defense and with the thesis printing. I am also grateful to the TU Delft Servicepunt and particularly to Eric van der Pol for his help with all IT matters and with my cherished Nastran, Fluent and Matlab software licenses. Finally, working on the AMEDEO, ReLOAD and MANTA EU projects with so many academic, research and industrial partners was extremely enriching and I would like to thank everyone involved in these consortiums.

A big thanks to Jurij who not only supervised me when I arrived in Delft for my internship but also became a trusted volleyball teammate and an ally in the ice/field hockey debate. Many thanks to Tito, Terence and Vega for the work we did together on aeroelasticity and optimisation which had quite an impact on this thesis as well. I would also like to thank Daniel for his important contribution to the dynamic FSI simulation framework developed during his internship with

us at TU Delft. A big thanks to Erik for proof-reading the Dutch parts of this thesis, and to Javier for being my go-to guy for all my graduate school questions during the last few months before the defence. It was also a real pleasure to work with Himanshu, Frederico, Dimitri, Srikanth and Roberto during their respective MSc Theses. Many thanks to the students and coaches of the DSE group 24 who made spring 2020 a bit brighter given the global context at the time and gave me a major motivational boost. Finally, a big thanks to Darwin for all the fun during the conference trips and for taking care of my plant after I left Delft.

Life and work at the office and in Delft would not have been the same without all my colleagues and friends: Noud, Kristofer, Ronan, Sebastian, Simon, Tigran, Mario, Zhi, Sherry, Yasir, Ines, Daniel, Boyang, Marta, Carlo, Tutu, Jens, Jaco, Meryem, Alex, Eddy, Sam, George, Sergio, Francesco, Natalia, Niels, Andres, Hammad, Nisarg, Giorgio, Marco, Saullo, Julien and the many I'm probably forgetting. Thank you for all the lunch debates, ASCM sports events, Papendal symposium, pizza at the sports centre and evenings at Doerak.

Special thanks to the volleyball friends and teammates Edgars, Kiran, Xu, Bala, Mohamed, Pietro, Santiago and all the others for the great games we had and which helped relieve a great deal of stress from work.

I wish to acknowledge Claude Le Quellenec for everything he taught me about model making, from electric boats to wooden gliders. The patience I gained while building these became really useful once I embarked on the PhD journey. I'm also grateful to Benjamin Depauw from the student exchange office and for my Professors in mechanical engineering of the University of Tours for helping me to get to Canada as an exchange student back in 2012-2013. It was a life changing experience which put me on the trajectory to later join TU Delft.

Most importantly, I would like to thank my parents Roland et Véronique, for their overwhelming support and continuous encouragement in following my current path in whatever country/continent I was in. And lastly, thank you Katie for your patience, proof-reading and for the uncompromised emotional and daily support I needed to finish this dissertation.

SUMMARY

The exponential growth of the aviation sector combined with environmental and energy supply challenges have led companies to innovate to reduce aircraft fuel consumption. Among the many areas currently under research this thesis investigates the possibility of making aircraft wings lighter thanks to innovative flight load alleviation systems and more accurate modelling methods. Reducing the loads on the wing means that the structure can be made with less material. Similarly, increasing the fidelity of the aircraft design tools can also lead to a weight reduction. This can in turn reduce the overall weight of the aircraft and improve its fuel consumption. A description of the state of the art advancements in both these areas is given in Chapter 1.

The second chapter serves as an introduction to linear aeroelasticity and aerodynamic identification. It covers the development of a passive load alleviation spoiler to reduce the forces acting on the wing during a gust encounter. The device uses a non-linear release system composed of a magnet and a linear mechanical spring which deflects upwards when a gust passes over the airfoil due to increased suction on the upper surface of the spoiler. Passive flaps and folding wingtips have been common in literature, however to the author's knowledge, a spoiler was never investigated for passive load alleviation purposes. The advantage of such a passive system is that it does not need complex logic or fast actuation. A spoiler can also be more easily integrated onto wings and they leave room on the trailing edges for other devices such as flaps.
The development of such a device is helped by a 2D airfoil aeroelastic model enhanced with RANS-CFD (Reynolds-averaged Navier–Stokes - Computational Fluid Dynamics) aerodynamic derivatives. The model has two degrees of freedom for pitch and plunge plus one for the spoiler deflection. The unsteady aerodynamic derivatives from the airfoil motion are derived from Theodorsen's unsteady aerodynamic theory. The gust aerodynamic derivatives are obtained using Küssner's implementation. The spoiler deflection derivatives are obtained by linearizing unsteady CFD results from the Ansys Fluent solver. All the contributions are summed together thanks to the load's superposition principle with the models running entirely using Simulink. An excellent agreement is obtained between the Theodorsen derivatives and the CFD derivatives. This shows the consistent level

of accuracy across all of the different aerodynamic components. With this model, we determined that a passive spoiler could reduce the gust incremental lift by up to 9% but needs an active system to fully retract the spoiler after a gust encounter rendering it semi-active.

In the third chapter, we focus on the unsteady non-linear aerodynamic modelling of an aileron in the transonic regime. This is a logical step from Chapter 2 as most commercial aircraft cruise at speeds generally between Mach 0.7 and Mach 0.9. Improving the modelling accuracy of control surfaces is paramount to better design load alleviation systems as these devices often have highly non-linear and unsteady aerodynamic responses.
On one hand, simulating the arbitrary aileron deflection with dynamic RANS-CFD analysis presents the challenges associated with mesh deformation and high computational cost. On the other hand, due to the presence of flow separation and transonic shocks, most potential flow aerodynamic panel methods cannot be used to predict the flow accurately around the control surfaces. Therefore, most research available in the literature chooses to only model the non-linear behaviour using quasi-steady aerodynamic models (from less expensive, steady RANS-CFD simulation or wind tunnel data), neglecting the unsteady aerodynamic part of the response, or to focus only on small disturbance linearized unsteady aerodynamic models obtained from RANS-CFD, which do not require large mesh deformation (as in Chapter 2).
To solve this dilemma, we opted to combine both approaches by summing up the steady loads produced by a non-linear quasi-steady aerodynamic model and the unsteady incremental loads produced by a linearized unsteady aerodynamic model. The quasi-steady model is simply a look-up table generated from a steady RANS-CFD analysis at each aileron deflection angles. The linearized unsteady model is obtained using transfer functions which are identified from unsteady RANS-CFD analysis with small disturbances. The resulting Reduced Order Model (ROM) runs using Simulink.
We found that this approach yields accurate lift prediction for a wide range of arbitrary control deflection amplitude and frequency. On a 2D example, we found an error of less than 5% compared with the RANS-CFD simulations for aileron oscillations up to +15 to -15 degrees of amplitude and deflection rates up to 94deg/sec.

In the fourth chapter, we investigate static aeroelastic load corrections on a 3D wing case. Static aeroelastic load analysis is important to derive the forces acting on the wing for structural sizing and has a direct impact on the weight of the airframe. The load correction is called the Hybrid Static Approach (HSA) and is already available with the NASTRAN static aeroelastic solver (SOL144). The HSA allows to correct SOL144 results using a high-fidelity aerodynamic database in the transonic regime thanks to the loads superposition principle, already experimented with in Chapter 2. To the author's knowledge, however, no source

in the literature have compared this method against high-fidelity Fluid-Structure Interaction simulation (FSI) previously.
Aerodynamic databases are generated from steady RANS-CFD analysis for different wing angles of attack , aileron and spoiler deflection. These so-called rigid aerodynamic loads are applied directly to the wing structural FEM model. This FEM model is coupled inside the NASTRAN solver to a linear aerodynamic panel mesh which provides the flexible loads as the wing bends and twists under the aerodynamic and inertia loads. The HSA method increases greatly the fidelity of the aeroelastic behaviour of the wing in the transonic domain, as demonstrated by comparing the results against high-fidelity FSI (NASTRAN coupled to Ansys Fluent). However, the stall behaviour of the wing (which starts around 3 degrees at Mach 0.85) is not well captured as the rigid loads are obtained at low angles of attack (0 to 1 degrees) and the aerodynamic database is extrapolated at higher angles of attack.
Nonetheless, the HSA method is ideal for wing structural sizing where we generally assume no stall on the wing and where only the flexible load changes as the structural design progresses. Flow separation around the control surfaces leading to a drop in effectiveness is also captured thanks to independent sets of the aerodynamic look-up tables covering their full range of deflection. The flexible aerodynamic behaviour of the wing is also more linear compared to the rigid wing results, with a delayed stall. This works in our favour as it reduces the impact of the non-linear incidence effect on the wing response.

In the fifth chapter, we describe the hybrid modelling approach to compute the wing dynamic aeroelastic response under the arbitrary motion of the control surfaces. Predicting the wing deformation with the control non-linear and unsteady aerodynamics is difficult. As for the aerodynamic response, research in the existing literature usually relies on quasi-steady models if a non-linear response needs to be captured. This can be the case for dynamic manoeuvres (dynamic roll, turn etc.) where the control surfaces may be deflected to their maximum. However, this method lacks the aerodynamic lag terms required to accurately simulate dynamic events like flutter or gust response. Therefore, the latter are often simulated using small disturbance linearized FSI (also referred as modal-based) or linear panel methods coupled with a FEM model. These methods are much faster than time marching high-fidelity FSI which is too computationally expensive to be included in the wing design loop. Nonetheless, they do not capture non-linear loads due to control surfaces deflection beyond their linear aerodynamic range.
Our hybrid modelling approach bridges the gap between both techniques by combining them. The control surface load aerodynamic ROM presented in Chapter 3 is reused and extended to a 3D wing case. It provides the non-linear and unsteady aerodynamic forces and moments from any large or sudden aileron or spoiler rotation. These rigid loads are applied directly onto the wing structural model as with the HSA presented in Chapter 4. We consider however that the

incremental dynamic aeroelastic wing response from the control surface deflection remains mostly linear and can be approximated using the NASTRAN linear dynamic aeroelastic solution (SOL146) which is very fast.
We demonstrate the accuracy of our hybrid model to predict the incremental wing loads and displacements against FSI with an error ranging from 5% to 10% in most of the cases. The loss of control effectiveness due to flow separation and shock wave interactions around the control surfaces and from the wing flexibility is captured too.

In the sixth chapter, we perform the aeroservoelastic optimisation of a wingbox of a typical airliner cruising at Mach 0.85. Both the structure and the gust load alleviation (GLA) system are optimised to reduce the wing weight. This framework also allows us to evaluate how changes in the aerodynamic fidelity of the control surfaces model used for GLA can affect the flight loads and the resulting optimised weight.
In most of the literature, wings are optimised with steady and dynamic loads but rarely with active control aside from manoeuvre load alleviation (MLA). There are notable exceptions where control parameters are optimised, but they rely on linear aeroelastic models to derive the loads. Not only do we use the HSA to correct the steady wing response, but we also use the control surface non-linear model described in Chapter 5 to estimate the GLA aerodynamic efficacy.
A bi-level approach is developed and the top level performs the GLA design parameters optimisation. This optimiser is heuristic and relies on a random search combined with an adaptive space to perform its task. For each design iteration, it prescribes the control surface motion (proportional to the gust profiles, but with variable lags and amplitudes) which will be used to generate the control surface aerodynamic loads used for GLA. Once the GLA contribution is obtained, a nested structural optimisation is performed. It relies on NASTRAN SOL200 (a structural gradient-based optimiser) and SOL144 and SOL146 (steady and gust loads with active control respectively). After the structural optimisation is converged, the resulting wingbox weight is sent back to the top level optimiser which will command the evaluation of the next set of control parameters.
Using this framework, we estimate that using linear aileron aerodynamic models instead of non-linear models overestimates the GLA capabilities and leads to 250kg lighter but non-conservative structural design. Results also highlight the diminishing return of increasing the aileron maximum deflection rate to minimise the wing weight.

Finally, we provide in Chapter 7 a discussion of the results and the recommendations to take this work further.

SAMENVATTING

De exponentiële groei van de luchtvaartsector in combinatie met uitdagingen op het gebied van milieu en energievoorziening hebben bedrijven ertoe aangezet te innoveren om het brandstofverbruik van vliegtuigen te verminderen. Van de vele gebieden die momenteel worden onderzocht, onderzoekt dit proefschrift de mogelijkheid om vliegtuigvleugels lichter te maken dankzij innovatieve systemen voor het verlichten van de vliegbelasting en nauwkeurigere modelleringsmethoden. Het verminderen van de belasting op de vleugel betekent dat de constructie met minder materiaal kan worden gemaakt. Ook het vergroten van de getrouwheid van de ontwerpgereedschappen voor vliegtuigen kan leiden tot gewichtsvermindering. Dit kan op zijn beurt het totale gewicht van het vliegtuig verminderen en het brandstofverbruik verbeteren. Een beschrijving van de stand van de techniek op beide gebieden wordt gegeven in Hoofdstuk 1.

Het tweede hoofdstuk dient als inleiding op lineaire aëro-elasticiteit en aërodynamische identificatie. Het behandelt de ontwikkeling van een passieve spoiler voor belastingvermindering om de krachten die op de vleugel werken tijdens een windvlaag te verminderen. Het apparaat maakt gebruik van een niet-lineair systeem om te openen dat bestaat uit een magneet en een lineaire mechanische veer en opent naar boven wanneer een windvlaag over het vleugelprofiel trekt door een verhoogde zuigkracht op de bovenkant van de spoiler. Passieve kleppen en opvouwbare vleugelpunten komen vaak voor in de literatuur, maar voor zover de auteur weet is een spoiler nooit onderzocht voor passieve belastingvermindering. Het voordeel van een dergelijk passief systeem is dat het geen complexe logica of snelle activering behoeft. Een spoiler kan ook gemakkelijker in de vleugels worden geïntegreerd en laat aan de achterranden ruimte voor andere voorzieningen zoals kleppen.
De ontwikkeling van een dergelijk toestel wordt ondersteund door een aëro-elastisch model in 2D van een aërodynamische vleugel met RANS-CFD (Reynolds-averaged Navier-Stokes - Computational Fluid Dynamics). Het model heeft twee vrijheidsgraden voor *pitch en plunge* plus één voor de spoileruitslag. De aërodynamische afgeleiden van de beweging van het vliegtuig worden afgeleid uit de theorie van Theodorsen over de aërodynamica. De aërodynamische afgeleiden van windvlagen worden verkregen met behulp van de implementatie van Küssner. De

spoilerafleidingen worden verkregen door het lineariseren van de niet-stationaire CFD-resultaten van de Ansys Fluent solver. Alle bijdragen worden bij elkaar opgeteld dankzij het superpositieprincipe van de belasting, waarbij de modellen volledig met Simulink werken. Er wordt een uitstekende overeenkomst verkregen tussen de Theodorsen-afgeleiden en de CFD-afgeleiden. Hieruit blijkt de consistente nauwkeurigheid van alle verschillende aerodynamische componenten. Met dit model hebben wij vastgesteld dat een passieve spoiler de lift bij windvlagen met 9% kan verminderen, maar dat een actief systeem nodig is om de spoiler volledig in te trekken na een windvlaag, waardoor hij semi-actief wordt.

In het derde hoofdstuk richten wij ons op de niet-lineaire aërodynamische modellering van een rolroer in het transonische regime. Dit is een logische stap vanuit hoofdstuk 2, aangezien de meeste commerciële vliegtuigenin in kruisvlucht doorgaans snelheden tussen de Mach 0.7 en Mach 0.9 bereiken. Verbetering van de modelnauwkeurigheid van stuurvlakken is van het grootste belang voor een beter ontwerp van systemen voor belastingvermindering, aangezien deze vaak sterk niet-lineaire en niet-stationaire aërodynamische reacties vertonen.
Enerzijds brengt de simulatie van een willekeurige rolroeruitslag met dynamische RANS-CFD-analyse uitdagingen met zich mee in verband met mesh-vervorming en hoge rekenkosten. Anderzijds kunnen de meeste aerodynamische paneelmethoden voor potentiële stroming, vanwege de aanwezigheid van loslating van de grenslaag en transonische schokken, niet worden gebruikt om de stroming rond de stuurvlakken nauwkeurig te voorspellen. Daarom wordt er in het meeste onderzoek in de literatuur voor gekozen om het niet-lineaire gedrag alleen te modelleren met behulp van quasi-stationaire aerodynamische modellen (op basis van minder dure, stationaire RANS-CFD-simulaties of windtunnelgegevens), waarbij het niet-stationaire aerodynamische deel van de respons wordt verwaarloosd, of om zich alleen te richten op gelineariseerde niet-stationaire modellen met kleine storingen, verkregen uit RANS-CFD, waarvoor geen grote itmesh-vervorming nodig is (zoals in Hoofdstuk 2).
Om dit dilemma op te lossen hebben wij ervoor gekozen beide benaderingen te combineren door de som te maken van de constante belastingen die worden veroorzaakt door een niet-lineair quasi-stationair aerodynamisch model en de niet-stationaire incrementele belastingen die worden veroorzaakt door een gelineariseerd niet-stationair aerodynamisch model. Het quasi-stationaire model is een opzoektabel die wordt gegenereerd uit een stationaire RANS-CFD-analyse bij elke rolroeruitslaghoek. Het gelineariseerde niet-stationaire model wordt verkregen met behulp van overdrachtsfuncties die zijn afgeleid van een niet-stationaire RANS-CFD-analyse met kleine verstoringen. Het resulterende *Reduced Order Model* (ROM) wordt uitgevoerd met Simulink.
Het blijkt dat deze aanpak een nauwkeurige voorspelling van de lift oplevert voor een groot bereik van willekeurige amplitude en frequentie van de stuuruitslag. Op een 2D-voorbeeld vonden wij een fout van minder dan 5% in vergelijking met de

RANS-CFD-simulaties voor rolroeroscillaties van +15 tot -15 graden amplitude en uitslagsnelheden tot 94deg/sec.

In het vierde hoofdstuk onderzoeken we statische aëro-elastische belastingscorrecties op een 3D-vleugel. Statische aëro-elastische belastingsanalyse is belangrijk om de op de vleugel werkende krachten af te leiden voor de dimensionering van de constructie en heeft een directe invloed op het gewicht van het vliegtuig. De belastingscorrectie wordt de Hybrid Static Approach (HSA) genoemd en is reeds beschikbaar in de NASTRAN statische aëro-elastische solver (SOL144). De HSA maakt het mogelijk de resultaten van SOL144 te corrigeren in het transonische regime met behulp van een hoogwaardige aerodynamische database dankzij het principe van superpositie van belastingen, waarmee reeds in hoofdstuk 2 is geëxperimenteerd. Voor zover de auteur weet, heeft echter geen enkele bron in de literatuur deze methode eerder vergeleken met hoogwaardige *Fluid-Structure Interaction* simulatie (FSI).
Aërodynamische stationaire worden gegenereerd uit databases RANS-CFD analyses voor verschillende invalshoeken van de vleugel, rolroer- en spoileruitslagen. Deze zogenaamde starre aerodynamische belastingen worden rechtstreeks toegepast op het FEM-model van de vleugelconstructie. Dit FEM-model wordt in de NASTRAN solver gekoppeld aan een lineair aerodynamisch paneel *mesh* dat de flexibele belastingen levert, aangezien de vleugel buigt en verdraait onder de aerodynamische en traagheidsbelastingen. De HSA-methode verhoogt de getrouwheid van het aëro-elastische gedrag van de vleugel in het transonische domein aanzienlijk, zoals blijkt uit een vergelijking van de resultaten met de hoogwaardige FSI (NASTRAN gekoppeld aan Ansys Fluent). Het overtrekgedrag van de vleugel (dat begint rond 3 graden bij Mach 0.85) wordt echter niet goed weergegeven omdat de starre belastingen worden verkregen bij lage invalshoeken (0 tot 1 graden) en de aërodynamische database wordt geëxtrapoleerd bij hogere invalshoeken.
Niettemin is de HSA-methode ideaal voor de dimensionering van de vleugelconstructie, waarbij in het algemeen wordt aangenomen dat de vleugel niet overtrekt en waarbij alleen de flexibele belasting verandert naarmate ontwerp van de constructie vordert. Stromingseparatie rond de stuurvlakken die het tot een afname van de effectiviteit wordt ook opgevangen dankzij onafhankelijke sets van de aerodynamische opzoektabellen die hun volledige bereik van hun uitslag bestrijken. Het flexibele aerodynamische gedrag van de vleugel is ook meer lineair in vergelijking met de resultaten van de starre vleugel, met een vertraagde overtrek. Dit werkt in ons voordeel omdat het de invloed van het niet-lineaire effect van de invalshoek op de vleugelrespons vermindert.

In het vijfde hoofdstuk beschrijven we de hybride modelbenadering om de dynamische aëro-elastische respons van de vleugel te berekenen onder de willekeurige beweging van de stuurvlakken. Het voorspellen van de vleugelvervorming bij een niet-lineaire en niet-stationaire aerodynamica is moeilijk. Voor de aërodynamis-

che respons wordt in de bestaande literatuur meestal gebruik gemaakt van quasi-stationaire modellen indien een niet-lineaire respons moet worden vastgelegd. Dit kan het geval zijn voor dynamische manoeuvres (dynamische rol, bocht etc.) waarbij de stuurvlakken maximaal kunnen worden uitgestuurd. Bij deze methoden ontbreken echter de aërodynamische vertragingstermen die nodig zijn voor een nauwkeurige simulatie van dynamische gebeurtenissen zoals flutter of windvlagen. Daarom worden deze laatste vaak gesimuleerd met behulp van gelineariseerde FSI met kleine storingen (ook wel modal-based genoemd) of lineaire paneelmethoden gekoppeld aan een FEM-model. Deze methoden zijn veel sneller dan hoogwaardige FSI, die te duur is om in het vleugelontwerp te worden opgenomen. Zij houden echter geen rekening met niet-lineaire belastingen als gevolg van uitslag van de stuurvlakken buiten hun lineaire aërodynamische bereik.
Onze hybride modelleeraanpak overbrugt de kloof tussen beide technieken door ze te combineren. Het in Hoofdstuk 3 gepresenteerde aerodynamische ROM voor de stuurvlakbelasting wordt hergebruikt en uitgebreid tot een 3D-vleugel. Het levert de niet-lineaire en niet-stationaire aerodynamische krachten en momenten van een grote of plotselinge rolroer- of spoilerrotatie. Deze starre belastingen worden rechtstreeks toegepast op het constructiemodel van de vleugel, zoals bij de in Hoofdstuk 4 gepresenteerde HSA. Wij zijn echter van mening dat de incrementele dynamische aëro-elastische vleugelrespons van de uitslag van het stuurvlak grotendeels lineair blijft en kan worden benaderd met de NASTRAN lineaire dynamische aëro-elastische oplossing (SOL146), die zeer snel is.
Wij tonen de nauwkeurigheid van ons hybride model door de incrementele vleugelbelasting en -verplaatsingen ten opzichte van de FSI te voorspellen met een fout die varieert van 5% tot 10% in de meeste gevallen. Het verlies aan controle-effectiviteit als gevolg van loslating en schokgolfinteracties rond de stuurvlakken en van de vleugelflexibiliteit wordt ook meegenomen.

In het zesde hoofdstuk voeren we de aeroservoelastische optimalisatie uit van een vleugeldoos van een typisch vliegtuig dat op Mach 0.85 vliegt. Zowel de constructie als het gustload alleviation (GLA) systeem worden geoptimaliseerd om het vleugelgewicht te verminderen. Dit kader stelt ons ook in staat te evalueren hoe veranderingen in de aërodynamische getrouwheid van het voor GLA gebruikte model van de stuurvlakken de vliegbelastingen en het daaruit voortvloeiende geoptimaliseerde gewicht kunnen beïnvloeden.
In de meeste literatuur worden vleugels geoptimaliseerd met constante en dynamische belastingen, maar zelden met actieve besturing, afgezien van manoeuvreerbelastingverlichting (MLA). Er zijn opmerkelijke uitzonderingen waarbij regelparameters worden geoptimaliseerd, maar die vertrouwen op lineaire aëro-elastische modellen om de belastingen af te leiden. Wij gebruiken niet alleen de HSA om de stationaire vleugelrespons te corrigeren, maar wij gebruiken ook het niet-lineaire model van het stuurvlak dat in Hoofdstuk 5 wordt beschreven om de aerodynamische efficiëntie van de GLA te schatten.

Er is een aanpak op twee niveaus ontwikkeld, waarbij het hoogste niveau de optimalisering van de GLA-ontwerpparameters uitvoert. Deze optimalisator is heuristisch en vertrouwt op een willekeurige zoektocht in combinatie met een adaptieve ruimte om zijn taak uit te voeren. Voor elke ontwerp iteratie schrijft hij de beweging van het stuurvlak voor (evenredig met de windvlaagprofielen, maar met variabele vertragingen en amplitudes) die zal worden gebruikt om de aerodynamische belastingen van het stuurvlak voor GLA te genereren. Zodra de GLA-bijdrage is verkregen, wordt een geneste structurele optimalisatie uitgevoerd. Daarbij wordt gebruik gemaakt van NASTRAN SOL200 (een op structurele gradiënten gebaseerde optimizer) en SOL144 en SOL146 (respectievelijk constante en windbelastingen met actieve regeling). Nadat de structurele optimalisatie is geconvergeerd, wordt het resulterende gewicht van de vleugeldoos teruggestuurd naar de topniveau-optimalisator, die de evaluatie van de volgende reeks regelparameters opdraagt.
Met behulp van deze methodiek, schatten wij dat het gebruik van lineaire aërodynamische rolroermodellen in plaats van niet-lineaire modellen de GLA capaciteiten overschat en leidt tot een 250 kg lichter maar niet-conservatief ontwerp van de constructie. De resultaten benadrukken ook het afnemende rendement van het verhogen van de maximale uitslag van de rolroeren om het vleugelgewicht te minimaliseren.

Ten slotte geven wij in Hoofdstuk 7 een discussie van de resultaten en aanbevelingen om dit werk voort te zetten.

ACADEMIC CONTRIBUTION OF THIS DISSERTATION

This dissertation presents a series of approaches to improve the wing and control surface loads analysis process during the preliminary design phase of an airframe. Refined load predictions allow a more accurate sizing of the wing structure. It also permits a better evaluation of the authority of the control surfaces to perform passive and active load alleviation. The contributions can be organised into the following three categories:

AERODYNAMIC MODELLING

- Linear unsteady models were identified from unsteady RANS-CFD and were combined with analytical models from Thordosen and Küssner's unsteady linear aerodynamic theories. The application was done on a 2D airfoil equipped with a spoiler, whereas most of the literature uses a flap. The analytical models were used for the airfoil pitch, plunge and gust encounter responses while the transfer functions derived from RANS-CFD were used for the aerodynamic derivatives of the spoiler. The analytical models were also compared to RANS-CFD directly to check for consistency of the results. The aerodynamic models were used to simulate a passive deploying spoiler for load alleviation purposes which in itself also represents a novelty.

- To improve the aerodynamic fidelity of the control surfaces in the transonic regime, a non-linear unsteady reduced order model was developed. Unlike other models found in literature that solely rely on either unsteady linearized models or quasi-steady non-linear aerodynamic databases, our modelling strategy combines both. Additionally, our models do not require full order simulations to be identified which are difficult to achieve using RANS-CFD due to mesh deformation and convergence issues. We first demonstrated the accuracy of this method on a 2D transonic rigid airfoil geometry equipped with an aileron. We compared the results given by our model against transient CFD-RANS analyses for a wide range of deflection rates and amplitudes. For most of the operational rate/amplitude combinations, our method was effective to replicate CFD results, predicting the lift increment within a 5%

error margin. The model was then extended to 3D cases and showed the same accuracy.

AEROELASTIC MODELLING

- We benchmarked a method to improve the static aeroelastic load analysis given by MSC NASTRAN. This method, called the Hybrid Static Approach (HSA), was introduced prior to this thesis but no comparison to Fluid-Structure Interaction (FSI) relying on RANS-CFD had been published in the open literature so far. The main advantage of the HSA lies in the simplicity of creating external aerodynamic databases using rigid CFD analysis to introduce the transonic flow corrections on the wing and control surfaces. We showed that this method gave satisfactory results compared to FSI and was suitable for wingbox structural sizing problems.

- We developed and compared an approach to improve the dynamic aeroelastic load analysis given by a linear aeroelastic solver. Following the same path as the HSA, the non-linear unsteady rigid incremental loads from control deflections obtained with our aerodynamic ROM were superimposed on a linear aeroelastic model. With this method, we could capture the loss of control effectiveness due to both non-linear aerodynamics and aeroelastic control reversal. We benchmarked our approach against a conventional time marching FSI method in the transonic regime. The results with the aileron showed a good agreement with our hybrid model when the wing is moderately flexible and provided a remarkable computation cost reduction against FSI which is traditionally warranted for such analysis.

APPLICATION TO A WINGBOX SIZING PROBLEM

- We have used non-linear aerodynamic models in wingbox optimisation problems featuring MLA and GLA whereas most studies in the literature rely on linear models to derive the loads. Therefore, we could investigate the impact aerodynamic fidelity had on the loads and on the subsequent optimised results. Concurrent optimisations of the control and structural design variables were performed using a novel bi-level scheme which was parallelised to improve the rapidity of finding the optimum solution. This allowed different scenarios to be evaluated with and without MLA and GLA and to perform a sensitivity analysis with different deflection speeds.

NOMENCLATURE

ABBREVIATIONS

AoA	Angle of Attack
CAD	Computer Aided Design
CFD	Computational Fluid Dynamics
CPU	Central Processing Unit
CRM	Common Research Model
CSM	Computational Structural Mechanic
DLM	Doublet Lattice Method
DLR	German Aerospace Center
DOF	Degree of Freedom
ESL	Equivalent Static Load solver
FEM	Finite Element Method
FSI	Fluid-Structure Interaction
HSA	Hybrid Static Approach
HuSA	Hybrid Unsteady Approach
LES	Large Eddy Simulations
MLA	Manoeuvre Load Alleviation
NACA	National Advisory Committee for Aeronautics
NASA	National Aeronautics and Space Administration
NASTRAN	NASA Structural Analysis
ONERA	French Aerospace Lab
RANS	Reynolds-averaged Navier–Stokes
RBF	Radial Basis Function
RFA	Rational Function Approximation
ROM	Reduced Order Model
SA	Spalart-Allmaras
SOLxxx	NASTRAN solution sequence

SST	Shear Stress Transport
TFEST	Matlab Transfer Function Estimate
UDF	User Defined Function
VLM	Vortex Lattice Method
ZDES	Zonal Detached Eddy Simulation

GREEK SYMBOLS

α	Angle of attack
δ	Control surface arbitrary deflection
δ_{ail}	Aileron deflection
δ_{spoil}	Spoiler deflection
ΔCl_c	Incremental lift coefficient due to control surface deflection
ΔM_x	Incremental bending moment
ΔN_z^{root}	Incremental load factor at the wingroot
ΔQ	Incremental loads from either the dynamic loads analysis or the aerodynamic ROM
ΔQ_c	Incremental control total loads
ΔQ_{ci}	Aerodynamic local ROM
ΔQ_{cs}	Incremental control quasi steady loads
ΔQ_{cu}	Incremental control unsteady loads
ΔQ_e	Generalized aerodynamic forces from the wing elastic response
ΔQ_{gust}	Incremental gust loads
ΔQ_{rigid}	Incremental aerodynamic rigid loads
ζ	Modal displacements vector
θ	Airfoil pitch
ρ	Flow density
χ	GLA control parameters
ψ	Structural design parameters
ω	Circular frequency

ROMAN SYMBOLS

$\tilde{M}_x$	Normalized bending moment
b	Airfoil semi-chord
C	Theodorsen function
Cl	Lift coefficient
Cm	Moment coefficient

d	Distance between the elastic axis and the center of pressure
G	Transfer function
h	Airfoil plunge
I^a	Airfoil inertia around its center of gravity
I^s	Spoiler inertia around its center of gravity
I_δ	Spoiler inertia around the spoiler hinge
I_θ	Airfoil inertia around the elastic axis
in	Transfer function input in the Laplace domain
K	Stiffness matrix
k	Reduced frequency
K_δ	Structural stiffness terms for the spoiler rotation
K_θ	Structural stiffness terms for the airfoil in pitch
K_h	Structural stiffness terms for the airfoil in plunge
L^a_δ	Airfoil lift due to spoiler deflection
L^a_θ	Lift due to airfoil pitch
L^a_h	Lift due to airfoil plunge
m	Total mass of the airfoil (including the spoiler)
M^a_δ	Airfoil moment due to spoiler deflection
M^s_δ	Spoiler moment due to spoiler deflection
M^s_θ	Spoiler moment due to pitch
M^s_h	Spoiler moment due to plunge
M^s_w	Spoiler moment due to gust
M_x	Bending moment
M_c	Control surface mass matrix
out	Transfer function output in the Laplace domain
P	Externally applied loads
q_∞	Dynamic pressure
Q_e	Flexible aerodynamic matrices
Q_r	Rigid aerodynamic matrices
Q_{eq}	Equivalent static loads
R_{ytip}	Wing tip rotation around y-axis
s	Laplace domain variable
S_δ	Inertia coupling term that relate the plunge with the spoiler deflection
S_θ	Inertia coupling term that relate the plunge with the airfoil incidence
$span$	Aircraft half wing span
t	Time

u	Nodal displacements
U_{ztip}	Vertical wing tip displacement
v_∞	Flow velocity at infinity
v_{gust}	Gust velocity
w	Aerodynamic gust state
X^a	Distance between the airfoil center of gravity and the airfoil elastic axis
$X^{s,a}$	Distance between the spoiler center of gravity and the airfoil elastic axis
$X^{s,s}$	Distance between the spoiler center of gravity and the hinge location
$y/span$	Normalized span-wise distance

CONTENTS

1

INTRODUCTION

Before the Covid pandemic, there were well over 100,000 commercial flights every day. After a historic 75% drop in April 2020, commercial traffic is now slowly getting back into shape. In some regions, such as China, passenger counts are even exceeding pre-pandemic levels, and the sector hopes for a full recovery by 2024. The number of commercial flights is expected to continue its growth, fuelled by an increased demand from Asia, India and Africa, and should double over the next 20 years. This forecast alone explains why the quest to reduce fuel consumption and the aviation industry's environmental footprint is as important as ever. Nonetheless, fuel economy in aviation is not a new topic. After the first oil crisis in the early 1970s, it became apparent that large, more efficient, passenger aircraft, such as the Boeing 747, would have a brighter future than their glamourous supersonic contemporaries. This trend later continued when the Airbus A300 entered service in 1974. With only two engines, this aircraft promised airlines significant savings on maintenance and fuel compared to the competing aircraft equipped with three or four engines.

Fuel economies, combined with improvements in air travel safety and economic development around the world, was met with a steep increase in ridership. Therefore, despite numerous crises, the number of air travellers has increased by a factor of 10 during the last 50 years. In contrast, energy consumption per passenger per kilometre has fallen by a factor of three. Although this is a remarkable reduction, it still fails to offset the growing aviation industry's environmental footprint and oil dependency.

Therefore, facing a dwindling energy supply coupled with climate and economic concerns, the commercial aviation industry needs to reduce fuel consumption aggressively in order to preserve itself. The steady progress in CO2 emission reduction of conventional aircraft propulsion is about 10% every 15 years on average. Aside from operational improvements (better route planning, higher passenger load factors), this represents the bulk of the reduction of the commercial aviation's environmental footprint so far. The improvements around jet engines (turbofan) generally rely on higher bypass ratios, hotter operating temperatures, geared turbofan and propfan. Projects to develop battery or hydrogen powered aircraft are also in full swing, but are only feasible for small commuter aircraft for the former, and require substantial investments for the latter. The use of new sources of energy are also contingent on the development of new aircraft architectures to accommodate battery storage or cryogenic tanks and new type of propulsion, such as distributed propellers. Therefore, improvement of the aircraft propulsion is only part of the answer, and significant improvements on the aircraft aerodynamics, systems and structures must also be achieved to push down CO2 emissions even further.

However, the incremental nature of aeronautical engineering usually means that any new technology needs to be proven before it is used on an aircraft. This tends to slow down innovation but is required to guarantee a high level of safety and reliability. In this context, trying to improve existing concepts becomes relevant. One significant improvement is to make the aircraft lighter. This translates to using less and lower-density materials for its structure. To achieve this, engineers must carefully determine the forces acting on the airframe and size its structure so that it will not become overstressed and break during service. These loads come from aircraft aerodynamics and inertia during manoeuvres, gust, landing and taxiing. Gusts mostly originate from atmospheric conditions (Hoblit, 1988) and control surfaces can be used to perform active lift control to reduce these forces. This is illustrated in Figure 1.1. For such a scheme to function adequately, however, sensors capable of probing the wind speed and the structural response along with fast actuation systems are required.

Load alleviation has been a field of research which has received increasing attention over the past decade. This is thanks to the development of light-weight, increasingly flexible wings for modern airliners, long endurance drones and wind turbines. It has been identified as an effective way to reduce structural fatigue and to improve aircraft handling as well as passenger safety and comfort. If accounted for early enough in the design, a snowball effect can lead to a significant weight reduction or permit higher wing aspect ratio, which in turn will reduce the fuel consumption and environmental footprint of the aircraft.

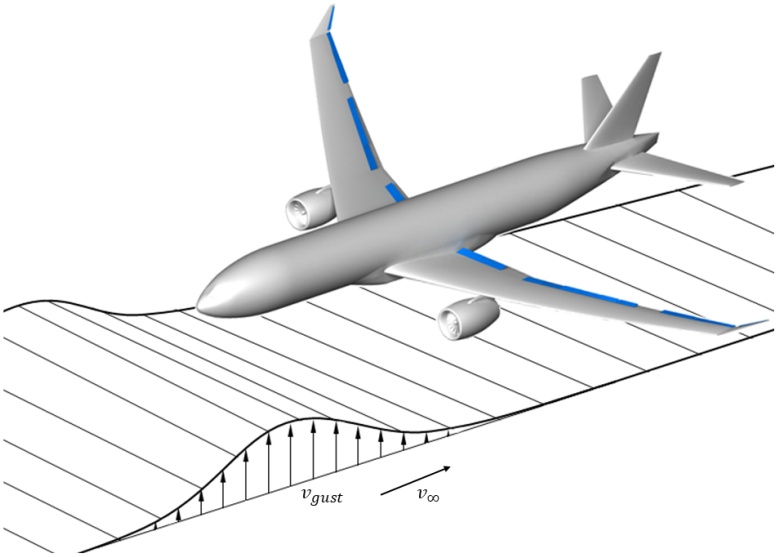

Figure 1.1: Illustration of a vertical gust hitting an aircraft in flight. Control surfaces (in blue) on the wings trailing edges and winglets can help reducing gust loads.

1.1 Active load alleviation

The idea of load alleviation is not new and such systems have been in operation since the 1970s. Lockheed engineers applied this technology on the C5 Galaxy to reduce fatigue load cycles on the wing structure as they had been underestimated during the design phase (Disney, 1977). Therefore, load alleviation was used to save weight, as extra airframe reinforcement would have been needed otherwise. At about the same time, Lockheed also implemented a similar system on its civil airliner, the L1011 Tristar (Ramsey and Lewolt, 1979), and nowadays, active lift control is common on civil aircraft (Regan and Jutte, 2012). Current load alleviation strategies mainly rely on the use of ailerons and spoilers because these devices are already present on most aircraft wings to fulfil other duties. Figure 1.2 is a photograph of a typical aircraft wing. We can see next to the wingtip the ailerons, which are primarily used for the aircraft roll control. To the left, we have a row of spoilers, which are mostly used as airbrakes. They also provide roll control as a back-up in certain flight phases or in case of an aileron failure. Finally, downstream to the spoilers, we have the flaps which are deployed during the take-off, approach and landing phases to maximise the wing lift coefficient. Active load control is, therefore, in most current aircraft a secondary feature of the control surfaces and must not interfere with their primary functions.

Active load alleviation also relies on the use of on-board sensors (angle of attack

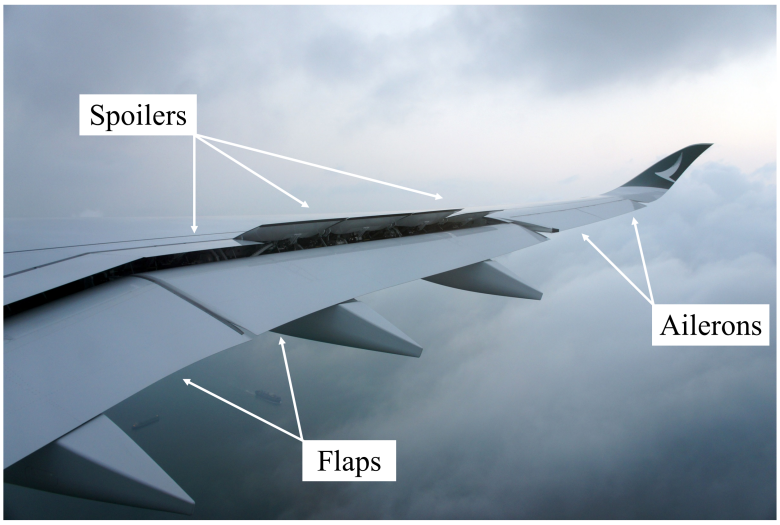

Figure 1.2: Control surfaces (also referred to as movables) on an Airbus A350-1000 wing.

sensor, Lidar, accelerometer) and controllers, programmed to react to disturbances such as gust (in the case of a feed-forward controller) or wingtip sudden acceleration (in the case of closed-loop feedback control) as shown by Fezans et al. (2019). There are a few challenges associated with active control: first is the reliability of the sensors, controllers and actuation systems. For this reason, there are multiple redundancies in place in the case of failure in the control loop. Another challenge associated with active control is the correct programming of the controller. The most simple type of controller is proportional. This means that the relation (or gain) between the input (gust disturbance, center of gravity or wingtip accelerations) and the output (control surface deflection) is linear and in phase. Finding the ideal value is a difficult process which requires adequate numerical simulation of the aircraft (Pusch et al., 2019), wind tunnel testing (Krag et al., 1980; Lepage et al., 2016; Ricci et al., 2017) and flight testing.

1.2 PASSIVE LOAD ALLEVIATION

Beside active gust load alleviation, passive systems have also been investigated in several studies. The advantage of a passive load alleviation system is to be a "fail-safe" alternative to active ones. Since there is no logic or actuation system involved, a passive system can potentially be less complex and more reliable. Many ideas of dedicated passive load alleviation devices are available in the literature. They usually involve using non-linear materials or springs to deflect a control

surface or to morph its shape passively. The non-linear behaviour is needed to maintain an optimal aerodynamic shape at 1g level flight while allowing sufficient deflection in case of a gust encounter. Another requirement is that the system needs to respond fast enough with limited latency to avoid any adverse effects such as an increase of the loads. As examples of passive load alleviation concepts, we can cite the rotating wingtip of Guo et al. (2015), the folding wingtip from Castrichini et al. (2016), the underwing control surface tested by Moulin and Karpel (2007), the very flexible winglet conceptualised by Ricci et al. (2013) and the bi-stable shape morphing airfoil tested by Kuder et al. (2016). Finally, aeroelastic tailoring using composite materials can also be used for passive load alleviation during manoeuvres (Sodja et al., 2021).

1.3 AERODYNAMIC MODELLING

Today's aircraft loads and sizing process still mostly relies on panel codes (doublet lattice or vortex lattice) as they are relatively accurate and very fast. However, they are limited to linear flow conditions and we cannot simulate transonic shock or flow separation with such methods. As highlighted by Bertram et al. (2021), the linear region of the aircraft's flight envelope shrinks as it accelerates towards the speed of sound.

These two aerodynamic phenomenons are of particular importance when designing a commercial jet aircraft wing because it will mostly fly in the transonic regime, between Mach 0.7 and Mach 0.9. Even if an aircraft is flying below the sound barrier, the air travelling around the wing accelerates in the process of generating aerodynamic lift, and can locally reach a supersonic speed. This, in turn, may lead to the apparition of a normal shock wave. It marks the sudden flow deceleration between the low-pressure area in front of the shock, and the rest of the airfoil behind it (Vos and Farokhi, 2015).

The occurrence of such an event has many implications, as it leads to an increase in aerodynamic drag (also called wave drag) and an important change in the lift distribution in the chord-wise direction. Besides the local Mach number, the strength and the location of the shock can change with the airfoil incidence and motion. The shock wave also interacts with the turbulent boundary layer, and flow separation can occur at the foot of the shock. This can lead to undesirable aerodynamic and aeroelastic effects such as buffet or aileron buzz. Although beyond the scope of this thesis, icing on wings and control surfaces can lead to similar aerodynamic non-linearity and have a great impact on the aircraft handling qualities (Baars et al., 2010).

As observed by Fillola (2006), the control surface deflections interact with the shock-wave position and strength. This is illustrated in Figure 1.3. If the aileron is deflected downwards (positively), the shock gains in strength and moves backwards. As it happens, the flow separation created by the shock wave leads

to a stall in the region around the aileron, reducing its efficacy. When the aileron is deflected upwards (negatively), the shock moves forwards and reduces in intensity. This is because the overall lift on the airfoil is decreasing and therefore the local airspeed and Mach number are also reduced. With potentially less flow separation emanating from the foot of shock-wave, the area around the aileron is not separated and the control surface maintains good effectiveness.

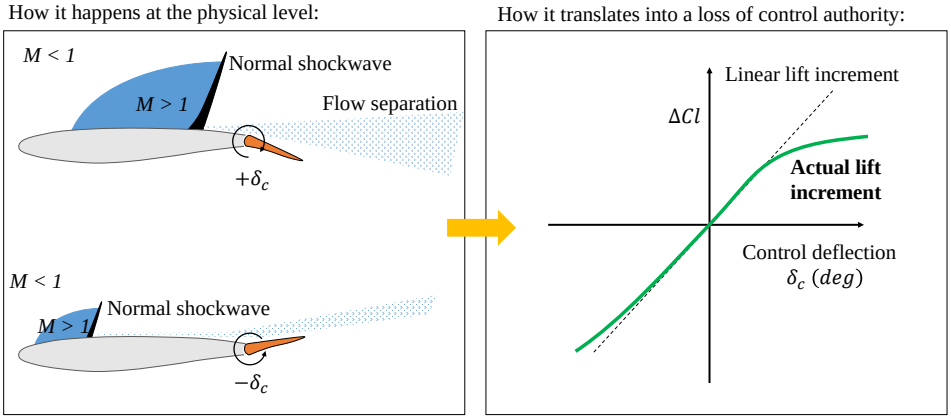

Figure 1.3: Illustration of the transonic shock position and its interaction with a control surface deflection.

Incidence effects on the spoiler deflection lift increment can also arise even at low angle of attack (AoA), denoted α, when flying at high speed. An example of this is given in Figure 1.4.

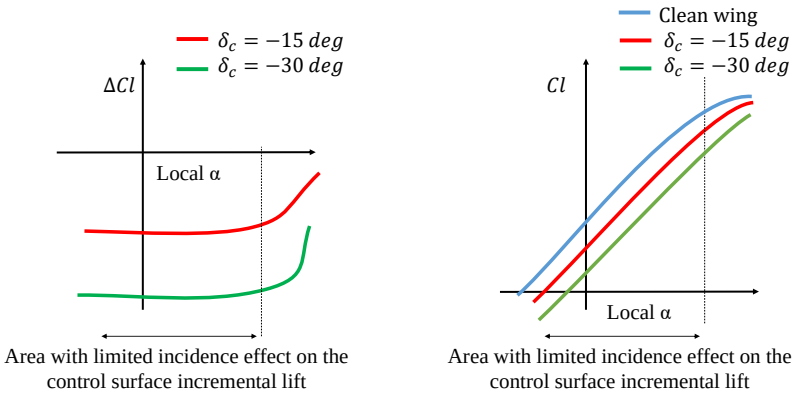

Figure 1.4: Incidence effects of the AoA on the spoiler incremental lift (left) and total lift (right). This is derived from Fillola (2006).

In these conditions, the load alleviation and manoeuvring capabilities of the control surfaces will also be affected. This means that a significant part of the sizing load cases for a regular passenger aircraft cannot be approximated with satisfying accuracy, leading to the necessity of important safety factors and generally heavier designs. Thus, the wing structure design is tied to the control surfaces performance assessment. Higher-order methods, such as computational fluid dynamics with Reynolds averaged Navier-Stokes (RANS-CFD) analyses are capable of approximating flight loads under transonic and detached flow regimes with higher fidelity. The computational time required for such simulations is nevertheless too long to be efficiently included in the sizing process of the airframe and is usually restricted to validation purposes only. Figure 1.5 is an overview of the various modelling approaches and fidelity levels used at the different stages of the aircraft design:

1.3.1 Control surfaces aerodynamic modelling

Fillola (2006) has characterised the aircraft movables performances using CFD-RANS and compared the results to experimental wind tunnel data. This was later extended with the development of a hybrid-fidelity model developed by Bertrand (2008). Both studies were centred around control surfaces steady aerodynamics and showed that RANS could be used reliably for such analyses. While steady-state problems have reached a certain maturity, modelling the dynamic behaviour of control surfaces is an active topic of research. The preferred approach is usually to use reduced-order models identified from CFD (Liu et al., 2011; Pohl et al., 2022; Prachař et al., 2018; Seidler et al., 2020) as these linear models are fast enough to be used in control problems. To handle any non-linearities that may arise at transonic speeds or high deflection angles, Ghoreyshi and Cummings (2014) propose to perform several identifications around various deflection points. The ONERA model was also successfully used for this purpose by Pohl et al. (2022) in the low-subsonic regime. Nonetheless, there is still no consolidated standard for control surfaces transonic non-linear unsteady aerodynamic modelling. This causes a rift in the modelling approaches between non-linear (quasi)-steady aerodynamic models chosen for handling qualities and manoeuvre load simulations and linear unsteady models primarily used to predict dynamic loads and gust cases.

1.3.2 FSI to account for flexibility

To account for the wing flexibility, several research groups have investigated the usage of transient CFD-RANS analysis coupled with a Computational Structural Model (CSM) in a staggered scheme (Huebner and Reimer, 2019; Huvelin et al., 2013; Reimer et al., 2019). While this approach captures all the relevant non-

Figure 1.5: Aerodynamic model fidelity for different stages of the aircraft design process.

linear aerodynamic and aeroelastic effects, it is also very time consuming and is not suitable for aerostructural optimisation. To bypass this issue, a modal approach can be used. It has been investigated by several researchers (Bekemeyer et al., 2019; Castells Marin, 2020; Halder et al., 2020; Hiller et al., 2020; Huang et al., 2018; Ritter and Roeser, 2020; Waite et al., 2019) and allows fast reduced-order models suitable for control optimisation problems. Nonetheless, in order to build the aeroelastic system, this method still requires at least one unsteady CFD simulation per retained mode shape to identify their aerodynamic derivatives. Therefore, this approach is only cost effective when a small number of modes is considered.

1.3.3 Hybrid models for rapid computations

Hybrid models which rely on multiple levels of aerodynamic fidelity can effectively be used for complex aeroelastic problems. For instance, to study the capability of a gust load alleviation system, Goggin (1992) proposed to scale the unsteady aileron lift increment generated by a panel code with non-linear experimental data. More recently, Binder et al. (2021) used a similar approach to calibrate the spoiler VLM aerodynamic loads using CFD-RANS. Additionally, Riso et al. (2020) introduced a rapid simulation method to assess aileron efficiency in the transonic regime using a steady-state aerodynamic database.
High-fidelity aeroelastic simulations were not required for any of these examples which reduced the need for expensive and complex simulations. Yet, their approaches capture some of the non-linear aeroelastic and aerodynamic effects. They were, however, limited to quasi-steady flow corrections.
For static aeroelastic problems, a competitor to these modelling techniques is the Hybrid Static Approach method (HSA) implemented in MSC NASTRAN by Vincenzo and Castrichini (2013) and which is used to size a wingbox by Bordogna et al. (2020). It replaces the rigid aerodynamic component of the aeroelastic system by an external aerodynamic database. Incremental loads from the wing aeroelastic deformation are captured using the native doublet lattice method (DLM) which also allows the solver to retain its capability to compute steady aeroelastic sensitivities. This method simplifies the load correction process and only requires the corrections to be computed once, from CFD or wind tunnel tests for instance. The rigid aerodynamic databases can also be swapped for different flow conditions if needed.
For unsteady problems, a similar philosophy to the HSA has been elaborated by Raveh (2010), where the rigid aerodynamic contribution of a gust is computed with CFD. The unsteady aeroelastic behaviour of the aircraft is captured using a panel method. The advantage of decoupling rigid and flexible aerodynamics during aircraft sizing is evident; the elastic deformation of the structure can vary from one iteration to another and therefore requires a fast analysis method. The rigid part remains unchanged and can be analysed using higher-fidelity tools.

1.4 Aircraft sizing with active control

Including manoeuvre and gust load alleviation (MLA and GLA) in the wingbox sizing has the potential to decrease the wingbox weight significantly thanks to a reduction of the loads. This idea dates back to the late 1970s, with studies from Ramsey and Lewolt (1979) and Sensburg et al. (1982). Their goal was to mitigate the potential increase in flight loads from wingtip extensions which would reduce the fuel consumption, by the mean of active load alleviation. As noted by Livne (1999), there are some challenges associated with combined optimisation of structural and control parameters: notably the increase in the number and types of design variables and the non-convex design space that may result from it. Design constraints regarding the reliability of the control must also be included, which is a shift towards system engineering. Additionally, some of the weight savings gained by load alleviation may be obtained through a reduction in the structure fatigue.
Few studies have been performed during the past few years, most relying on a gradient based algorithm. These were performed on conventional and futuristic configurations, using ailerons spanning the entire wing and showing significant flight performance improvements from Xu and Kroo (2014) and Stanford (2020). Wildschek (2015) included a winglet tab for gust load alleviation purpose in the sizing process of a wingbox using a feed-forward controller. Handojo et al. (2018) also included the GLA function in the sizing of a composite wingbox and showed the effect of control delays on the resulting wing root loads. This optimisation was sequential with fixed control parameters. Bussemaker (2018) and more recently Binder et al. (2021) used a more integrated approach allowing concurrent optimisation of both control and structural parameters. This type of optimisation architecture is considered to be more efficient but makes it harder to integrate existing solvers in the chain. It also requires full access to the code to compute the sensitivities efficiently. Finally, most of these studies relied on linear aerodynamic method neglecting non-linearities due to transonic flow.

1.5 Scope and aims of this thesis

We saw in the introduction that load alleviation can be a key driver in reducing aircraft structural weight, improving flight performance and hence reducing commercial aviation fuel burns. Since decreasing the aeroelastic loads mostly relies on aerodynamic control surfaces, accurately modelling their performances is critical. Additionally, it needs to happen early in the design process, so the wing can be sized to leverage the lower stress on the wing structure from gust and manoeuvres. Therefore, we formulate the following main research question:

How can we predict aircraft control surfaces unsteady non-linear aerodynamics and aeroelastic response, and how can we integrate this assessment into the early phases of airframe sizing?

This is a highly multi-disciplinary endeavour that encompasses several aspects of aircraft development. It interacts with wing shape and structural optimisation, control laws and actuator design. It must also account for requirements in handling qualities, loads and flight performance. More importantly, the design and simulation tools required for each discipline may require CAD, CFD or FEM software and greatly vary in fidelity, computational time and level of expertise to use them. Therefore, to achieve any progress on this topic, we must limit the scope of the research to only a few selected areas. In Figure 1.6, we show an overview of the wing moveables development process and what will be covered in this thesis. We will cover the aerodynamic characterisation of the control surfaces, the load analysis on the wing and the following structural sizing, accounting for steady and dynamic analysis, with MLA and GLA.

Whereas until now, conceptual wing design with control surfaces has relied on linear aerodynamic modelling with steady aerodynamic corrections, we aim to reach the accuracy of CFD with rapid aeroelastic simulations during structural sizing. This will be achieved by deriving reduced-order models (ROM) of the aircraft movable aerodynamics from rigid CFD analyses and using these as higher fidelity models for the loads in the aeroelastic simulation. The goal of this methodology is to remain non-intrusive and compatible with commercial analysis and optimisation tools such as NASTRAN. Building a fast aerodynamic model of the control surfaces also allows control optimisation to evaluate the load alleviation potential of the devices, which can in turn affect the sizing of the wingbox. This will deliver more accurate load predictions earlier in the design process of the aircraft and its control surfaces, and by doing so, can yield better trade-off opportunities.

Regarding the validation of the aerodynamic and aeroelastic models developed in this thesis, most of it will be performed through cross-comparison with results obtained using established steady and unsteady RANS-CFD and FSI methods. Wind tunnel aeroelastic experiments with control surfaces have been achieved in the transonic regime (Huvelin et al., 2019; Wiart and Carrier, 2012) but openly accessible data remains generally scarce to completely reproduce these test setups. Additionally, to the author's knowledge, wind tunnel testing at such speeds also constrains the maximum achievable control surface deflection and wing elastic deformation. This makes using these experimental results for validating models built to simulate large control surface deflection with more realistic wing elastic deformation challenging.

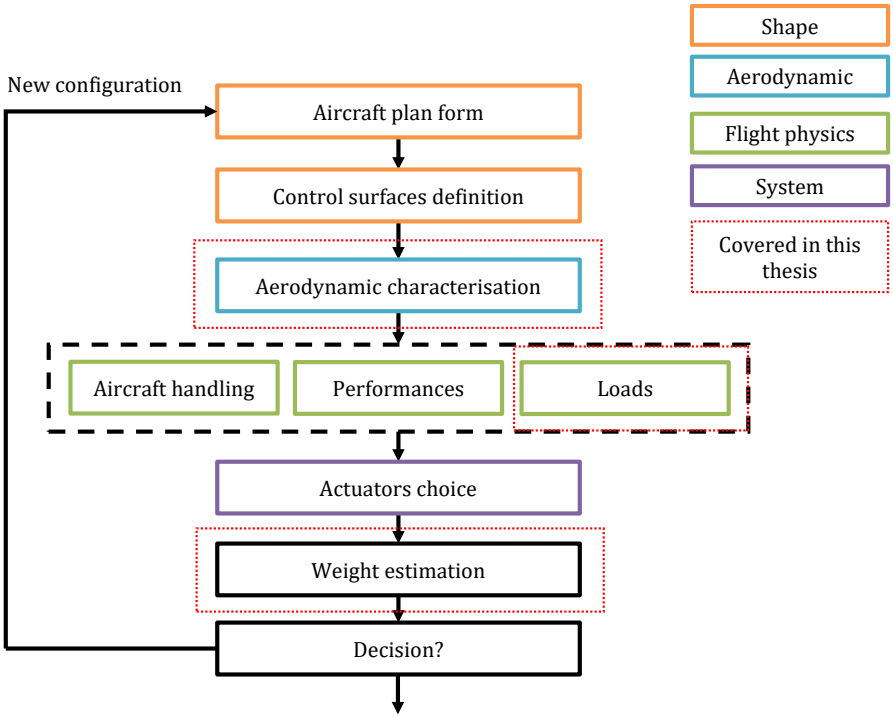

Figure 1.6: Industrial process for sizing control surfaces. Illustration adapted from Bertrand (2008).

1.6 DISSERTATION OUTLINE

In Chapter 2, we introduce a linear aeroelastic model relying on Theodorsen's unsteady flow theory for a typical airfoil section. To cope with the limitations of this type of model for spoiler aerodynamics, corrections are brought from unsteady high-fidelity flow simulations using transfer functions. The outcome is a 2D aeroelastic model with three degrees of freedom. It describes the spoiler contribution to the overall aeroelastic behaviour of the airfoil in the event of a gust encounter.

A more complex aerodynamic non-linear unsteady ROM is presented in Chapter 3. We describe the different components of this model and the steps to proceed to its identification using CFD data. Finally, we perform a first benchmark of the approach on a 2D airfoil equipped with an aileron at transonic speeds.

The different steady aerodynamic models available for load analysis and load alleviation are then discussed in Chapter 4. Possible levels of fidelity for such models are presented and benchmarked on a 3D wing model. Hybrid models and corrections techniques are introduced to speed up calculation. Finally, we analyse the effect of deflecting the aileron and the spoiler on the lift distribution, demonstrating how the wing flexibility and aerodynamic level of fidelity interact on loads.

A similar investigation to Chapter 4 is carried out in Chapter 5 on the same 3D geometry, but for unsteady loads. Due to their transient nature, these loads are more computationally expensive because they vary in time. Using the ROM from Chapter 3, we develop an hybrid aeroelatic model that accounts for the unsteady non-linear aerodynamics of control surfaces. The method is validated against a traditional FSI simulations.

Finally, in Chapter 6, we apply the load corrections and models derived in Chapters 4 and 5 to the sizing of a commercial passenger aircraft wing. We assess how the aerodynamic fidelity impacts the weight of the optimised structure. This chapter also presents methods to integrate structural design variables, and flight control design parameters within the same optimisation loop.

2

LINEAR DYNAMIC AEROELASTIC MODELLING

This chapter[1] introduces the basis for our hybrid-fidelity modelling strategy. For this purpose, we choose a 2D aeroelastic airfoil equipped with a passively actuated spoiler as an application case. As stated in the introduction however, many studies have already looked at developing passive load alleviation devices. Yet, most of them have focused on the wingtip, aileron or flap-like devices to achieve their goal of reducing the lift increment from gusts or manoeuvres and have dismissed the use of a passive spoiler for such task. Nonetheless, the spoiler remains a common type of control surface that can be installed next to the flaps. Being such a common occurrence on aircraft wings, we believe it can be a prime candidate for the job.

One major hurdle when dealing with spoilers however, is that the aeroelastic and unsteady aerodynamic behaviour of a wing equipped with deflected spoilers is not well documented. Most researchers rely on wind tunnel tests or high-fidelity simulations such as RANS or LES CFD (Deck et al., 2014; Geisbauer and Löser, 2017; Wentz et al., 1975; Xu and Yeung, 1999). Whereas RANS simulations rely on statistical averages to model small scales flow structures, LES (Large Eddy Simulation) resolves the Navier-Stokes equations at a smaller scale for more accurate

[1] This chapter is based on the conference paper Lancelot, P., De Breuker, R. (2016). "Passively actuated spoiler for gust load alleviation". In *International Conference on Adaptive Structure and Technologies, Lake George, NY, USA.*

modelling of vortexes and turbulence. LES is still to this day very computationally expensive, and while RANS is faster, it is not suitable for rapid aeroelastic simulations. Therefore, to realise any conceptual study of a passively actuated spoiler, a quicker model needs to be developed.

2.1 2D AIRFOIL AND SPOILER MODELS

In the following sections we describe the hybrid-fidelity models we are developing using classical linear aeroelastic formulations and CFD.

2.1.1 LINEAR AEROELASTIC MODELLING

The unsteady aeroelastic model developed by (Theodorsen, 1935) provides the basis to understanding the interactions between aerodynamics and structural dynamics. His original model had three degrees of freedom; one for the airfoil pitch θ, one for the plunge h and one for the control surface deflection δ. With such a simple model, one can quickly solve and understand aeroelastic problems such as flutter, control reversal and gust response. In Figure 2.1 we show an overview of the aeroelastic system equipped with the spoiler:

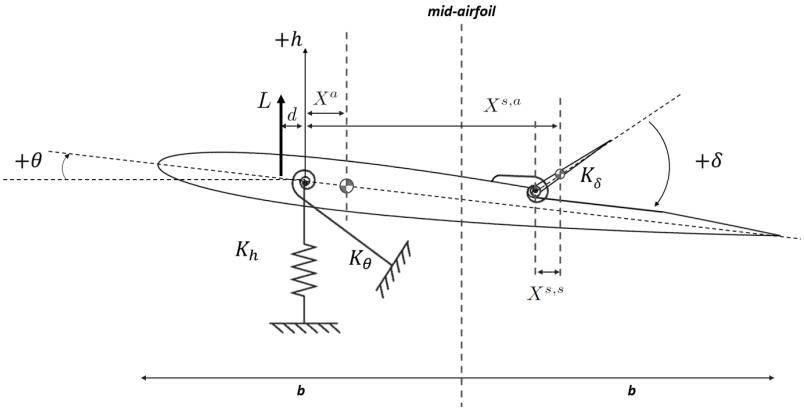

Figure 2.1: Overview of the aeroelastic system with three degrees of freedom: airfoil pitch, plunge and spoiler deflection.

The coupled system can be represented in matrix form shown in Equation 2.1. It is solved with Matlab/Simulink (MathWorks, 2020b) which allows non-linear multidomain computations. We decompose the forces acting on the airfoil into

discrete inputs for the system. This requires us to estimate the coupling terms between each degree of freedom but simplifies the identification process as it can be done individually for every input, without needing the full order system right away.

Each line of the system of equations is used for a degree of freedom. In addition to the aerodynamic effects from the airfoil pitch and plunge, we are also accounting for the spoiler deflection δ and vertical gust inputs w. Their individual aerodynamic contributions are summed for each degree of freedom in the right hand side of the system. The superscript on the aerodynamic terms indicates if the force is generated by the airfoil (^{a}) or by the spoiler (^{s}). The subscript indicates the degree of freedom or gust input on which the aerodynamic contribution is a function of.

$$\begin{bmatrix} m & -S_\theta & -S_\delta \\ -S_\theta & I_\theta & S_{\delta\theta} \\ -S_\delta & S_{\delta\theta} & I_\delta \end{bmatrix} \begin{Bmatrix} \ddot{h} \\ \ddot{\theta} \\ \ddot{\delta} \end{Bmatrix} + \begin{bmatrix} K_h & 0 & 0 \\ 0 & K_\theta & 0 \\ 0 & 0 & K_\delta \end{bmatrix} \begin{Bmatrix} h \\ \theta \\ \delta \end{Bmatrix} = \begin{bmatrix} L^a_\theta + L^a_h + L^a_w + L^a_\delta \\ M^a_\theta + M^a_h + M^a_w + M^a_\delta \\ M^s_\theta + M^s_h + M^s_w + M^s_\delta \end{bmatrix} \tag{2.1}$$

The variables m, I_θ and I_δ are, respectively, the total mass of the airfoil (including the spoiler), the inertia of the airfoil around the elastic axis and the inertia of the spoiler around the spoiler hinge. Similarly K_h, K_θ and K_δ are the structural stiffness terms for the airfoil in plunge and pitch, and for the spoiler rotation. m is obtained as follows:

$$m = m^a + m^s \tag{2.2}$$

With I_θ and I_δ derived from the airfoil and spoiler inertia around their respective center of gravity I^a and I^s by the means of the parallel axis theorem (Haas and Verschoyle, 1928). X^a is the distance between the airfoil center of gravity and the airfoil elastic axis, $X^{s,s}$ is the distance between the spoiler center of gravity and the hinge location. Finally, $X^{s,a}$ is the distance between the spoiler center of gravity and the airfoil elastic axis.

$$I_\theta = m^a (X^a)^2 + m^s (X^{s,a})^2 + I^a + I^s \tag{2.3}$$

$$I_\delta = m^s (X^{s,s})^2 + I^s \tag{2.4}$$

With S_θ and S_δ the coupling terms that relate the different states between them:

$$S_\theta = m^a X^a + m^s X^{s,a} \tag{2.5}$$

$$S_\delta = m^s X^{s,a} \tag{2.6}$$

The inertia coupling term between the airfoil rotation and spoiler deflection is defined as follows:

$$S_{\delta\theta} = I^s - S_\delta X^{s,a} \tag{2.7}$$

The lift and moment values related to the airfoil pitch and plunge can be evaluated directly from Theodorsen's model. Each set of forces and moments can be split into a circulatory and an added mass part. The circulatory part relies on the Jones approximation (Brunton and Rowley, 2013) of the Theodorsen function $C(k)$ to account for phase shift and change in response amplitude as function of the reduced frequency k (Leishman, 2000). b is the length of the semi-chord and d is the distance between the elastic axis and the center of pressure located at the airfoil quarter-chord. L^a_θ and L^a_h are computed at the quarter chord of the airfoil, while the moment is evaluated around the elastic axis:

$$L^a_\theta = \rho b^2(v\pi\dot{\theta} - \pi b d\ddot{\theta}) + 2\pi\rho v b C(k)(v\theta + b(\frac{1}{2} - d)\dot{\theta}) \tag{2.8}$$

$$L^a_h = \rho b^2(\pi\ddot{h}) + 2\pi\rho v b C(k)\dot{h} \tag{2.9}$$

$$M^a_\theta = -\rho b^2(\pi(\frac{1}{2} - d)vb\dot{\theta} + \pi b^2(\frac{1}{8} - d^2)\ddot{\theta}) + 2\pi\rho v b^2(d + \frac{1}{2})C(k)(v\theta + b(\frac{1}{2} - d)\dot{\theta}) \tag{2.10}$$

$$M^a_h = -\rho b^2(-d\pi b\ddot{h}) + 2\pi\rho v b^2(d + \frac{1}{2})C(k)\dot{h} \tag{2.11}$$

Regarding the forces induced on the airfoil by a gust encounter, Küssner is used instead of Theodorsen because it evaluates the lift as the airfoil penetrates into a vertical gust defined as a velocity profile v_{gust}. The two formulations (Equations 2.12 and 2.13) that are used for the lift and the moment are taken from Berci et al. (2010).

$$L^a_w = 2\pi\rho v b(0.565(\frac{v}{b})\dot{w} + 0.13(\frac{v}{b})^2 w) \tag{2.12}$$

$$M^a_w = L^a_w d \tag{2.13}$$

The variable w is the additional aerodynamic contribution created by the vertical gust profile and is uncoupled from the airfoil motion. It is defined in Equation 2.14.

$$v_{gust} = \ddot{w} + 1.13(\frac{v}{b})\dot{w} + 0.13(\frac{v}{b})^2 w \tag{2.14}$$

For the responses that involve the spoiler, limited work has been found on this topic. Therefore, no low fidelity model was found that describes the unsteady

aerodynamic behaviour of a spoiler. The approach chosen here is to generate transfer functions which can be used to approximate L^a_δ, M^a_δ, M^s_δ, M^s_w, M^s_h and M^s_θ.

2.1.2 Aerodynamic model identification from CFD

The transfer function $G(s)$ gives the relation between an input $in(s)$ and output $out(s)$ in the Laplace domain by matching the phase shift and amplitude of the response to the input as shown in Equation 2.15:

$$G(s) = \frac{out(s)}{in(s)} = \frac{f_m s^m + f_{m-1} s^{m-1} + ... + f_1 s + f_0}{s^m + e_{m-1} s^{m-1} + ... + e_1 s + e_0} \tag{2.15}$$

In our case, $in(s)$ and $out(s)$ are the Laplace transforms of the system states (w, h, θ, δ) and responses (L, M). We achieve the identification of the transfer function polynomials using Matlab TFEST toolbox MathWorks (2020c).
To demonstrate the accuracy of this method, we show the process for the aerodynamic identification below, using the OAT15A airfoil equipped with an aileron. It is different from the NACA0010 airfoil we use for the rest of this chapter, but the conclusions we derive still apply. The OAT15A setup is presented in more detail in Chapter 3 where the non-linear modelling is also introduced. In this section, we focus only on the linear aerodynamic response identification.
As shown in Figure 2.2, we can derive an aerodynamic transfer function from the step impulse on the control surface. The data to perform the identification is achieved with RANS-CFD. While this type of analysis is expensive to perform, using a step impulse is an effective way to reduce the time needed to generate the time-series.

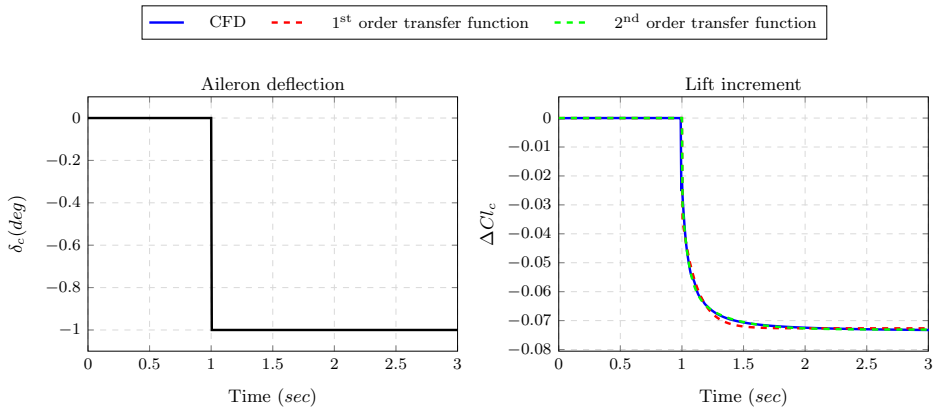

Figure 2.2: Aerodynamic response to a step impulse of the aileron on the OAT15A airfoil. This setup is presented in more detail in Chapter 3.

We can see above that 1st and 2nd order transfer functions provide a good approximation of the step response, with a 5% and 1% error respectively. To test the validity of this on a broad spectrum of frequencies, we perform the same CFD analysis with a chirp signal driving the aileron instead. The oscillation reaches 8Hz at 10 sec of simulation. We show the results in Figure 2.3. The accuracy of the 2nd order transfer function decreases as the oscillation frequency increases, with the error growing from 1% to 15%. The reduced frequency value of $k = 0.2$ is reached at 4.7Hz, which indicates a highly unsteady flow. For this value of k, the accuracy of the model remains good, with an error below 5%.

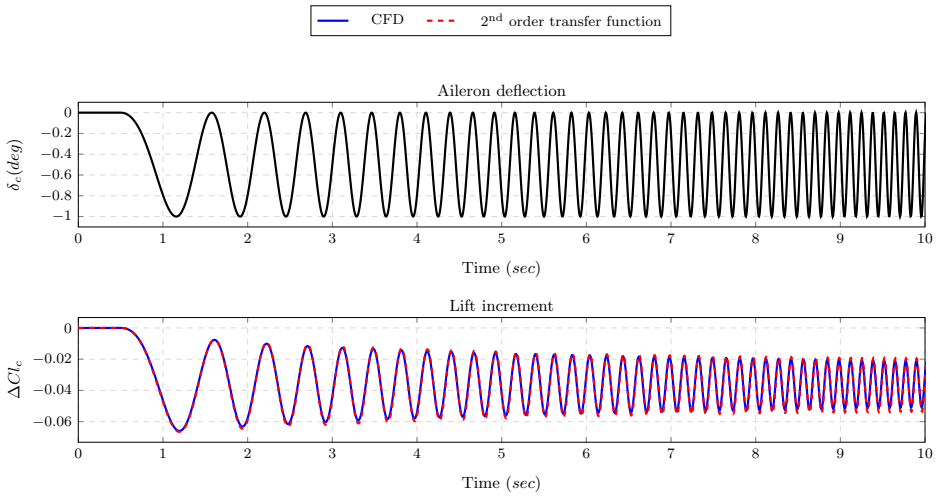

Figure 2.3: Aerodynamic response to a chirp motion from the aileron.

We plot in Figure 2.4 the frequency response of the chirp command obtained with transient CFD, 2nd and 5th order transfer functions. As the frequency increases, we also note a decreasing accuracy, in both gain and phase. This is consistent with the observation of the chirp results in the time domain.

Additionally, we can say that increasing the order of the transfer functions polynomial do not yield to a significant increase in accuracy. We conclude our demonstration with Figure 2.5 in which we show a comparison with two square signals with different amplitudes. The accuracy of our identified model is very good on the first input, with an error below 1%. The error slightly increases up to 3% with the second impulse. This is a sign of a subtle flow non-linearity. The transfer functions we are using are inherently linear, and the amplitude of the stabilised response must be strictly proportional to the input. We tackle this issue in Chapter 3. The accuracy of the current linear model is however sufficient for the purpose of the current chapter.

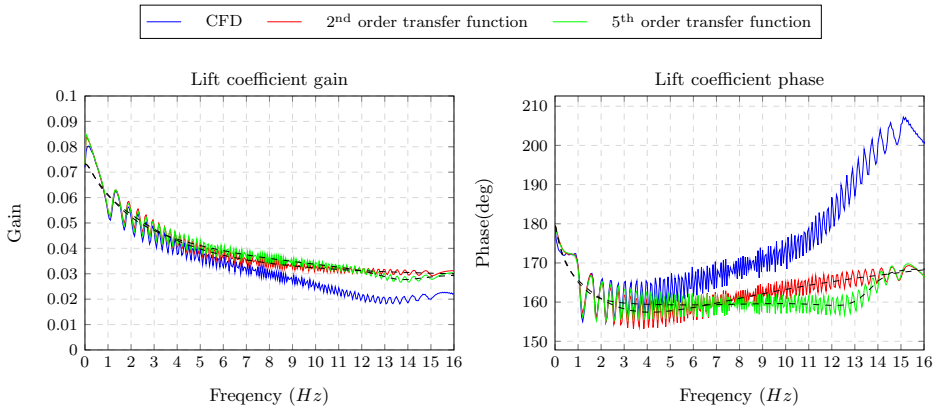

Figure 2.4: Frequency response plot of the CFD and transfer function results. The black dashed line indicates the exact response derive from the RFA polynomials.

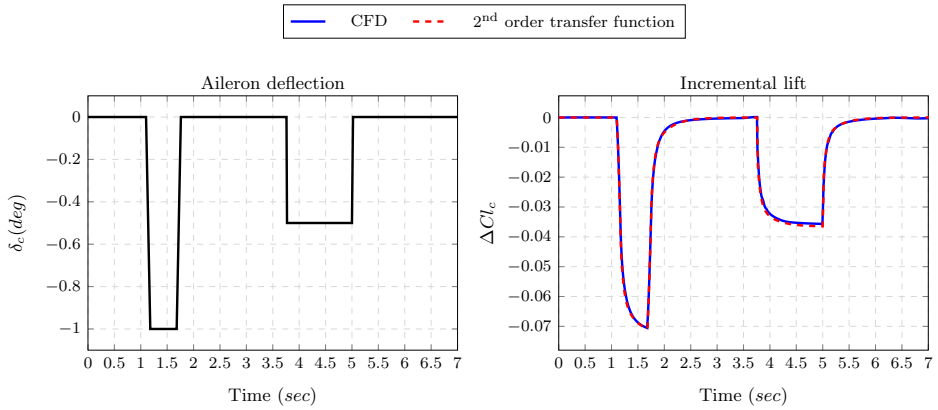

Figure 2.5: Square deflection signal.

2.1.3 SPOILER MODEL IDENTIFICATION

Four simulations are required to generate the six different transfer functions for the spoiler aerodynamic. L^a_δ, M^a_δ, M^s_δ can be evaluated in the same run since they are function of the same input. It is important to note that new transfer functions would need to be evaluated in case of any important change related to spoiler location or geometry since the identification would not be valid anymore. However, the effect of the spoiler deflection δ is assumed to vary linearly for small angles. A frequency sweep is performed to account for a realistic range of reduced frequency k. In the present work, the reduced frequency range of the different inputs varies from 0.209, which is highly unsteady, to 0.026 which is

quasi-steady. The flow speed is 30 m/s and the chord is 1 m. The spoiler hinge is located at 65% of the chord and its length is 10 cm. We set the flow speed and airfoil dimensions in such way it would be possible to reproduce this setup as a wind tunnel experiment in the TU Delft Open Jet facility (Lancelot et al., 2017). However we dropped this plan to focus on numerical investigations instead.

CFD simulations are performed using ANSYS Fluent R17.1 using an overset grid. The mesh is comprised of nearly 500,000 triangular and rectangular elements. As shown in Figure 2.6, they are distributed between the global mesh around the airfoil, and a local mesh that moves along the spoiler. Overset grids have the advantage to be much quicker to account for the rigid body motion of the geometry because it does not require any mesh deformation, unlike other mesh motion techniques. Therefore they can lead to significant time saving during transient simulations. However, overset grids can remain computationally challenging in the areas of overlap between the different grid zones with a risk of unexpected orphan cells and convergence issues. During the preparation of this thesis, dynamic mesh motion combined with compressible flows was only a beta feature of the overset grid solution in Ansys Fluent, and it was therefore decided for the following chapters that we would revert to more traditional spring-based smoothing and diffusion smoothing methods (Ansys, 2009a) to tackle studies with transonic flow.

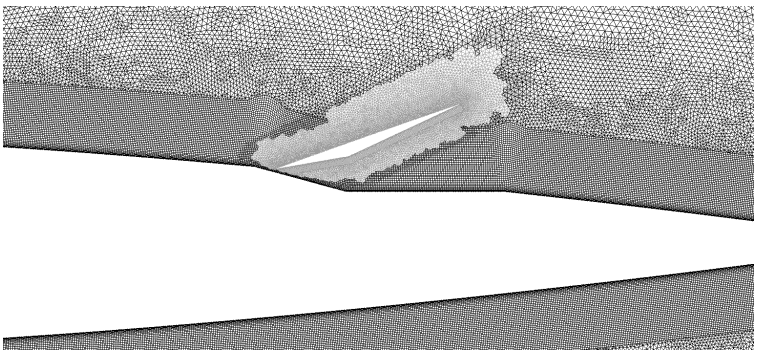

Figure 2.6: Mesh around the spoiler at the rear of a NACA0010 symmetrical airfoil. The cells which are redundant between the two mesh layers are suppressed.

The spoiler and airfoil motions, as well as gust inputs, are prescribed using Fluent user define functions (UDF). Since the flow is separated behind the spoiler when deployed, a $k-\omega$ turbulence model is used as well. For the simulations which do not require the spoiler to deflect, a regular "monolithic" mesh is used with a more classical mesh deformation for the displacements of the whole airfoil.

In Figure 2.7 on the left plot, the lift coefficient resulting from the arbitrary pitch and plunge motion of an airfoil is approximated using two transfer functions. Although Theodorsen's model is used for this purpose in the coupled aeroelastic

system, the comparison shows good agreement and demonstrates the validity of the methodology described above.

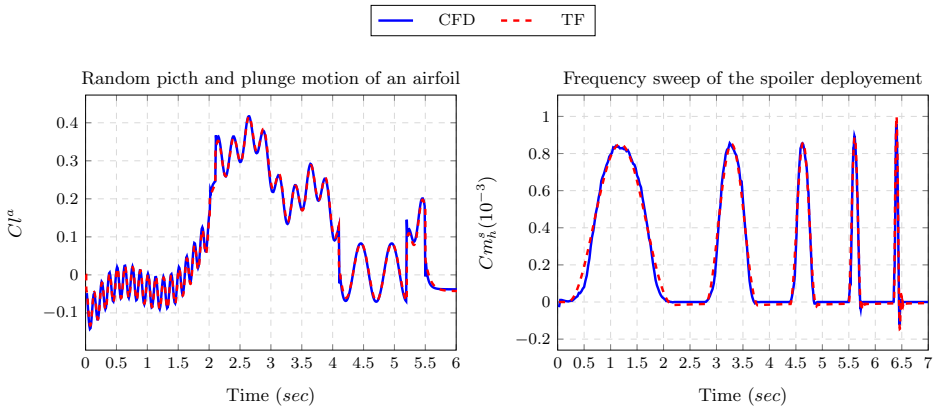

Figure 2.7: Comparison between CFD results and their approximations with transfer functions.

On the right plot in Figure 2.7, a spoiler is deployed at various speeds with an amplitude of 2.5 degrees. The incremental moment coefficient at the spoiler hinge is recorded and the results show that a transfer function can approximate it well, with less than a 5% error in magnitude. The procedure is repeated successfully for L_δ^a, M_δ^a, M_w^s and M_h^s.

2.2 Results

Once the aeroelastic system is constructed with all the required aerodynamic derivatives, we solve it using Matlab/Simulink to evaluate the effectiveness of the spoiler for load alleviation. For a fully passive load alleviation system to work, a non-linear behaviour needs to be introduced to maintain an optimal aerodynamic shape at 1g level flight while allowing sufficient deflection in case of a gust encounter. If we use a linear relation between the loads and the passive alleviation mechanism, the system will start deflecting as the forces acting on the device increase. This is sub-optimal, as it means that the spoiler may already deflect while the wing is not experiencing high loads factor or gust. This can create additional aerodynamic drag which would be detrimental to the flight performance of the aircraft. The amount of force acting on the device at 1g flight can also slightly vary because of the change in aircraft weight due to fuel consummation or the change in aircraft speed and altitude. Therefore, we must ensure that the spoiler will remain retracted for a whole range of nominal flight conditions, and only deflect when needed, as illustrated on the right plot in Figure 2.8.

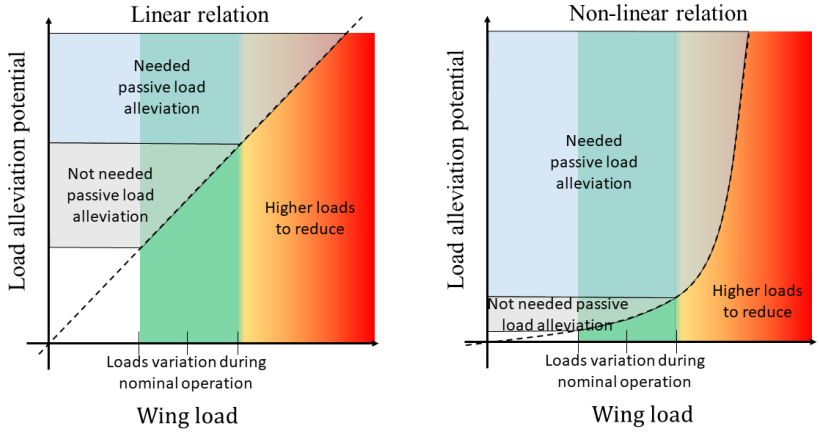

Figure 2.8: Illustration of why passive load alleviation systems must have a non-linear behaviour.The load alleviation potential is the achievable force and moment reduction acting on the airfoil or wing.

In the present work, the passive spoiler relies on the use of a linear spring and permanent magnets, which here serve the purpose of the non-linear element. Indeed, the attraction force between two magnets can be approximated by Coulomb's law and varies with the inverse of the distance squared. Therefore it provides the equivalent behaviour of a non-linear spring. The system is shown in Figure 2.9.

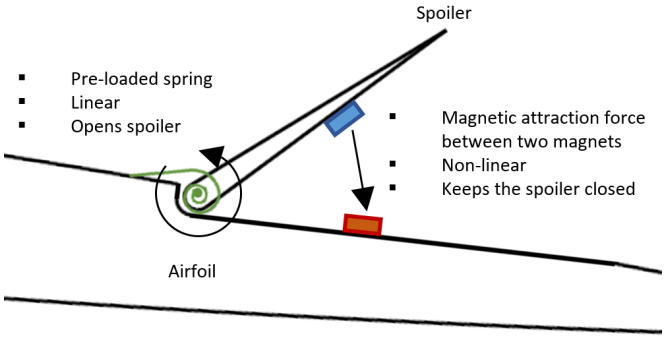

Figure 2.9: Schematic of the passive spoiler. The pre-loaded linear spring is installed to help the spoiler deflection, while the permanent magnets keep the spoiler retracted when there is no gust.

The main advantage of this combination is to allow a quick deployment of the

spoiler to mitigate the loads efficiently with little delay and no control logic involved. The combined stiffness is shown in Figure 2.10:

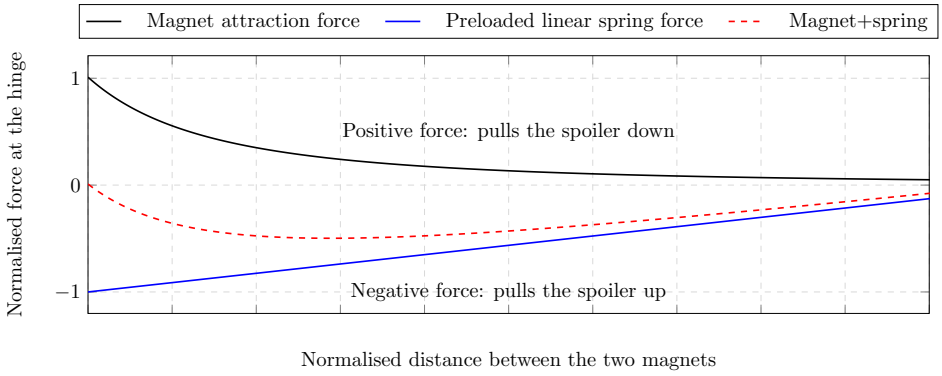

Figure 2.10: Force/displacement curve of the magnets and the spring.

The strong attraction force from the magnets prevents the spoiler to open if there is no gust. When a positive gust hits the airfoil, this is equivalent to a temporary change in the angle of attack and therefore creates lift and a drop in pressure on top of the airfoil. This pressure drop creates a suction force that pulls open the spoiler and moves the two magnets apart (one is attached to the airfoil, the other to the spoiler), therefore causing their attraction to drop non-linearly. The pre-loaded linear spring is installed to help the spoiler deflection by counteracting aerodynamic forces that will build up on it when deflected. To show the necessity of such a mechanism, a free-floating spoiler (without a spring nor magnets) is also investigated.

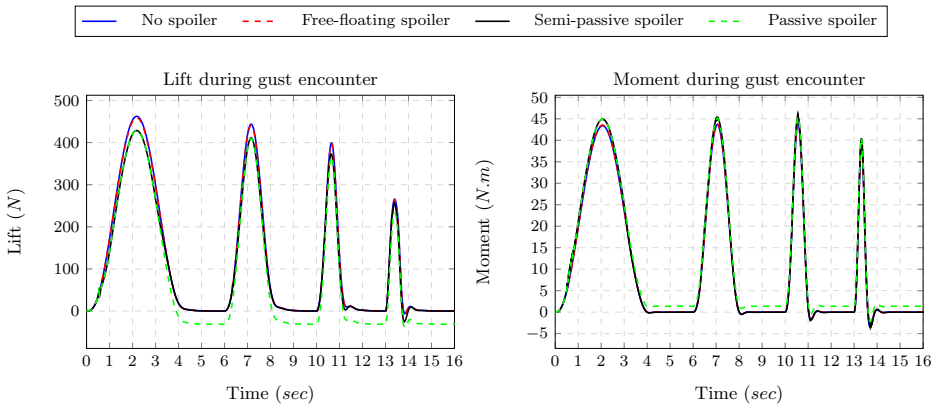

Figure 2.11: Lift and moment after four gust inputs. The airfoil angle of attack is set to 0 degree.

Results shown in Figure 2.11 and Figure 2.12 indicate that the spoiler never fully retracts after a gust encounter, reducing the lift during steady flight. This would affect the lift/drag ratio of the airfoil. The solution here could be a semi-passive system, which would still rely on a fully passive strategy for the deployment, but would require an actuator to completely close the spoiler again once the gust has passed. For this solution, it is necessary to evaluate when the spoiler needs to be retracted. In the present work, the spoiler will start to be pulled down when the gust load rate is negative. As shown in Figure 2.11 up to 9% of the lift from the gust is reduced, however because the spoiler is located at the rear of the airfoil, an additional moment around the elastic axis is added up to 4%.

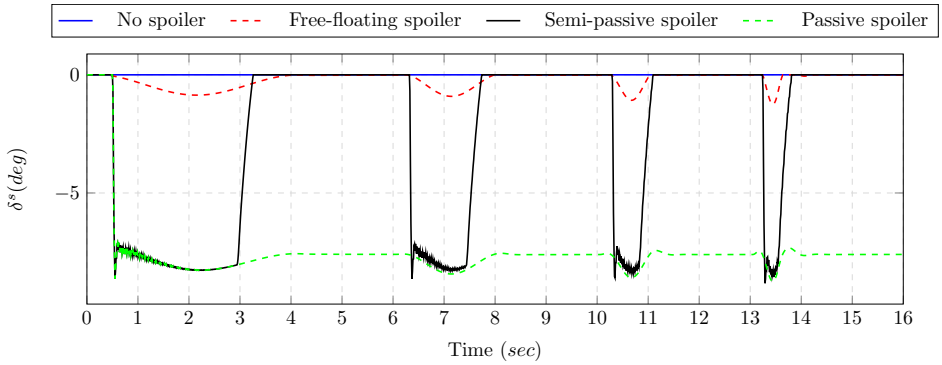

Figure 2.12: Spoiler deflection after four gust inputs.

Figure 2.12 highlights the effect of the actuator on the spoiler motion. If no actuator is used, the spoiler will stay deflected. On the other hand, if no spring is installed to help the spoiler to deflect, only a small deployment angle is reached, with limited effect on the lift (about 1% load reduction). While requiring an actuator, a semi-passive system would also conserve the other capabilities of the spoiler for brake and roll, and would render this device truly multipurpose. The feasibility of having magnets on a real aircraft wing also needs to be assessed; however other solutions such as bi-stable laminates could be used for the same purpose.

2.3 CONCLUSION

In this section, an innovative solution for a passively actuated spoiler for loads alleviation is presented. This device relies on the use of linear pre-loaded springs and magnets. The main advantage of this combination is to allow a quick passive automatic deployment of the spoiler to mitigate the loads efficiently with little delay and no control logic involved. Within Matlab/Simulink, a model that fea-

tures a two-dimensional airfoil is equipped with a spoiler and is subjected to gust disturbances. This airfoil can also pitch and plunge. The aerodynamic behaviour of the spoiler is determined using transfer functions from high-fidelity CFD simulations. Results based on the developed model show that in order to function properly, the spoiler needs to be retracted actively. Nonetheless, the present system can react to gust loads passively and achieve up to 9% load reduction on the 2D section. In the next section, we extend the control surface aerodynamic identification methodology to the transonic regime.

3

NON-LINEAR UNSTEADY AERODYNAMIC REDUCED ORDER MODEL FOR CONTROL SURFACES

Most modern airliners fly within the transonic regime and this can potentially have implications for the performance and aerodynamic effectiveness of the wing control surfaces. As illustrated in Figure 1.3, aerodynamic non-linearities can appear due to the shock motion on the top of the wing and the flow separation around the control surface hinge. This means that the evaluation of the control surfaces effectiveness for roll, pitch, yaw or load alleviation cannot solely rely on linear aerodynamic models which do not capture transonic and viscous effects. Therefore the characterisation of control surfaces aerodynamic capabilities must be done through flight testing (Biannic et al., 2016; Boely et al., 2009), wind tunnel testing (Fillola, 2006), RANS-CFD (Bertrand, 2008) and higher-order aerodynamic simulation methods (Deck et al., 2014; Gand, 2013).

While flight and wind tunnel testing are expensive and require months of preparation, numerical approaches also present several difficulties. The first is the computational time required to solve Navier-Stokes equations. Transient CFD analysis requires numerous time steps to converge, and a few seconds of simulation time may easily take hours to simulate on a high-performance computer. This is not compatible with requirements from loads and handling qualities disciplines,

which necessitate up to several thousand flight points to be covered, yielding to hundreds of virtual flight test hours that must be simulated. The second problem is how to cope with mesh deformation along with the deflection of the control surface. CFD cells can easily get crushed and distorted during control surfaces dynamic simulations, as illustrated in Figure 3.1. Distorted elements can lead to numerical errors resulting in erroneous values or crashes of the solution. Chimera meshing techniques (Blanc et al., 2009) can help bypass this issue but are also very expensive in labour cost as the construction of such meshes is not yet automated. Chimera meshing is also not available to all CFD solvers.

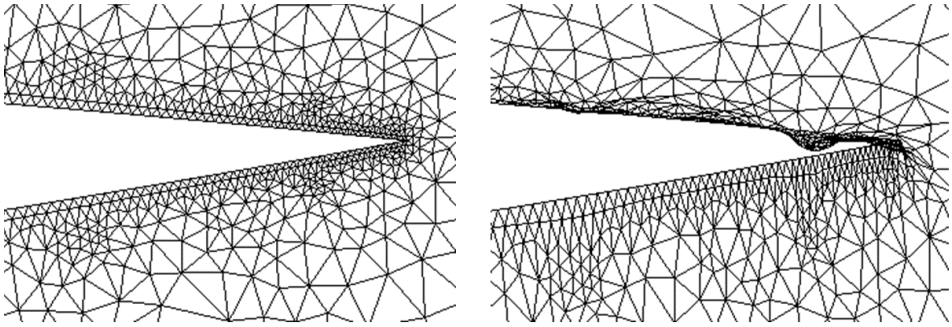

Figure 3.1: Illustration of crushed CFD cells, reproduced from Ansys Fluent User Guide (Ansys, 2009a).

Therefore, in this chapter[1], we introduce a non-linear unsteady aerodynamic model for control surfaces. This model does not require a complex CFD setup as it only relies on small disturbance dynamic simulations and static simulations for the model identification. Conventional mesh smoothing techniques are sufficient to handle small control rotations (in the order of a few degrees) on 2D or 3D cases, while static simulations can be re-meshed directly to tackle large control surface rotations with no limitation on the deflection angle. For this chapter, we focus on a simplified 2D transonic aileron case. The ROM is also compared against a linearized model and a quasi-steady model.

[1]This chapter is based on parts of the journal paper Lancelot, P., De Breuker, R. (2021). "Unsteady Non-linear Control Surface Modelling for Aeroservoelastic Applications". *Journal of Aeroelasticity and Structural Dynamics.*

3.1 METHODOLOGY

The modelling strategy we describe proposes to separately identify the incremental non-linear steady aerodynamic contribution of the control surface deflection, ΔQ_{cs}, and the linear unsteady contribution, ΔQ_{cu}. We sum these two components to obtain the full load increment value, ΔQ_c, as shown in Equation 3.1:

$$\Delta Q_c = \Delta Q_{cs} + \Delta Q_{cu} \tag{3.1}$$

We define the load increment as the variation in force and moment over the wing caused by the control surface arbitrary deflection δ_c. This is summarized in Equation 3.2 and is used for the steady and transient analyses.

$$\Delta Q_c = \begin{pmatrix} \Delta F_x \\ \Delta F_y \\ \Delta F_z \\ \Delta M_x \\ \Delta M_y \\ \Delta M_z \end{pmatrix} = \begin{pmatrix} F_x - F_x(\delta_c = 0) \\ F_y - F_y(\delta_c = 0) \\ F_z - F_z(\delta_c = 0) \\ M_x - F_x(\delta_c = 0) \\ M_y - F_y(\delta_c = 0) \\ M_z - F_z(\delta_c = 0) \end{pmatrix} \tag{3.2}$$

When looking at control surfaces, a non-linear steady aerodynamic behaviour can be characterised by a non-linear relation between the deflection angle and the resulting incremental lift and moment. We show an example of this relation in Figure 3.7. This can be identified using steady-state CFD simulations for a range of movable settings. The resulting loads can be stored in look-up tables, as illustrated in Figure 3.2 and noted as ΔQ_{cs}. Such simulations are much faster to compute than transient CFD solutions and do not require dynamic mesh deformation. Therefore, this approach can be easily scaled to include multiple flight points and configurations. This method is not restricted to RANS-CFD, and wind tunnel results or high-order methods could be used instead to create the steady aerodynamic database.

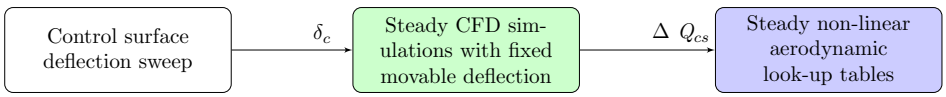

Figure 3.2: Steady aerodynamic modelling to capture large control surface deflection responses.

The unsteady effects around control surfaces are the changes in aerodynamic phase lag and amplitude due to the frequency of actuation. They can be captured using transfer functions derived from unsteady CFD analysis. To avoid any excessive grid distortion, we are performing the analysis with small deflection

angles. The accuracy of this approach for linear aerodynamic response is already demonstrated in Chapter 2.

The variable $\delta_c(t)$ is an arbitrary deflection command for the control surface given in the time domain. $\Delta Q_{cu}(t)$ is the incremental unsteady load response due to a dynamic surface deflection. We obtain $\Delta Q_{cu}(t)$ by removing the quasi-steady non-linear component $\Delta Q_{cs}(t)$ from the control load increment $\Delta Q_c(t)$. This operation is shown in Figure 3.3 and is required because the transfer function used is only valid for approximating linear time-invariant systems.

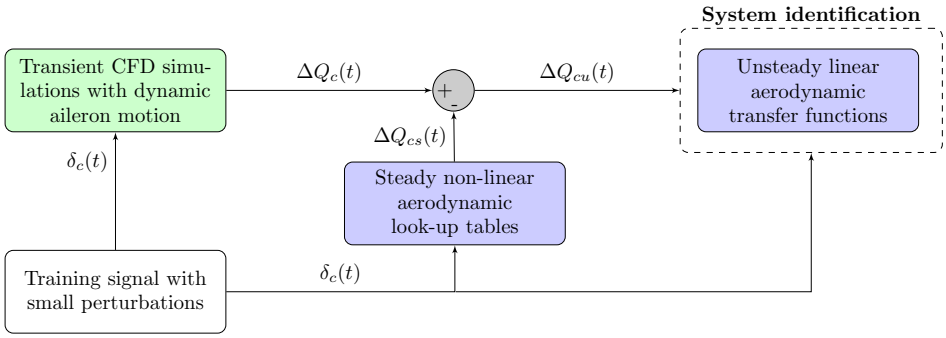

Figure 3.3: Transfer functions identification procedure.

Following the process shown in Figure 3.4, we combine the results produced by the look-up tables and the transfer functions to capture the full response. We run our ROM using the Matlab/Simulink platform (MathWorks, 2020b) which handles both time and frequency domains.

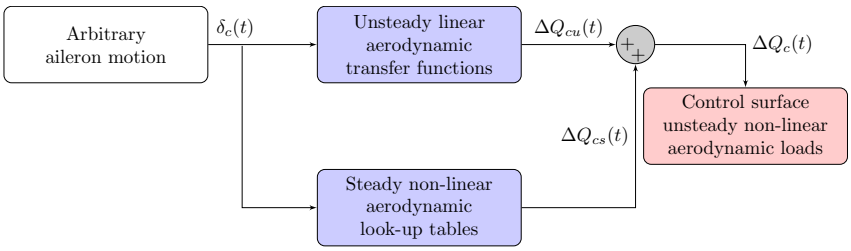

Figure 3.4: The unsteady non-linear aerodynamic ROM is comprised of the look-up tables and the transfer functions.

3.2 Application to a 2D case with the OAT15A airfoil

In this section, we assess the accuracy of the hybrid unsteady non-linear aerodynamic model on a 2D example.

3.2.1 Validation of the steady CFD setup

To assess the validity of the modelling approach presented in Section 3.1, we are doing the aerodynamic identification using the Onera OAT15A airfoil equipped with an aileron. The airfoil geometry is shown in Figures 3.5 and 3.6 on the left. We perform CFD using Ansys Fluent with a RANS K-ω SST turbulence model (Ansys, 2009b). Steady wind tunnel results for this airfoil are used as validation using the conditions described by Fillola (2006). The airfoil angle of attack is set at 1.5 degrees, the aileron is deflected down by +6 degrees and up by -3 degrees, and the Mach number is Mach 0.73. When the aileron is at +6 degrees, the transonic shock materialises as a sudden increase in pressure at 0.55 chord length on the airfoil, as shown in Figure 3.5 on the right. On the contrary, when the aileron is up, the pressure distribution is a lot smoother as the negtaive aileron deflection reduces the overall lift and mitigates the creation of a transonic shock. We see a very good agreement between the CFD results and the experiment in Figure 3.5 while the match is satisfactory in Figure 3.6 with a slight error on the pressure increase at 0.15 chord length.

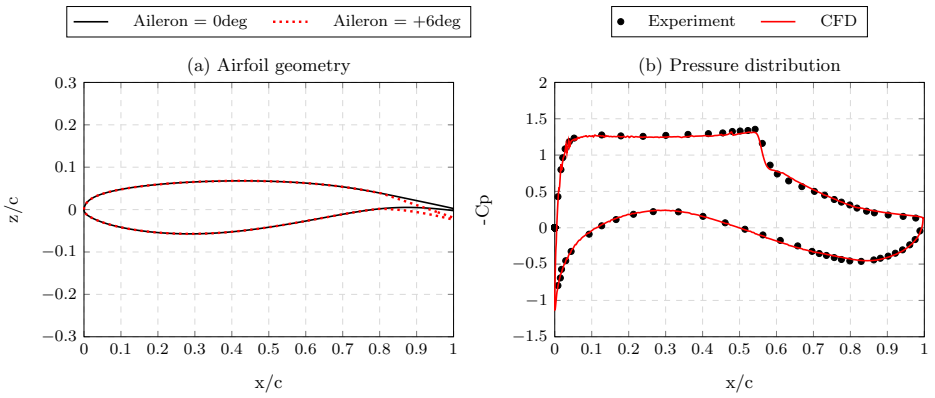

Figure 3.5: In (a) is the OAT15A airfoil geometry and in (b) the pressure distribution with the aileron deflected at +6 degrees.

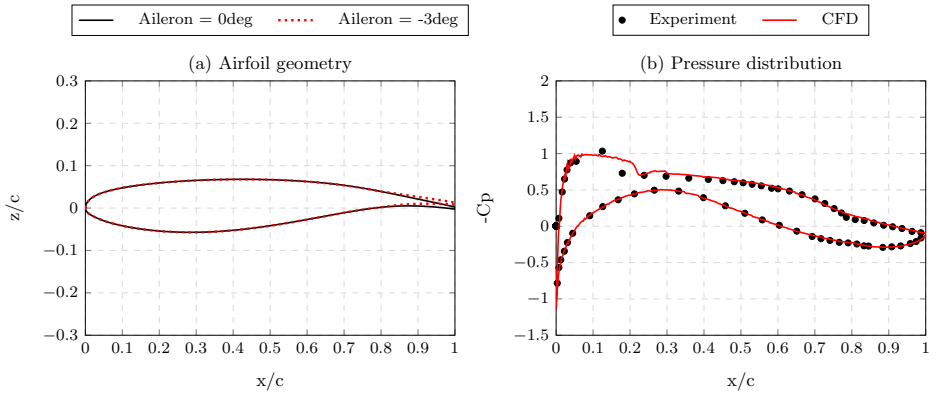

Figure 3.6: In (a) is the OAT15A airfoil geometry and in (b) the pressure distribution with the aileron deflected at -3 degrees.

3.2.2 IDENTIFYING THE AILERON ROM

For the subsequent study, we use a 20 times scaled-up version of the original OAT15A airfoil geometry, increasing its chord length from 15cm to 300cm. A scale-up is required to maintain the aileron actuation speed and reduced frequency consistent with a full-scale aircraft wing while preserving the Mach number of Mach 0.73. The definition of the reduced frequency k is given in Equation 3.3, where ω is the circular frequency of the control surface deflection, b is the airfoil semi-chord and v_∞ the flow velocity.

$$k = \frac{\omega b}{v_\infty} \tag{3.3}$$

The static aileron sweep in Figure 3.7 highlights the non-linearity of the lift increment. This can be explained by the shock position moving downstream when the aileron is deflected down, as shown in Figure 3.8. The linear region in Figure 3.7 is sustained longer for high negative deflection angles due to the shock being mitigated on the upper surface of the wing when the aileron is deflected up. Similar observations were already made by Fillola (2006) and are illustrated in Figure 1.3 in Chapter 1.

We describe the four steps to create the aerodynamic ROM as follows:

1. We first perform a dynamic CFD simulation, where the aileron deflection is driven by a square command $\delta_c(t)$ varying from -2.5 degrees to +2.5 degrees as shown in Figure 3.9 (a). Small amplitudes make it easier to handle mesh deformation for the CFD solver with a smoothing deformation technique (Ansys, 2009a), as the overset grid capabilities of Ansys Fluent

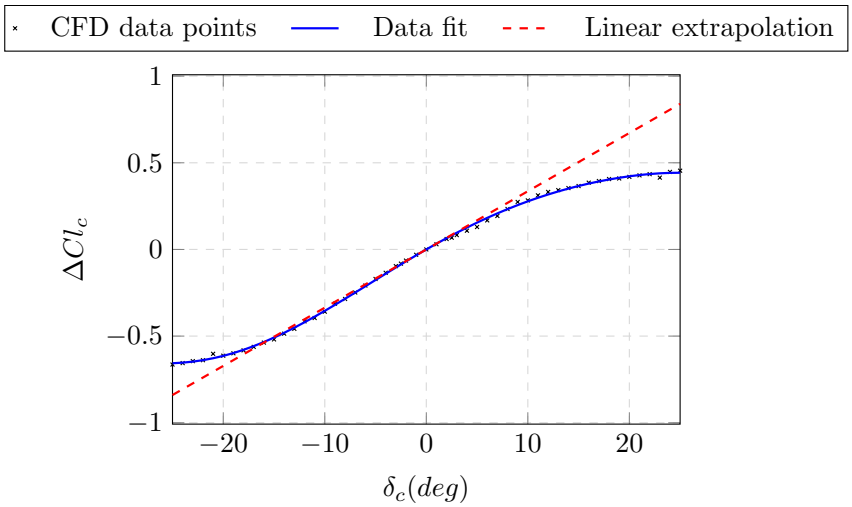

Figure 3.7: Lift coefficient increment from -25 to +25 degrees aileron deflection. The fitted data is used for the look-up table in the aerodynamic ROM. The linear extrapolation is performed around the neutral aileron deflection.

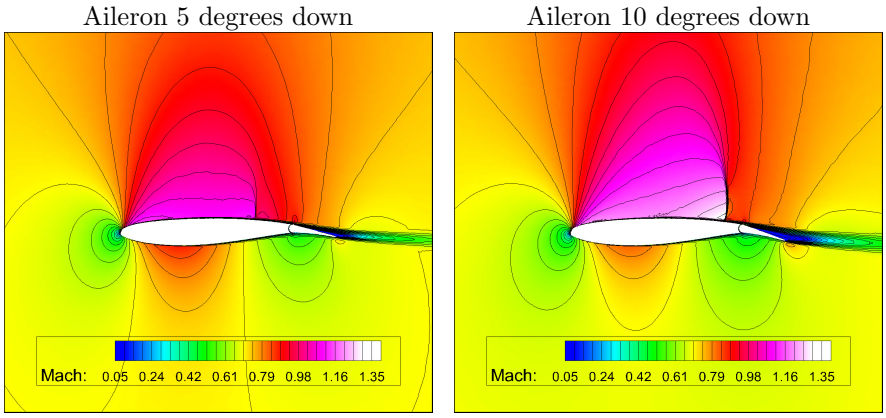

Figure 3.8: Mach flow contours around the airfoil with AoA = 0deg. The shock moves to the rear as the aileron is deflecting.

remain limited for transonic flow conditions. The resulting incremental lift $\Delta Cl_c(t)$ from the aileron motion is plotted in Figure 3.9 (d).

2. We create a non-linear quasi-steady lift response $\Delta Cl_{cs}(t)$ from the aileron command using the look-up tables, plotted in Figure 3.9 (b). The process to create the look-up tables is shown in Figure 3.2, and only requires steady-state CFD analysis. In this example, the aerodynamic database is comprised of 53 simulation results ranging from -25 degrees to +25 degrees aileron deflection angles.

3. The non-linear quasi-steady lift response $\Delta Cl_{cs}(t)$ is subtracted from the transient CFD response $\Delta Cl_c(t)$ to extract the unsteady lift component $\Delta Cl_{cu}(t)$ from the aileron motion. We show this operation in Figure 3.3. By doing so, we make sure to perform the transfer function identification over a linear signal. The identification process for a linear signal is explained in Section 2.1.2. In Figure 3.9 (c), we see a very good match, within 1% error, between the transfer function and the training data obtained from CFD.

4. We recompose the full response $\Delta Cl_c(t)$ by summing the non-linear quasi-steady lift increment $\Delta Cl_{cs}(t)$ with the linear unsteady lift increment $\Delta Cl_{cu}(t)$, as depicted in Figure 3.4. We observe from the comparison with the CFD in Figure 3.9 (d) a small error of only 1%. While the amplitude of the deflection signal is moderate, we can already notice some non-linearity on how the lift increment is not exactly proportional to the deflection angle. Along with the unsteadiness, this effect is well captured using the steady look-up tables.

3.2.3 COMPARISON AGAINST UNSTEADY CFD FOR A RANGE OF AMPLITUDES AND FREQUENCIES OF AILERON OSCILLATION

The model described above is evaluated on signals varying from ± 1 to ± 15 degrees of deflection and from 0.5 Hz to 8.0 Hz in frequency. Such deflection amplitude is typical for an aileron (Bertrand, 2008; Sensburg et al., 1982). We show the results against the CFD responses in Figure 3.10. Overall, the model gives good prediction for aileron deflection rates up to 60 deg/sec. This rate is considered to be practical for active load alleviation, as shown by Pusch et al. (2019). Furthermore, motions with high deflection amplitudes but moderate frequencies are also well captured.

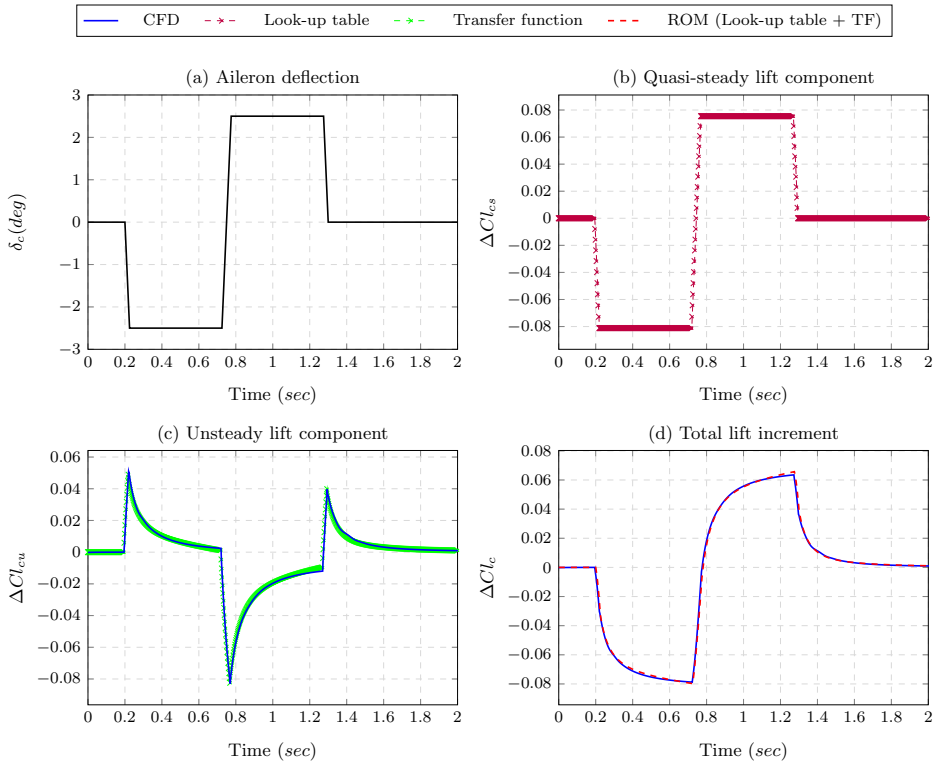

Figure 3.9: Unsteady non-linear lift increment modelling components.

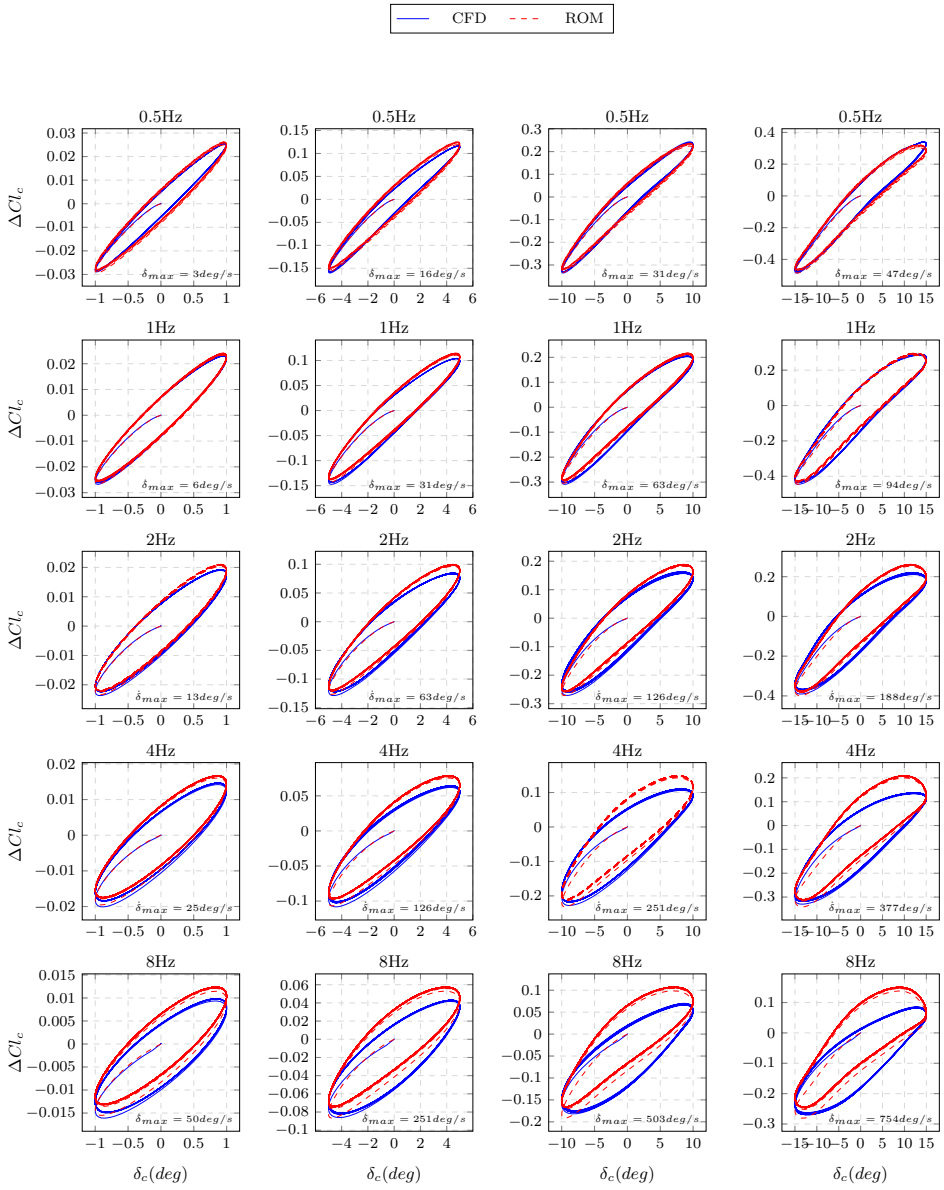

Figure 3.10: Dynamic aileron lift increment plotted against the deflection angle for different amplitudes and frequencies of actuation.

In Figure 3.11, we select a few cases where we also show the comparison against the non-linear quasi-steady and linearized unsteady models. We see that the quasi-steady model gives results which are too optimistic in terms of lift increment

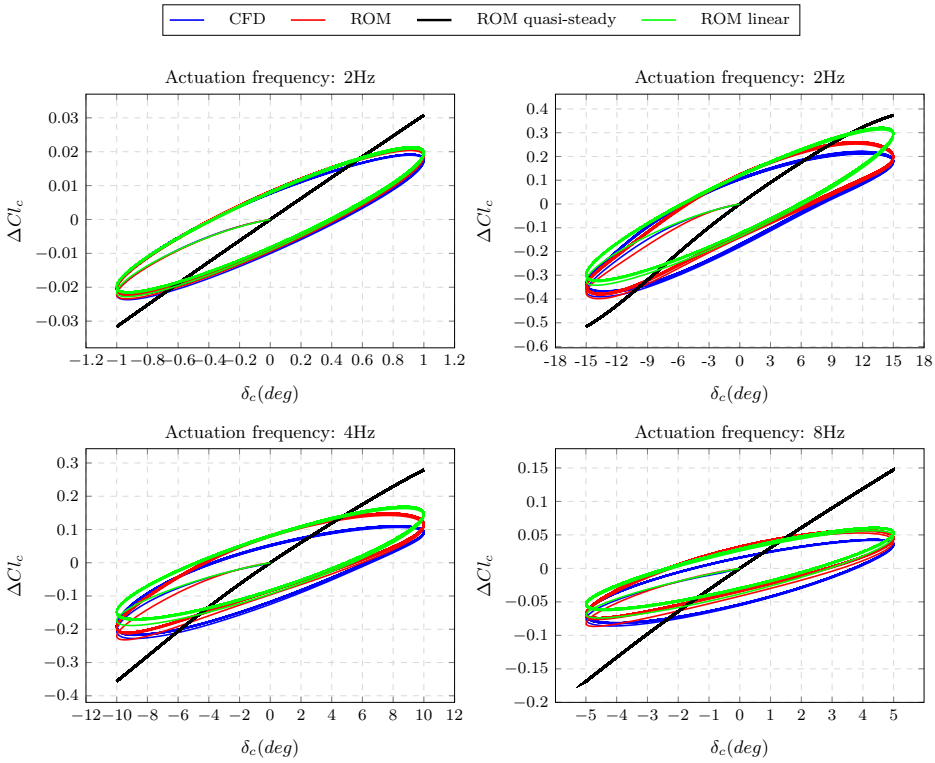

Figure 3.11: Dynamic aileron lift increment plotted against the deflection angle for a selected set of amplitudes and frequencies of actuation.

and do not account for the phase shift, as shown by the lack of hysteresis in the response. The linearized model gives closer results to our ROM for small deflections but loses in accuracy for higher deflection amplitude by also being too optimistic.

3.3 Conclusion

In this chapter, we have introduced a data-driven method to capture the unsteady non-linear incremental loads from arbitrary aileron motion. For a given device, Mach number and dynamic pressure, we perform several steady-state CFD analyses with a range of rotation angles to fill look-up tables capturing the steady non-linear aerodynamic behaviour of the control surface. We then perform a single transient CFD analysis with small control deflections to capture the unsteady effects. This approach makes it possible to use standard dynamic smooth-

ing deformation techniques without risk of stretching the mesh excessively. Before identifying the transfer functions, we remove the steady aerodynamic component of the transient CFD response from the training data using the look-up tables. We do this to perform the transfer functions identification on the unsteady linear aerodynamic component of the control response. Finally, we sum up the unsteady linear and steady non-linear aerodynamic contributions to restitute the complete control loads. We compared the results given by our model against transient CFD-RANS analyses for a wide range of deflection rates and amplitudes. Results showed that for most of the realistic rate/amplitude combinations, our method was effective to replicate CFD results, predicting the lift increment within a 5% error margin. Our model also showed a better prediction than linearized or quasi-steady approximations.

4

STEADY AERODYNAMIC LOAD CORRECTION AND MANOEUVRE LOAD ALLEVIATION

The standard load analysis procedures that rely on aerodynamic panel methods have limitations as highlighted in the recent work from Dillinger (2014), Voß (2019) Jovanov (2019) and Crovato et al. (2020). Using linear potential flow methods often yields a conservative estimate of wing loading during manoeuvres because stall is not accounted for. However, this can also lead to an overestimation of the control surface effectiveness because non-linear aerodynamic effects such as transonic shock and flow separation over the control surfaces are ignored. This produces an over-optimistic assessment of the benefit of using MLA in terms of optimised wing structural weight.

The DLM is one of the most widely used panel methods in academia and industry. It was introduced by Albano and Rodden (1969) to be used in a large number of aeroelasticity problems, including static and dynamic loads, divergence, control effectiveness and flutter. It is included in MSC NASTRAN and despite being able to account for the flow compressibility (Johnson and Rodden, 1994), this method remains essentially linear. To illustrate this, we show in Figure 4.1 the pressure difference on the wing surface obtained at Mach 0.85 produced by DLM and the RANS-CFD analysis. Both simulations are trimmed to achieve the same total lift. The location of the shock-wave on the RANS-CFD results is visible while

being absent on the DLM plot. This creates different aerodynamic loading on the wing based on the type of aerodynamic model used and therefore also impacts the wing sizing.

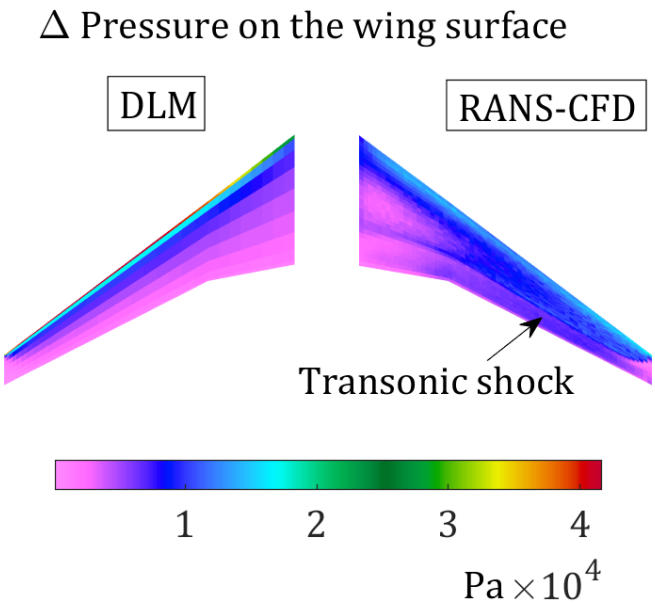

Figure 4.1: Pressure gradient on the wing surface in the transonic flow condition (Mach 0.85). The CFD results are re-projected onto a coarser mesh to compute the pressure difference between the two sides of the wing.

In Chapter 1, we presented several approaches that are already available for load corrections, but none of them suit every application. Recently, MSC Software implemented the Hybrid Static Approach (HSA) in NASTRAN (Bosco et al., 2016; Vincenzo and Castrichini, 2013) which replaces the rigid aerodynamic contribution of the wing with higher-order CFD results stored in a database. In this chapter, we describe and benchmark this method.

4.1 HYBRID STATIC APPROACH

The static aeroelastic equation of motion is shown below in Equation 4.1:

$$[K - q_\infty Q_e]u + [M]\ddot{u} = q_\infty Q_r(\alpha) + P(\delta) \tag{4.1}$$

With K being the structural stiffness matrix, M the structural mass matrix, q_∞ the dynamic pressure, u the nodal displacements, P the externally applied loads and Q_e and Q_r the flexible and rigid aerodynamic matrices. P, Q_e and Q_r can be scaled with the dynamic pressure. Q_e brings the influence of the elastic deformation of the wing on the loads, as illustrated in Figure 4.2. The wing flexibility generally leads to a reduction of the lift slope curve thanks to the washout effects of backward swept wings (Weisshaar, 1995). Conversely, Q_r is a function of the aircraft trim variables such as the angle of attack α. With the HSA method, Q_r is built from an external aerodynamic database, obtained with a higher-order method, while the Q_e relies on the DLM aerodynamic panels.

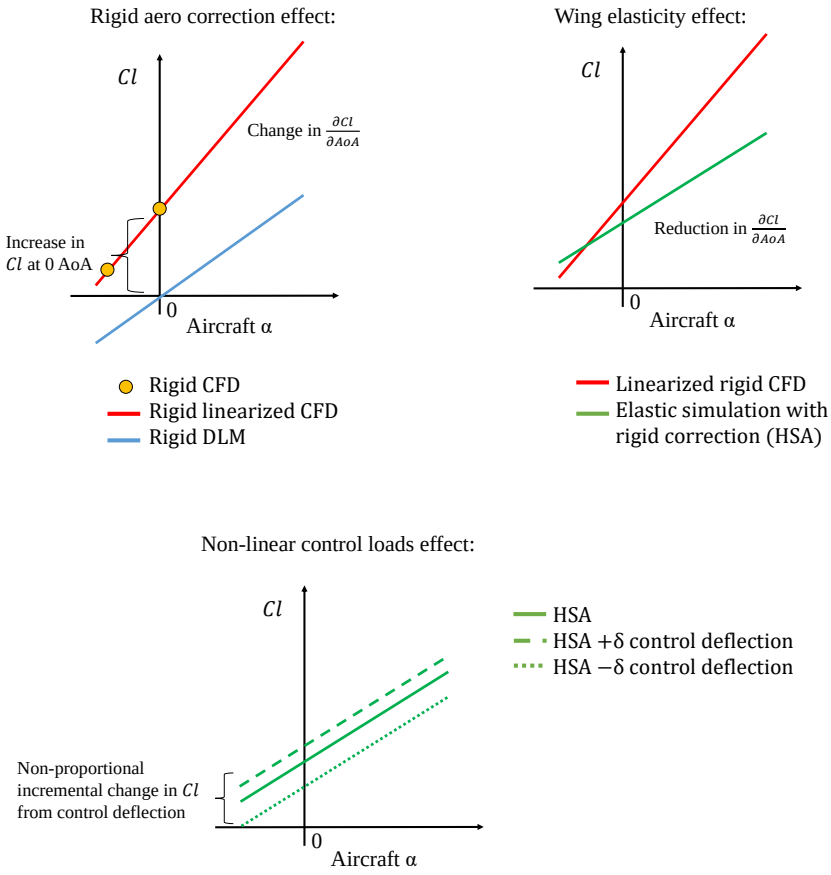

Figure 4.2: Illustration of the effect of rigid aerodynamic corrections, wing flexibility and control surface loads on the lift.

In our case, for a given Mach number, the aerodynamic database is obtained

from two rigid RANS-CFD analyses at -1 and 0 degrees AoA as illustrated in Figure 4.2. These two points are extrapolated for higher AoA. This method is an aerodynamic loads correction to account for the wing camber and transonic shock effects on the lift slope and 0 degrees AoA lift value. It is only valid for attached flow conditions.
The incremental control surface loads are obtained from RANS-CFD analyses as well. We restrict our study to flight conditions at which the incidence effect on the control loads can be neglected and below the aircraft AoA at which the buffet occurs. Therefore, during the aeroelastic analysis, the aerodynamic control loads are solely a function of the control deflection δ and can be considered as externally applied loads. These loads can be the resultant of flow simulations including flow separation or interaction with the transonic shock over the wing surface, creating a non-linear relation between the control deflection and the incremental loads, as shown in Figure 3.7 and illustrated further in Figure 4.2.

4.2 APPLICATION TO AN AIRCRAFT MODEL

To test the HSA method, we use the undeformed common reference model (uCRM) developed from the NASA CRM by Brooks et al. (2018). With this geometry, we create two aerodynamic models: one low fidelity to capture the elastic flexible loads with DLM and one to perform RANS-CFD analysis to derive the rigid aerodynamic database. The latter is also used for the FSI simulations for validation of the HSA method. Both models are shown in Figure 4.3. The DLM aerodynamic mesh is created from four CAERO1 cards (MSC Software Corporation, 2019), which all define a trapezoid shaped region of the aircraft half-planform. Two are used for the wing because it is not possible to model the Yehudi break (kink in the wing trailing edge) with a single CAERO1 card.

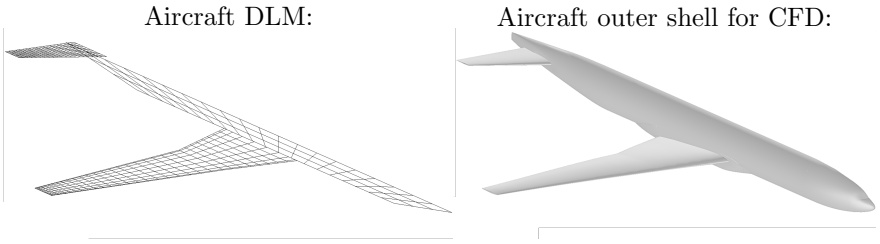

Figure 4.3: CRM aerodynamic representations.

To investigate the effectiveness of using the HSA method with control surfaces, we have modified the uCRM geometry to include an aileron and a spoiler as depicted in Figure 4.4.

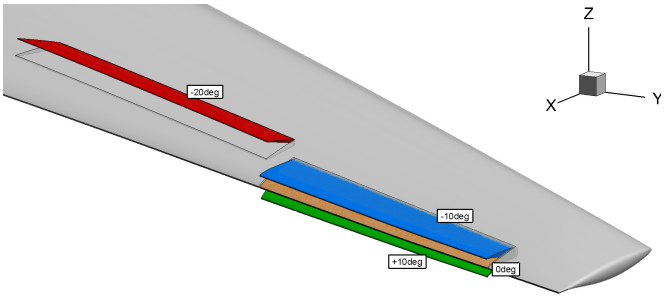

Figure 4.4: uCRM wing model fitted with an aileron and a spoiler.

4.3 FLUID-STRUCTURE INTERACTION FRAMEWORK

To validate the HSA method, we rely on a FSI framework which couples a structure solver with an aerodynamic solver for static aeroelastic analysis. We use MSC NASTRAN SOL101 (MSC Software Corporation, 2012b), a linear structure solver, to compute the elastic deformation of the wing. ANSYS FLUENT is used again for the CFD. The fluid domain mesh has 15 millions cells and we use the K-ω SST turbulence model (Ansys, 2009b).

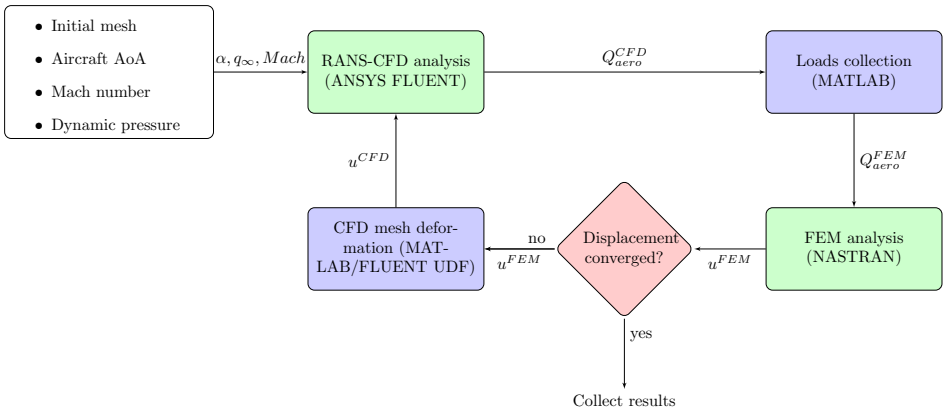

Figure 4.5: Iterative FSI workflow, which allows computing of the static aeroelastic response of the wing.

The framework is illustrated in Figure 4.5. The coupling is achieved with a MATLAB script that controls the sequential execution of both ANSYS FLUENT and MSC NASTRAN. The CFD analysis is performed first. Then, the aerodynamic loads are integrated on the FEM model degrees of freedom using

a nearest-neighbour algorithm (MathWorks, 2020a). Once the FEM analysis is completed, the resulting displacements are extracted. These displacements are applied to the CFD mesh so that a new aerodynamic analysis can start. This cycle runs until the lift value falls below the convergence tolerance of 0.1% error between the current and the previous iterations. Convergence is reached within 7 to 10 cycles, which takes up to two hours of simulation time on a 32 cores Intel CPU machine clocked at 2.3Ghz. For comparison, a static equilibrium can be reached within five seconds using the HSA approach and MSC NASTRAN. The two rigid CFD solutions to generate the HSA aerodynamic database takes 30 minutes on the same computing setup, however multiple subsequent analyses with different wing flexibility or AoA can then be performed with little additional computing cost. In Figure 4.6, we show the result of the coupling between the structural FEM and the external surface of the wing.

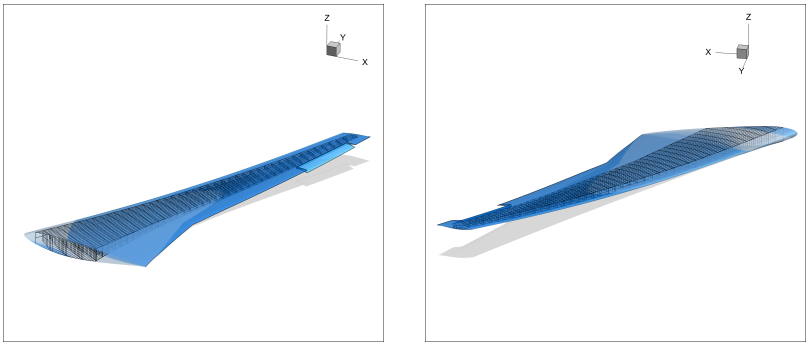

Figure 4.6: The CRM deformed structural FEM model overlayed with the resulting deformed aerodynamic wing shape, from two different angles. The grey shade indicates the undeformed wing shape. The wing is clamped at the root.

4.4 COMPARISON BETWEEN FSI AND HSA

We looked at two different wing stiffness behaviours as shown in Table 4.1. This range is conform to modern airliners in service today (Sensburg et al., 1982). While wing A and B have the same mass properties, wing B has a wing material stiffness twice lower than wing A, which allows a higher wing deformation as highlighted in Figure 4.7.

Table 4.1: Frequencies in Hz of the two models.

mode	wing A	wing B
1^{st}	2.96	2.09
2^{nd}	7.53	5.32
3^{rd}	8.34	5.90
4^{th}	13.08	9.25

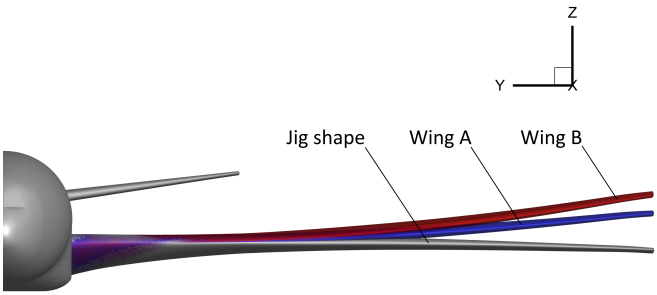

Figure 4.7: Wing A and wing B aeroelastic deformation calculated using the FSI scheme. The aircraft is trimmed at 2 degrees AoA with a dynamic pressure of 11,100Pa at Mach 0.85.

In Figure 4.8, we have the results with the stiffer wing A and without control surfaces. The dynamic pressure is set to 11,100Pa at Mach 0.85, which is a typical cruise speed for an airliner. We compare four sets of results: FSI, HSA, DLM and rigid CFD. FSI results are produced with the setup described in Section 4.3. Corrections needed by the HSA are also evaluated on the same CFD setup.

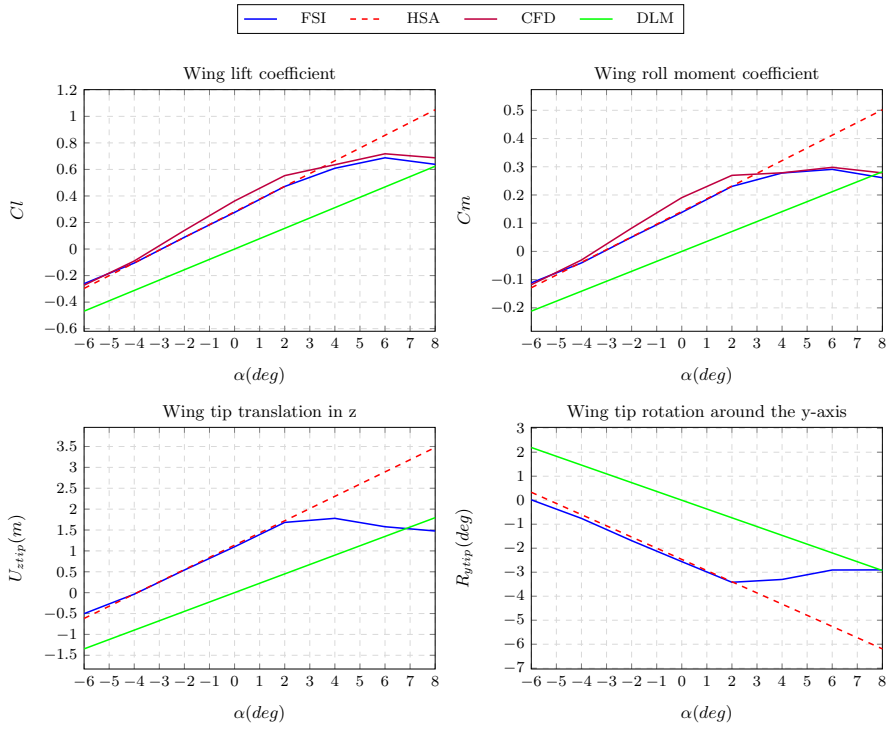

Figure 4.8: Lift, moment and tip displacements for various angles of attack obtained with the FSI, rigid CFD, HSA and pure DLM methods for the wing A at 11,100Pa Mach 0.85.

If we recall Figure 4.2, the first thing to establish is that despite the use of an aerodynamic database from CFD results, the response given by the HSA method is linearized between two points. These points are obtained at -1 and 0 degrees AoA with the same dynamic pressure and Mach number. In this case the HSA does not predict stall. The possibility to build the external database from CFD results closer to the stall point is possible, but not investigated in this thesis. The main goal for these load corrections is to be used for sizing.
Despite this, the HSA and the FSI give comparable results in the linear region for all metrics while the pure DLM is quite off. This is explained by the lack of airfoil camber of the DLM model (hence the mismatch at the 0 degrees AoA lift coefficient) and the impossibility to model the transonic shock on the wing surface.
Rigid CFD has the least linear aerodynamic behaviour of all. In contrast, flexible simulations tend to have a more linear behaviour. When the wing deflects, the natural bend-twist coupling of a back-swept wing induces a rotation of the wing tip, also known as wash-out (Weisshaar, 1995). As the wing tip rotates, a reduction of the local AoA occurs which delays stall and flow separation as illustrated in Figure 4.9. This has been observed by Tinoco (2008) along with Schewe and Mai (2018) in their respective studies.

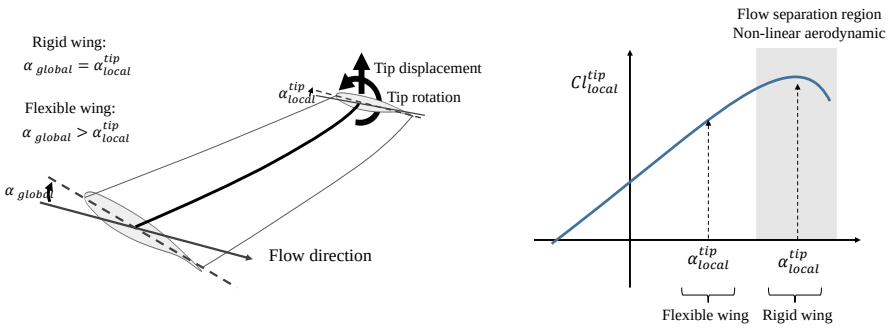

Figure 4.9: Wash-out induced by structural bend-twist coupling and its effect on the local aerodynamic behaviour of the wing.

We show the effect of varying the wing flexibility and the dynamic pressure on the wing response in Figure 4.10. The HSA correction is derived from the same two rigid CFD simulations performed at 11,100Pa and Mach 0.85 from Figure 4.8. In Figure 4.10, the Mach number remains constant but we have to adjust the dynamic pressure term q_∞ from Equation 4.1. This will in turn scale both rigid and flexible aerodynamic matrices Q_r and Q_e. We recall that Q_r is effectively what we refer to as the rigid component HSA database.
The increase in flexibility and dynamic pressure lead to the same reduction in lift coefficient but a higher wing deflection. This is well accounted for by the flexible

component of the HSA method (Q_r). Whereas the stall is initiated at 2 degrees AoA for the most rigid case (wing A at 11,100Pa), it is delayed to 4 degrees AoA for the most flexible scenario (wing B at 16,500Pa).

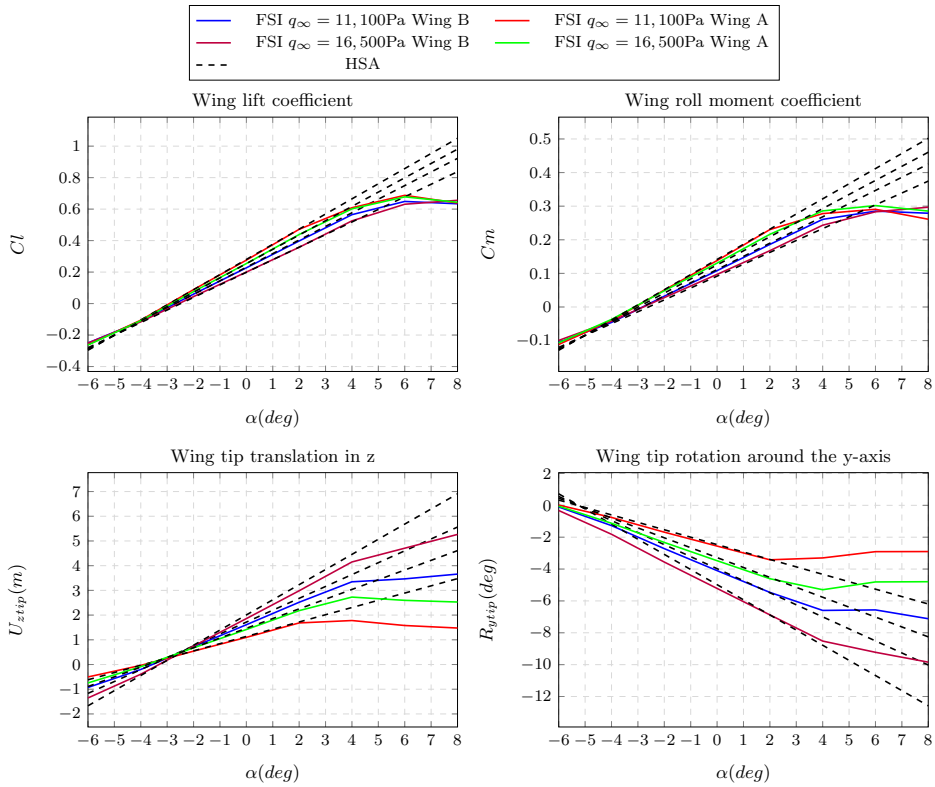

Figure 4.10: Lift, moment and tip displacements for various angles of attack obtained with the FSI and HSA methods for the two wing models at two different speeds.

For the following comparisons, we look at the spanwise lift distribution. This is one of the main parameters when looking at the wing loading. In Figure 4.11 we first take the results with the least flexible wing (model A) at the dynamic pressure of 11,100Pa. The lift is normalized with respect to the total wing surface area. For the DLM solution, we trim the NASTRAN SOL144 analysis (Johnson and Rodden, 1994) to make the comparison against FSI based on equal lift rather than equal angle of attack. Otherwise, the DLM results would be too off because of the lack of camber modelling with this approach. The FSI, CFD and HSA on the other hand are set to the same angle of attack. Additionally, we show the rigid HSA lift component which is obtained from the CFD database. The

flexible lift component of the HSA obtained from the DLM is shown as well. Both contributions are summed up to obtain the actual HSA prediction.

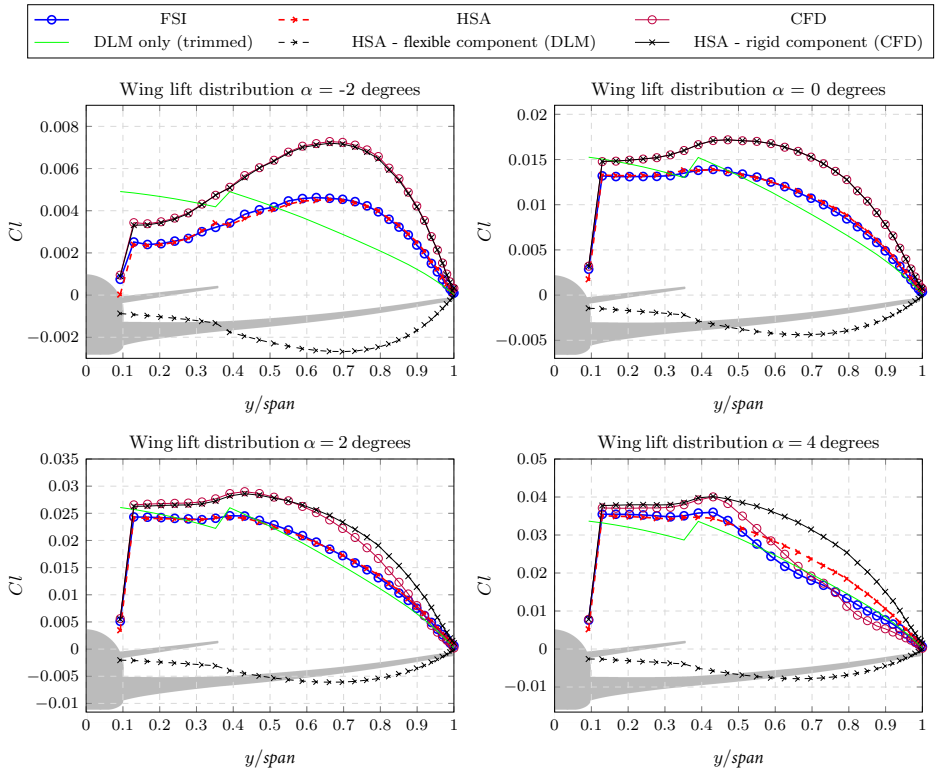

Figure 4.11: Normalized lift distribution span-wise for various angles of attack obtained with the FSI, rigid CFD, HSA and pure DLM methods for the wing A at 11,100Pa Mach 0.85.

We see that for -2 and 0 degrees AoA, the FSI and HSA are in good agreement, with an average error below 2%. Furthermore, at -2 degrees, the rigid CFD and the rigid HSA, which are extrapolated from the stored aerodynamic database, are matching too. At 2 degrees AoA, the CFD and rigid HSA start to have divergent results, as the extrapolation breaks down near the wingtip. The FSI and HSA remain close (less than a 2% error) at this AoA thanks to the wing flexibility, which prevents the wingtip from stalling due to the wing washout effect. At 4 degrees AoA, the lift drops further from the outboard part of the wing on both the rigid CFD and the FSI computations. This is most likely due to local flow separations and buffet, which can occur even at a moderate AoA in the transonic regime (Belesiotis-Kataras and Timme, 2018; Giannelis et al., 2018). These phenomenons are outside the scope of the thesis and are not accounted for by the rigid aerodynamic database of the HSA. This leads to an overestimation of the

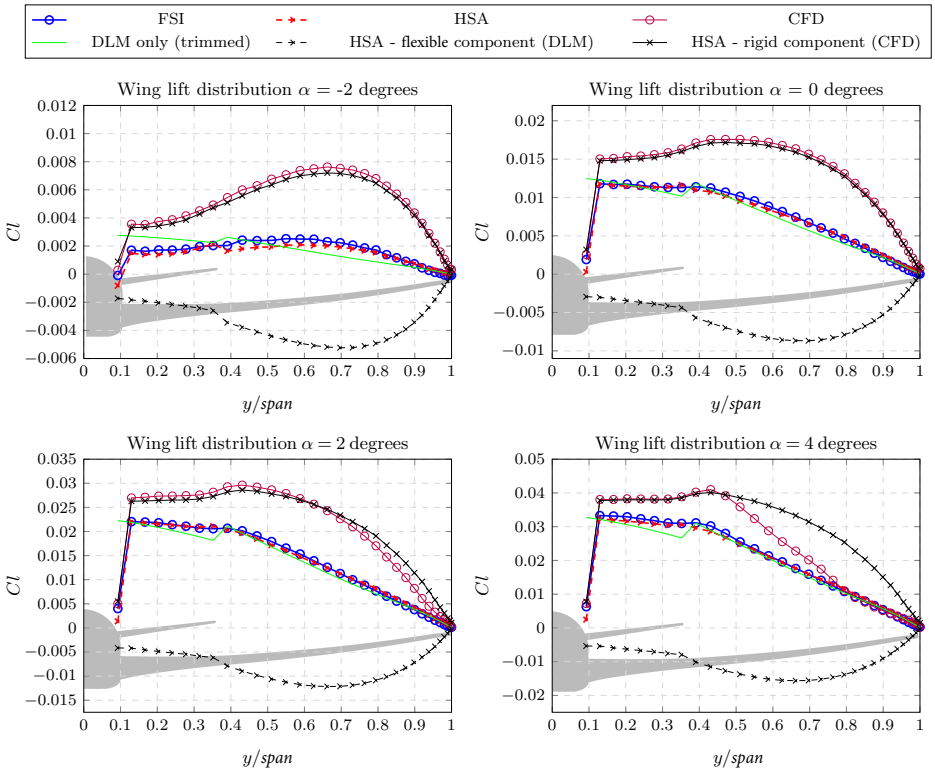

Figure 4.12: Lift distribution span-wise for various angles of attack obtained with the FSI, rigid CFD, HSA and pure DLM methods for the wing B at 16,500Pa Mach 0.85.

lift outboard from the HSA method.
The HSA aerodynamic flexible component is directly a function of the wing flexibility. It increases negatively after the Yehudi break at around 0.35 of the semi-span as a result of washout. The discontinuity in the DLM lift distribution at the Yehudi break is because of a small mismatch in displacements between the two aerodynamic CAERO panels which form the full wing surface.
Despite being trimmed, DLM gives completely off results from -2 to 2 degrees AoA, with a lift distribution which is too much inboard. This is due to the lack of twist and camber on the DLM model. Interestingly, the DLM accuracy improves when the lift from FSI starts to diminish near the wingtip due to stall. This is mostly a coincidence however, as the DLM cannot predict stall.

We now compare the HSA and FSI lift distribution on the wing model B, which is more flexible. These simulations are performed at 16,500Pa to further exacerbate the aeroelastic effects.

The results in Figure 4.12 show that the rigid CFD and HSA rigid components follow the same behaviour as with the wing model A, with a difference in lift emerging at 2 degrees AoA. Nonetheless, both FSI and HSA are in good agreement with less than a 3% error in average. The drop in lift near the wing root is also well captured by the HSA method and match the FSI results. We can see an increase in the negative lift coefficient from the HSA flexible component which correspond to the lower total Cl seen in Figure 4.10 at iso-AoA.
Finally, the increased flexibility of wing B and the higher dynamic pressure are also beneficial to the accuracy of the pure DLM results. This is again mostly a coincidence as the DLM does not capture all the relevant flow phenomenons (transonic shock, viscosity etc.) but it does highlight that elasticity can lead to a linearization of the wing flexible aerodynamic response.

4.5 AEROELASTIC PREDICTION WITH CONTROL SURFACE DEFLECTION

As for the 2D example in Chapter 3, non-linear aerodynamic effects arise when deflecting the control surfaces. In Figure 4.13, the lift increment from the aileron deflection largely deviates from the linear trend, when deflected down. Similarly, the spoiler, when deflected up, exhibits a non-linear behaviour, especially at low deflection angles of less than 15 degrees.

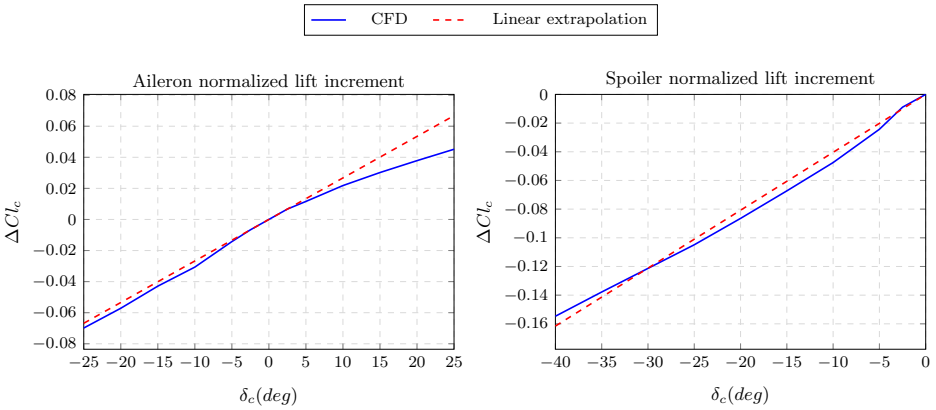

Figure 4.13: Lift increment obtained on the 3D wing for the aileron and the spoiler. The linear trends are interpolated around the 0 degrees position for the aileron, and with a least square fit for the spoiler.

As mentioned in the introduction, MLA capabilities are very important. We saw in the previous chapter that a linear approximation of the aileron is not good at

high deflection angles. To the author's knowledge, there is no example of spoiler aerodynamics modelling solely relying on linear panel codes such as DLM. Due to the inherent flow characteristics around a deflected spoiler, the most practical option is therefore to rely on RANS-CFD.
We therefore opted for the use of external CFD databases containing the lift and moment increments from control surfaces deflection. These databases can take the form of a load vector for each control surface deflection settings and Mach number. As stated in Section 4.1, the incremental lift and moment can be scaled with the dynamic pressure.
In Figure 4.14, we look at the integrated loads and wingtip displacements for the wing model A at cruise speed. The aileron is used at -25 and +25 degrees deflection. Overall, a good agreement is found between the FSI and HSA methods within the linear region. Beyond 2 degrees of AoA, the wing stalls and the error in the results increases. The response given by HSA method remains conservative at AoA above 3 degrees and would remain safe to use for wing sizing.

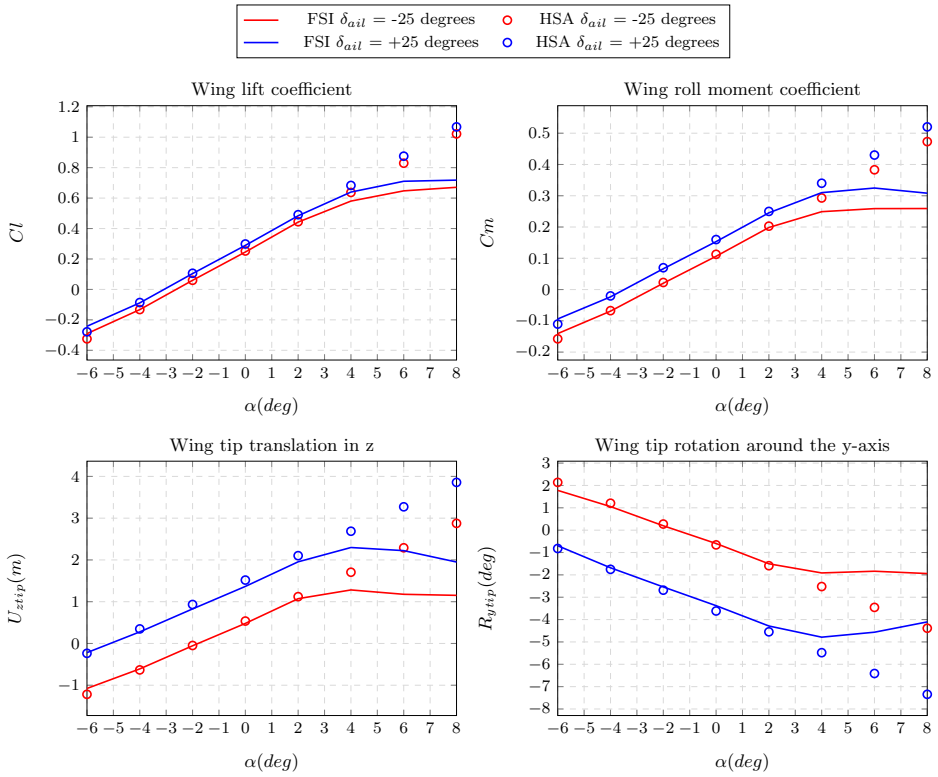

Figure 4.14: Lift, moment and tip displacements for various angles of attack with the aileron deployed. This is obtained with the FSI and HSA methods for the wing A at 11,100Pa Mach 0.85.

In Figure 4.15, we show the same simulations but output in terms of lift distribution. We see that for +25 and -25 degrees deflection settings, the lift distribution given by the two methods are very close until 2 degrees AoA. The agreement breaks down at AoA = 4 degrees, yet, it is a good demonstration of how the superposition of loads (rigid, flexible and control) can work effectively for aeroelastic transonic prediction.

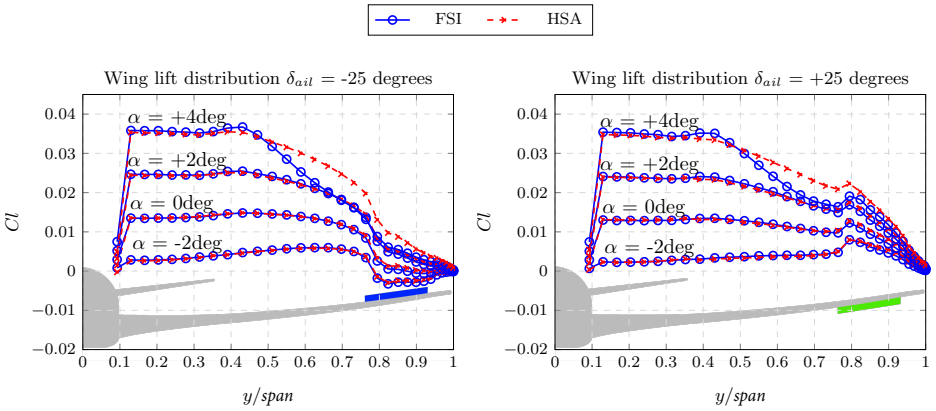

Figure 4.15: Lift distribution span-wise for various angles of attack with the aileron deployed. This is obtained with the FSI and HSA and methods for the wing model A at 11,100Pa Mach 0.85.

For the simultaneous deployment of both the spoiler and the aileron, we used two distinct databases. If we recall the external aerodynamic load vector P from Equation 4.1, it is now equal to:

$$P = P_{ail}(\delta_{ail}) + P_{spoil}(\delta_{spoil}) \tag{4.2}$$

This way, it is not necessary to simulate all the possible combinations of deflection between the two movables with RANS-CFD. We show in Figure 4.16 the sum of both aileron and spoiler individual aerodynamic loads and compare it to CFD results where both control surfaces are deflected. This approach tends to slightly minimise the control effectiveness by less than 5% when both the spoiler and aileron are deflected up. In contrast, when the aileron and spoiler have conflicting deflections, the results are not as good, with a slight underestimation of the negative loads over the spoiler section of the wing and an overestimation of the loads over the aileron section. The total error in lift increment is 10%. We attribute the difference in accuracy between both scenarios to the increase of the flow complexity pattern which our approach could not capture. However, this control surfaces setting, with the exception of flight control malfunction events (GPIAAF, 2020), can be considered as unusual in regular operation.

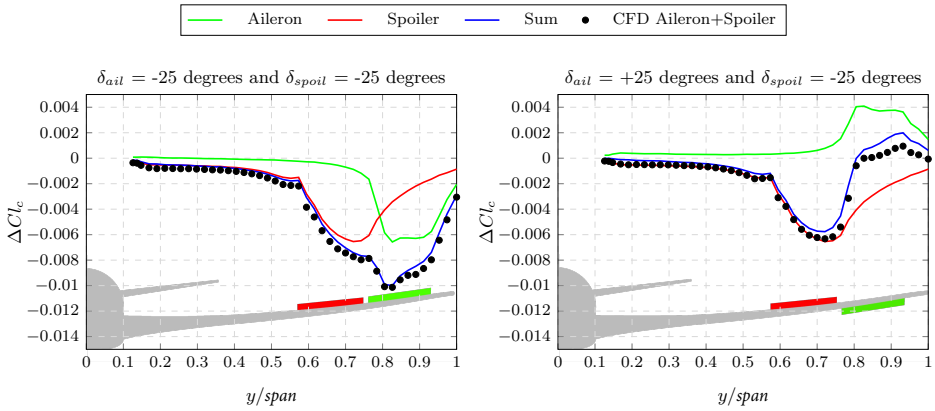

Figure 4.16: Rigid incremental lift distribution span-wise obtained with both the aileron and spoiler deployed.

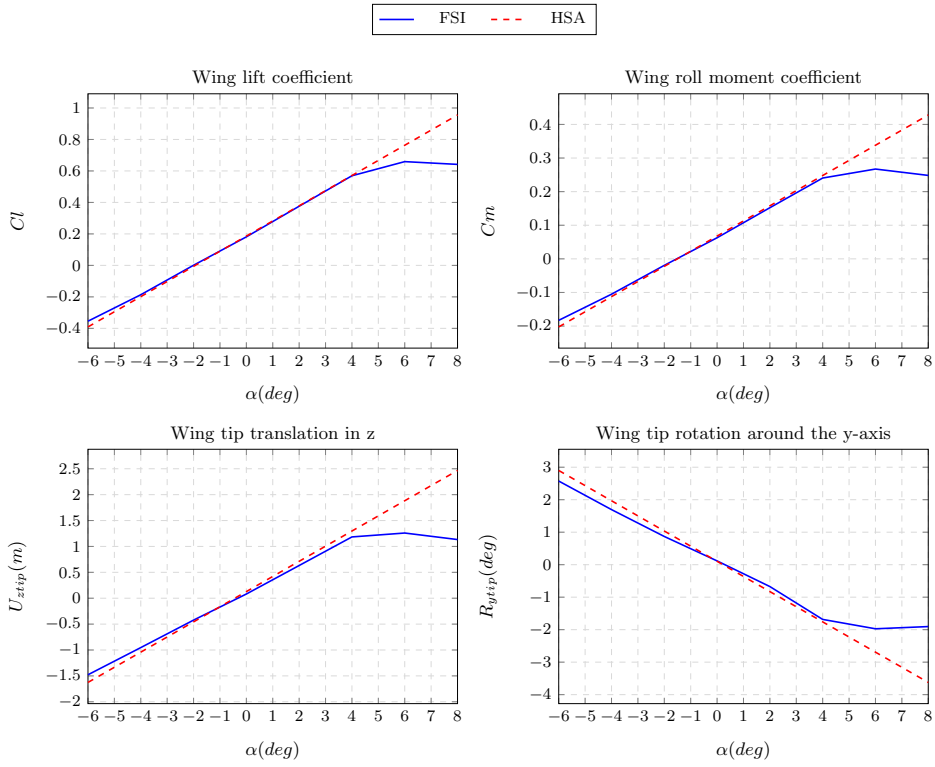

Figure 4.17: Lift, moment and tip displacements for various angles of attack with the aileron and spoiler deployed at -25 degrees obtained with the FSI and HSA methods for the wing model A at 11,100Pa Mach 0.85.

In Figure 4.17 we show the aeroelastic polars where both the spoiler and the aileron are deflected up. We see an improvement of the HSA accuracy up to 4 degrees AoA with a delayed non-linear response compared to the previous cases. When a control surface acts to reduce the amount of lift, it usually mitigates the transonic shock and flow separation over the wing. This is amplified by the combined deflection of the control surfaces. The span-wise lift distributions in Figure 4.18 reflect this with a good agreement up to 4 degrees AoA between the FSI and HSA predictions. We can also note that in this configuration, the control surfaces alleviate a lot of the loads which leads to little aeroelastic deformation and therefore almost no incremental flexible lift. This is in sharp contrast to the results shown in Figure 4.11. Because the aeroelasticity of the wing contributes less to its overall response, the accuracy of the prediction is therefore mostly based on the rigid forces estimation provided by the RANS-CFD simulations.

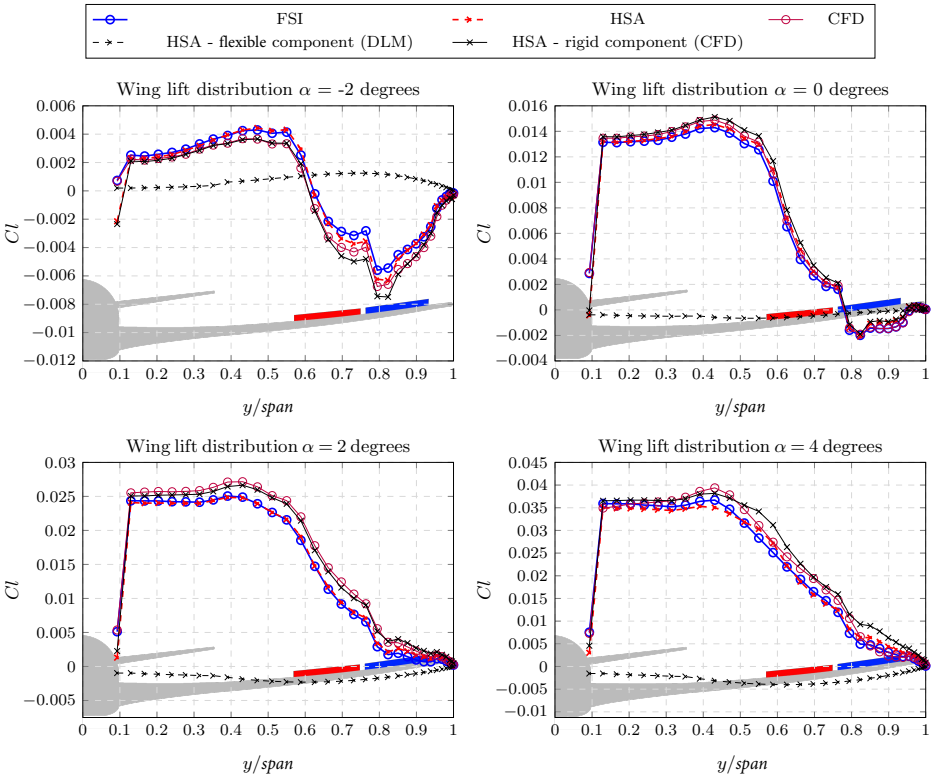

Figure 4.18: Lift distribution span-wise for various angles of attack with the aileron and spoiler deployed obtained with the FSI, CFD and HSA methods for the stiffer wing model at 11,100Pa Mach 0.85.

4.6 Conclusion

In this section, we benchmarked the HSA method against FSI simulations and the NASTRAN SOL144 DLM-based solver. Comparisons were made with two different wing models and two dynamic pressures in the transonic regime. Total lift, span-wise lift distribution, roll moment and wing tip displacements were plotted for a range of AoA from -6 to 8 degrees. Additionally, HSA and FSI were also pitted against each other with control surfaces deflection.
When compared against the FSI results, HSA tends to over-predict the loads while the outer wing would normally stall at high AoA. The results are slightly better when we use control surfaces to reduce the loads, mitigating aerodynamic non-linearities and extending the linear region of the wing response. Trimmed DLM analyses gave good predictions at higher AoA, but it is only a conjuncture as the lift distribution moves inboard when stall occurs on the wing outer part in the FSI and CFD simulations. Overall, SOL144 under-estimates the root bending moments.
The main advantage of the HSA method lies in the simplicity of creating external aerodynamic databases using rigid CFD analysis to introduce the transonic flow corrections. We also showed that it was practical to superpose multiple sets of control surfaces loads and to account for their potential non-linear incremental responses when deflected. Finally, because the aerodynamic corrections and external loads are all based on the rigid geometry, the wing stiffness can be changed if required.
Despite giving a conservative loads estimate, the HSA method remains a pertinent choice for wingbox sizing problems thanks to its aforementioned benefits. It also gave very accurate results at lower AoA more typical of 1g cruise flight point, which is important when computing gust loads.

5

UNSTEADY AEROELASTIC SIMULATIONS WITH DYNAMIC CONTROL SURFACES DEFLECTIONS

5.1 INTRODUCTION

In this chapter[1] of the thesis, we tackle the modelling of a flexible wing with dynamic control surfaces deflections. We have seen in the previous two chapters that non-linear flow behaviour occurs when control surfaces are deflected with large amplitudes. Moreover, the aeroelasticity of the wing can reduce control effectiveness, especially at high speed.
Performing unsteady aeroelastic analysis in the transonic regime generally requires high-fidelity FSI which is expensive. It is even more so in a wingbox sizing problem where the structural properties of the design may change at each optimisation loop. Therefore, developing a fast approach to model the wing response to dynamic control surface deflection is paramount. The latter could then be used to estimate the performance of a gust load alleviation system or to enhance the movables kinematic design to improve the ride comfort of the aircraft (Delannoy,

[1] This chapter is based on parts of the journal paper Lancelot, P., De Breuker, R. (2021). "Unsteady Non-linear Control Surface Modelling for Aeroservoelastic Applications". *Journal of Aeroelasticity and Structural Dynamics*.

2007).
Building aerodynamic corrections as in Chapter 4 is not as straightforward for dynamic simulations because of the unsteady nature of the flow. In the following sections, we extend the methodology presented in Chapter 3 to the modified uCRM wing already presented in Chapter 4. To account for the wing dynamic aeroelastic response, we couple our control surface ROM to the unsteady aeroelastic solution of NASTRAN. We compare this method against coupled high-fidelity FSI simulations for the two wing models (A and B from the previous chapter) equipped with the aileron and the spoiler.

5.2 CONTROL SURFACES ROM APPLIED TO A 3D RIGID WING

The methodology we described in Chapter 3 is applied to a 3D rigid wing. We use Ansys Fluent with a $k-\omega$ SST two equations turbulence model (Ansys, 2009b). We set the simulations at Mach 0.85 with a dynamic pressure of 11,100Pa similar to the conditions in Chapter 4. Simulations are achieved with an aircraft AoA of 0 degrees.
For the 3D simulations, we need to capture the span-wise variations in lift and moment due to the control surface deflection. The wing is divided into strips on which the aerodynamic loads are collected. Each strip corresponds to the location of one of the condensed structural degrees of freedom (DOF). These strips are defined as shown in Figure 5.1.

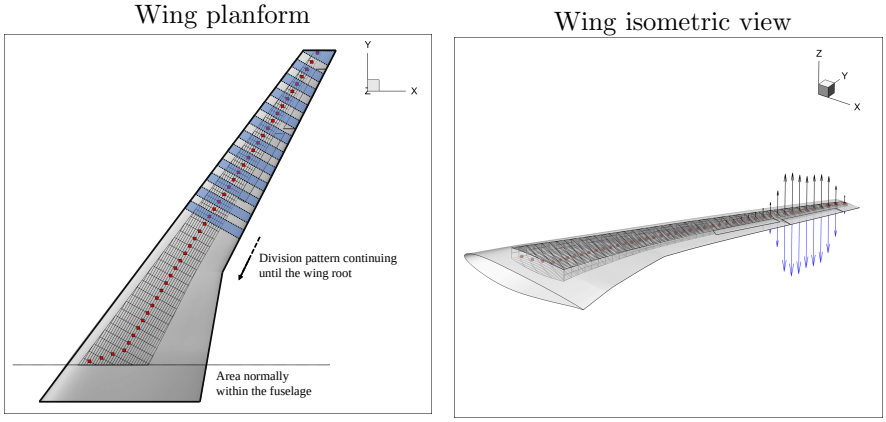

Figure 5.1: The wing outer mould and control surfaces are overlaid with the wingbox structural model. The red squares represent the condensed DOF on which the CFD aerodynamic loads ΔQ_c from each strip are integrated. The black and blue vectors represent the aerodynamic forces produced on the wing by the aileron when deflected down or up.

5.2.1 ROM VERIFICATION WITH UNSTEADY CFD FOR DIFFERENT CONTROL SIGNALS

We identify the loads on each strip following the same process as described in Section 3.1. To build the look-up tables for the 3D wing, we perform the steady CFD analyses with control deflection ranging from -25 to +25 degrees (see Figure 4.13). Then we use the CFD results shown in Figure 5.2 to identify the unsteady contribution of the aerodynamic model. For these dynamic simulations, we set the time steps to 0.01 seconds, which provides the best compromise between numerical convergence and computational effort. The incremental lift predictions from the ROM are overlaid on the CFD results. In this plot, we move both control surfaces with a square signal going from -5.7 to +5.7 degrees (0.1 radians) similar to what is done in Figure 3.9. The spoiler deflection signal is centred around 20 degrees to simplify the mesh deformation. The lines correspond to the local incremental lift coefficient produced by the unsteady aerodynamic models of each strip.

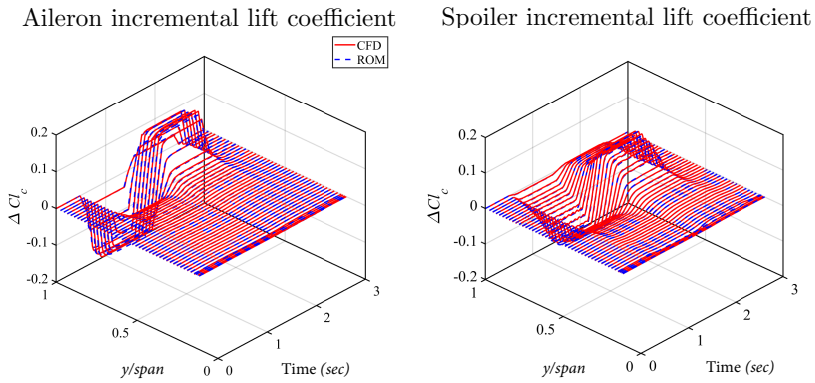

Figure 5.2: Time dependent visualization of the span-wise lift increment during the aileron and the spoiler dynamic deflections. The lift is normalized with respect to each strip surface area.

In Figure 5.3, we take two snapshots of each aforementioned simulation at 1 and 2 seconds. The maximum error in the incremental lift in the span-wise direction is in the order of 5%. This indicates that not only the amplitude of the unsteady aerodynamic response is correctly approximated for both the aileron and the spoiler, but also its phase over the span of the wing is well accounted for. The spoiler results are particularly relevant because there is currently no widespread aerodynamic model for this type of control surface aside from high-fidelity CFD or empirical formulas and it remains one of the most challenging control surfaces to model as summarised by Chyczewski et al. (2020).

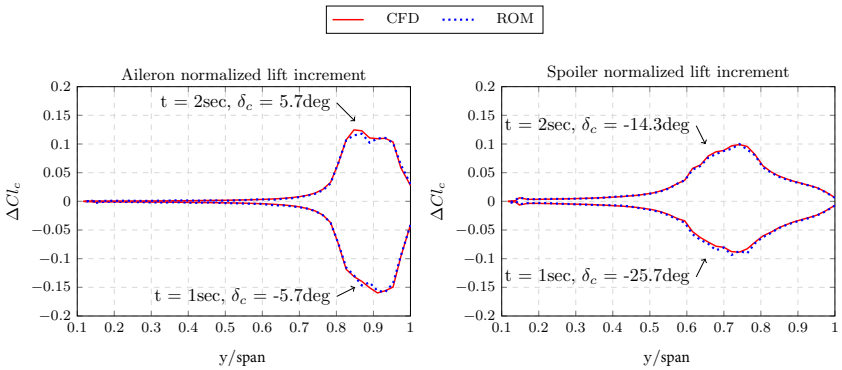

Figure 5.3: Rigid aileron and spoiler lift increment over the span. The spoiler lift increment is zeroed around a 20 degrees baseline deflection angle.

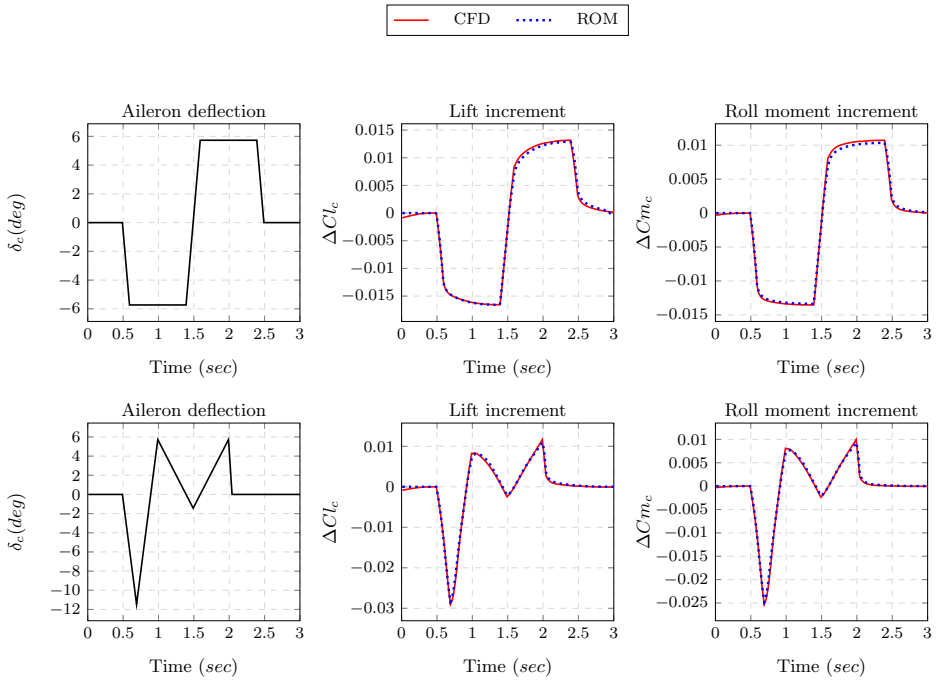

Figure 5.4: Time dependent visualization of the lift and roll moment increment coefficients for various aileron dynamic deflections.

We show the aileron integrated incremental loads (ΔCl_c and ΔCm_c) in Figure 5.4. The ROM produces good results compared to the rigid CFD analysis, also below a 5% error. The aileron deflects up and down at a velocity of 57.3 deg/sec

for the square signal and at range varying from 14.3 to 114.6 deg/sec for the triangular signal. As already highlighted in Chapter 3, the unsteady part of the ROM is suitable for a wide range of deflection speeds since it is identified over a step response.

We show the spoiler integrated incremental loads in Figure 5.5. Here, due to limitations in our CFD setup, we are making a piecewise comparison between the ROM and the rigid CFD. We are indeed limited to the amplitude at which we can deflect the spoiler without distorting excessively the mesh. Nonetheless, the ROM for the spoiler is generated following the same process as for the aileron. We only need to perform the unsteady identification around a single spoiler deflection since we assume that the unsteady aerodynamic contribution in the model is not affected by static deflection angle. The construction of the look-up tables for the steady non-linear aerodynamic data of the spoiler is also not affected by the mesh deformation limitation, since the mesh can be completely re-meshed for each angle. Leaning on this single model, the results in Figure 5.5 are in good agreement with the CFD for the whole range of deflections within 5%. The difference in amplitude of the incremental lift response for different baseline deflection angles is also well approximated and is consistent with the static polar in Figure 4.13.

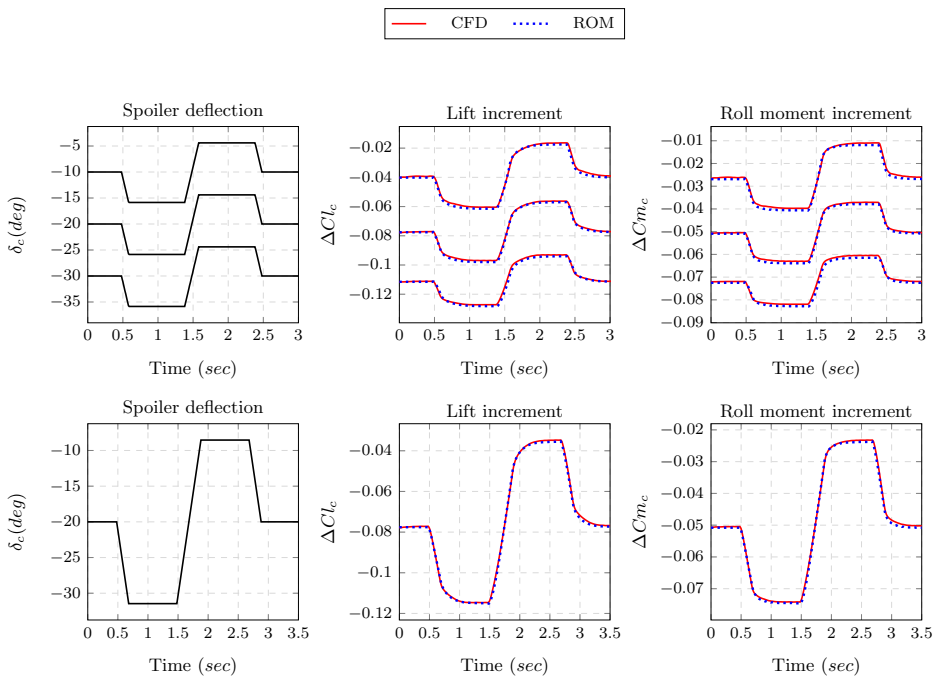

Figure 5.5: Time dependent visualization of the lift and roll moment increment coefficients for various spoiler dynamic deflections.

5.3 CONTROL SURFACES ROM APPLIED TO A 3D FLEXIBLE WING

In cruise flight, the static aeroelastic response can be tackled using the HSA method described in Chapter 4. This method however does not account for any dynamic response of the wing. To resolve this situation, we assume that the main source of aerodynamic non-linearity is the control surfaces deflections and not the wing elastic response itself, which would remain mostly linear. There are examples in the literature of small disturbances aeroelastic problems (typically flutter) where linear methods provide sufficient approximation even in the transonic regime (Begnini et al., 2016; Dequand et al., 2019). Therefore, we choose to superpose the non-linear aerodynamic contribution of the aileron and spoiler deflections to a linear aeroealstic wing model. This has been used with gust loads (Raveh, 2010) and buffet loads (Mamelle et al., 2013) as well. The following sections describe and verify this method for control surfaces.

5

5.3.1 HYBRID AEROELASTIC METHODOLOGY

In our model, transonic incremental loads on the wings, ΔQ_c, are only a function of the deflection command δ_c, as shown in the aeroelastic equation of motion shown in Equation 5.1 on the right-hand side. Variables M and K are the aircraft mass and stiffness matrices derived from MSC NASTRAN. The variable ΔQ_e is the generalized aerodynamic forces from the wing elastic response and is obtained from the DLM method implemented in MSC NASTRAN. The matrix M_c which represents the control surface mass is not included in our analysis for simplicity. The dynamic pressure is q_∞. The variable ζ is the modal displacements vector while s is the Laplace domain variable.

$$([M]s^2 + [K] + q_\infty[\Delta Q_e(s)])\zeta(s) = -([M_c]s^2 + q_\infty[\Delta Q_c(s)])\delta_c(s) \tag{5.1}$$

We describe the integration of the model in Figure 5.6. The MSC NASTRAN dynamic aeroelastic module (SOL146) is used to solve the system in the frequency domain (Johnson and Rodden, 1994). We use the 50 first modes during the NASTRAN analysis. However, the aerodynamic loads due to the aileron deflection, ΔQ_c, are included through time domain direct force inputs (DLOAD tables, see MSC Software Corporation (2019)). MSC NASTRAN converts them to the frequency domain using the Fourier transform. For every condensed structural DOF on the flexible wing, we derive one matching aerodynamic local ROM ΔQ_{ci}. This allows capturing the load increments along the wingspan from the movable deflection δ_c. We build the ROMs for the incremental forces in the z and moments in the y directions.

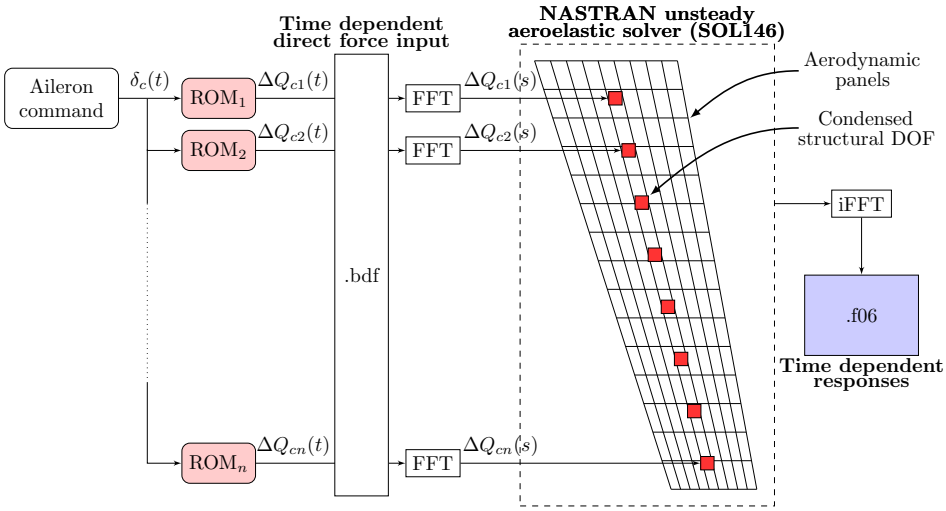

Figure 5.6: Hybrid unsteady approach: we add the control loads generated by the aerodynamic ROMs to the MSC NASTRAN aeroelastic solver.

With this setup, we can then extract the loads and stresses on the entire aircraft in the time domain from MSC NASTRAN. Our method retains the non-linearities due to control surface deflection, while greatly simplifying the rest of the simulation. For structural sizing, we can therefore quickly update our structural wing design because SOL146 is fast to run (see Figure 5.8) while keeping the ROM untouched. This is the same logic as the HSA method presented in Chapter 4 but for dynamic simulations. Also, because the method is non-intrusive, we could rely on a different aeroelastic model, such as unsteady vortex lattice (UVLM) or linearized CFD for improved fidelity. Corrections to the unsteady aerodynamic matrices Q_e in SOL146 are also compatible with our approach.

5.3.2 Setup of the verification with high-fidelity FSI

In this section we perform a verification of our hybrid approach for the incremental flexible loads caused by control deflection. To do this, we use a traditional high-fidelity FSI approach as described in Section 4.3 but extended to dynamic simulations using a time domain staggered scheme. It is adapted from the FSI framework developed by Piñeiro Rielo (2019) to handle control surface motion as illustrated in Figure 5.7. A Newmark scheme is used to solve structural dynamics since it is straight forward to implement in Matlab. The stiffness and mass matrices are extracted from MSC NASTRAN using the DMIGPCH command MSC Software Corporation (2019). As with the setup described in Section

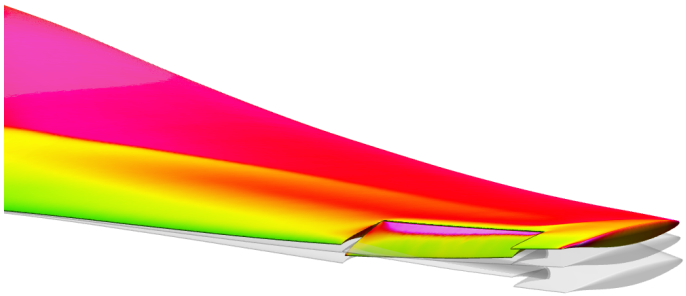

Figure 5.7: Illustration of a dynamic aileron deflection using high-fidelity FSI simulation.

4.3, the CFD simulation is run with Ansys FLUENT using a k-ω SST turbulence model and time steps of 0.01sec. Mesh deformation is achieved with a smoothing deformation technique Ansys (2009a) and therefore limits the maximum wing tip displacement achievable to about $\pm$ 300mm and control surface deflection to $\pm$12 degrees as we will see later in this chapter. The wing deformation is obtained by extrapolating the structure displacements via radial basis functions (RBF) implemented with a user-defined function (UDF) in Ansys FLUENT (Beckert and Wendland, 2001). The CFD loads are transferred back to the structure using the nearest neighbour approach (MathWorks, 2020a).

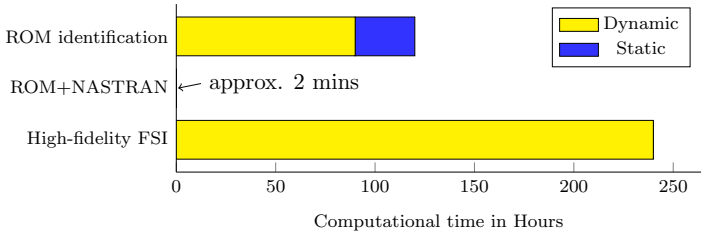

Figure 5.8: All CFD simulations run on a 32 cores Intel CPU clocked at 2.30Ghz. Simulink and NASTRAN analyses run on a single core.

In Figure 5.8, we show a time comparison between our hybrid approach and the high-fidelity FSI analysis. The ROM is identified in Section 5.2, from a single rigid transient CFD analysis and in this case, 15 rigid static analyses with a range of control surfaces deflections going from -25 to +25 degrees. We identify one ROM per type of control surfaces and per Mach number. A single ROM supports any arbitrary control motion and the loads ΔQ_c can be scaled up with the dynamic pressure q_∞. For simplicity, all the subsequent simulations are run at a fixed

Mach 0.85 and $q_\infty = 11,100$Pa. When it is combined with MSC NASTRAN SOL146, the wing mass and stiffness properties can be varied at minimum cost (a couple of minutes). Therefore, this solution is less time consuming than a direct coupled high-fidelity FSI analysis. Also, because static aerodynamic CFD analyses are comparatively cheap to perform (about 2 hours per deflection setting and flight point), the aerodynamic look-up tables of the loads increments from control surfaces deflection can be refined at a relatively low computational cost.

5.3.3 Flexible wing and aileron verification

We look at the load and displacement increments induced by the aileron and spoiler deflections. The wing AoA is set to 0 degrees. In Figure 5.9, we deflect the aileron from -5.7 to +5.7 degrees. We are comparing three different wings: one rigid, and two flexible wings: A and B.

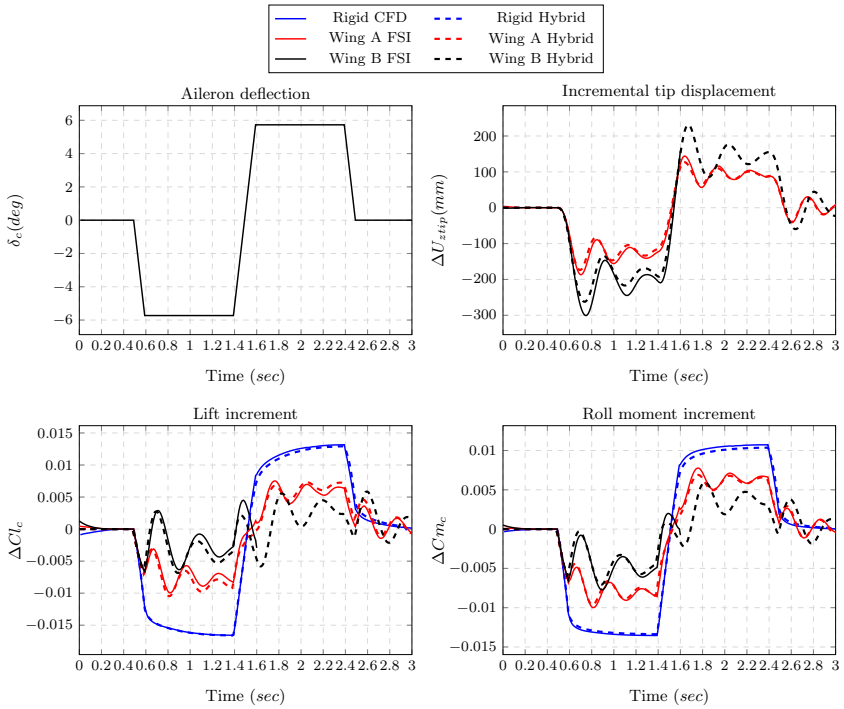

Figure 5.9: FSI compared against the hybrid model with dynamic aileron deflections. The deflection range varies from -5.7 to +5.7 degrees. A video of the simulation with wing A is available at the following reference Lancelot and De Breuker (2023).

Due to an excessive mesh deformation, the simulation with the B model crashed

mid-way. This shows the difficulty of modelling such problem using a high-fidelity method, but the author still deemed these results relevant as they provide comparison for the more flexible wing B. Looking at the wing tip vertical displacement, ΔU_{ztip}, we see that the amplitudes are in the same order of magnitude for both the FSI and the hybrid model. The relative error is however higher for wing B and reaches 13% during the negative displacement peak. The error in the stiffer wing A remains below 12%. When looking at the incremental lift coefficient ΔCl_c and roll moment ΔCm_c, we see similar trends for the tip displacement where the stiffer wing and the rigid wing have a lower error at the peak values, around 5%, as compared to the more flexible wing B. We also see that the amplitudes are different when deflecting the aileron up or down, highlighting aerodynamic non-linearities which our ROM captures effectively. Finally, we see that the rolling moment and lift coefficients significantly reduce when the wing stiffness is decreased. This aeroelastic effect is fully captured by our hybrid model. It can lead to control reversal and is a key driver of the aircraft sizing, as the wings may have to be reinforced to avoid such issue (Klimmek, 2014).

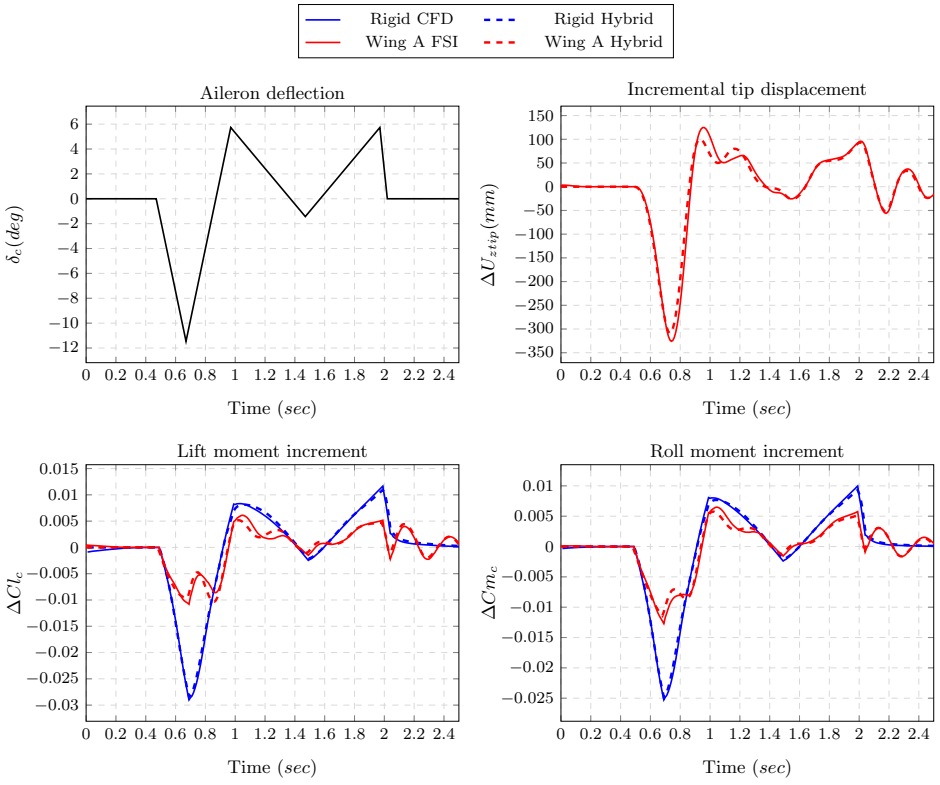

Figure 5.10: FSI compared against the hybrid model with dynamic aileron deflections. The deflection range varies from -11.4 to +5.7 degrees.

In addition to the square signals, we test our hybrid approach with a different deflection input as shown in Figure 5.10. The aileron moves from -11.4 to +5.7 degrees with deflection rates varying from 14.3 to 114.6 deg/sec while the flight parameters remain the same as the previous set of simulations. This command signal is arbitrary but covers a realistic range of deflection rates. We see a good agreement overall for both the rigid and the flexible wings.

5.3.4 Flexible wing and spoiler verification

When comparing the results for the spoiler deflection, we are limited by the range of dynamic deflection possible with our CFD and mesh deformation setup. To avoid distorting the mesh excessively around the spoiler, we perform a piecewise comparison of our hybrid model against several FSI runs with the spoiler positioned at 10, 20 and 30 degrees. As for the aileron, the spoiler ROM identification only needs a single small disturbance transient CFD analysis to capture the unsteady flow response to the movable deflection, and a set of nine steady CFD simulation from 0 to -40 degrees to capture the non-linear aerodynamic response at large deflections.

We start the comparison with static aeroelastic results plotted in Figure 5.11. Results with the AoA set to $\alpha = 0$ degrees generally match well, with errors ranging from 0% to 5% for both wing type in vertical tip displacement, lift and moment coefficients.

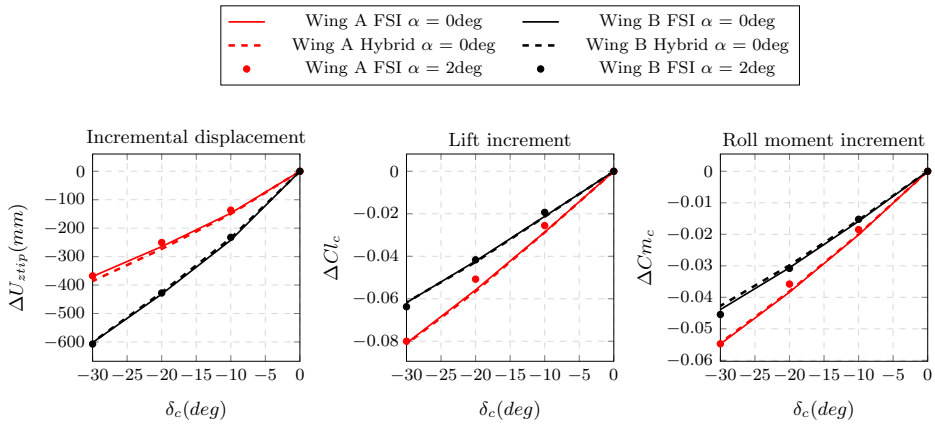

Figure 5.11: FSI compared against the hybrid model with static spoiler deflections.

We also looked at the possible interactions between the spoiler deflection and the aircraft AoA. In their combined wind tunnel and numerical studies, Wiart and Carrier (2012) showed that limited coupling could be observed at small AoA (less than 2 degrees) in the aileron response. However, for the spoiler, Wilkinson et al.

(1996) described the risk of spoiler rigid aerodynamic reversal at transonic speeds and positive aircraft angles of attack. They explained it by the complex shock motion being influenced by both the aircraft incidence and the spoiler setting. In our results, we can also see higher discrepancies at 2 degrees AoA between the FSI analyses and our hybrid approach. However, despite the aircraft incidence increasing, the wing washout limits the local angle of attack, and hence the shock motion due to the change in AoA. Further evidence of this is in the smaller relative error with the more flexible wing B compared to results with wing A. The hybrid approach for both cases relies on a ROM identified at an AoA of 0 degrees.

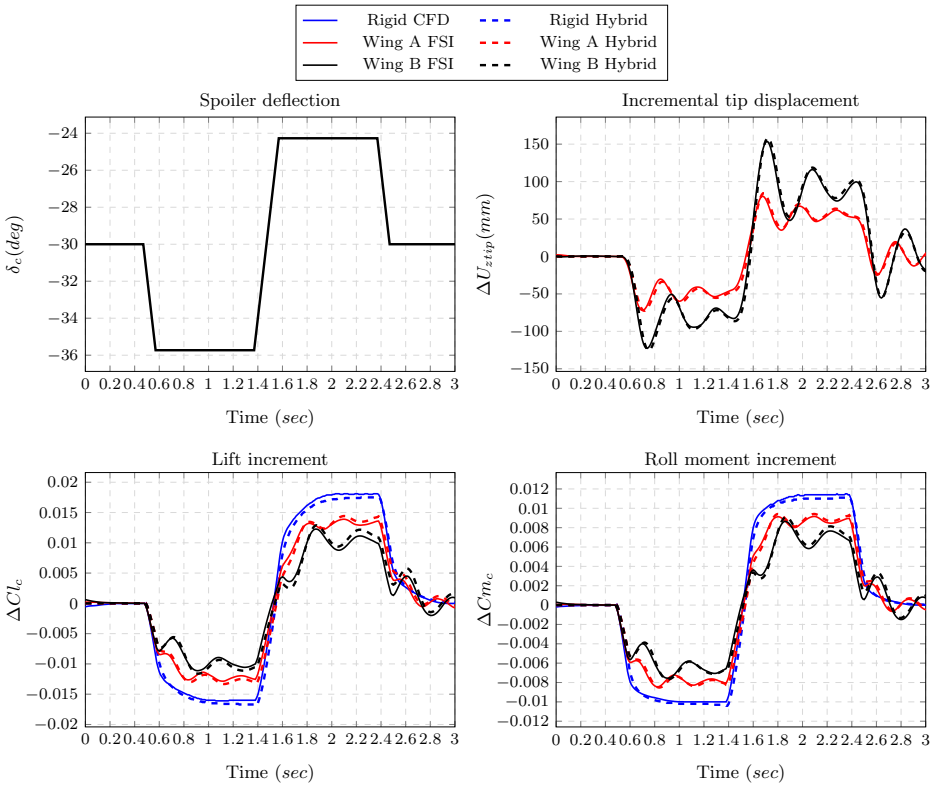

Figure 5.12: FSI compared against the hybrid model with dynamic spoiler deflections. The deflection range varies from -5.7 to +5.7 degrees around a baseline position of 30 degrees. A video of the simulation with wing B is available at the following reference Lancelot and De Breuker (2023).

For the unsteady cases, we show in Figure 5.12 the results for a dynamic spoiler moving from -5.7 to +5.7 degrees around a baseline deflection of 30 degrees with the aircraft AoA at 0 degrees. We compared the rigid wing, and the wings A and B, in a similar setup as for the aileron. The results have been zeroed around this

baseline spoiler position. For ΔU_{ztip}, ΔCl_c and ΔCm_c, we have a good agreement between our hybrid model and the FSI simulations. The error at the peak values is at a maximum of 5.3%. The results for the spoiler are generally better than for the aileron. We attribute this to the lower wing deformation induced by the spoiler deflection. It is due to its more inboard position and therefore its lower influence on the wing bending. Similarly, we observe a lower decrease in spoiler effectiveness as the stiffness is reduced. We can also conclude that our hybrid approach could perform equally well in modelling other control surfaces located closer to the root, such as flaperons.

5.4 Conclusion

We have tested our unsteady non-linear hybrid model on a realistic 3D transonic wing equipped with an aileron and a spoiler. The spoiler is a control surface whose aerodynamics are difficult to approximate using potential flow theory because it inherently creates flow separation. Its modelling is restricted to empirical models or CFD and higher-order methods but those are computationally expensive. We approached this problem by discretizing our wing in span-wise strips, on which incremental loads from CFD simulations are integrated to create local ROMs capturing the load increments along the span from the movable deflection. As for the 2D example in Chapter 3, we only needed for the ROM identification one transient simulation with small deflection amplitudes and nine static CFD analyses. Using the resulting ROM, we were able to replicate the incremental loads calculated with transient CFD for any arbitrary spoiler motion. We also obtained good results with the aileron, for which the ROM yielded a good agreement against the reference CFD simulations.
Finally, we developed and compared an approach where we combined our aerodynamic ROM with a linear aeroelastic solver which is the SOL146 from MSC NASTRAN. Here, the non-linear unsteady rigid incremental loads from control deflections are superimposed on the aeroelastic model. With this method, we can capture the loss of control effectiveness due to both non-linear aerodynamics combined with linear aeroelasticity. We benchmarked our approach against a conventional time marching coupled FSI method in the transonic regime. The results with the aileron showed a good agreement with our hybrid model when the wing is moderately flexible (wing A). For the more flexible cases (wing B), the difference is higher but remains within 13%. The results with the spoiler are also promising, with the error at the peak values on the tip displacement, lift and moment increment coefficients below 6%.

6

AEROSERVOELASTIC OPTIMISATION PROCESS

In this chapter, we apply the load corrections derived in Chapter 4 and Chapter 5 to the sizing of a large passenger aircraft wing. Including load alleviation (MLA and GLA) in the wingbox sizing can potentially decrease the wingbox weight thanks to a reduction of the flight loads. One challenge is to include structural design variables and flight control parameters in the same optimisation pipeline. The former usually includes panel thickness or material stiffness and strength properties, while the latter is about aircraft wing layout and control surfaces gain and scheduling. This heterogeneity means that the wing structural optimisation problem becomes multidisciplinary. To tackle this issue, we apply a hybrid optimisation technique. We use a gradient-based optimiser that is efficient to size the wing structure nested within a global heuristic method to optimise the load alleviation parameters. Finally, we assess how the aerodynamic model fidelity impacts the weight of the optimised structure.

6.1 AEROSERVOELASTIC OPTIMISATION SETUP

Mixing different types of parameters makes optimisation difficult. The design variables do not all have the same influence on the objective and constraints, and the possibility of a non-convex design space is high. The use of a global optim-

isation approach (particle swarm optimisation, genetic algorithm, multi-starts) is usually a remedy to this but can become very inefficient if the optimisation problem contains many design variables and requires an expensive objective function to evaluate (Martins and Ning, 2021). This is why structural optimisation requires a gradient-based approach. Therefore we rely on the industry-proven MSC NASTRAN solution 200 (SOL200) optimiser (MSC Software Corporation, 2012a), a powerful structural optimiser. SOL200 handles structural optimisation problems with static aeroelastic load cases (manoeuvres) and flutter but does not directly account for aeroelastic gust responses, let alone cases with active load alleviation (GLA). The approach we propose has the structural optimisation performed as a nested function within an adaptive random search. A notable use of a multi-level approach to efficiently tackle multiple types of design variables is the work from Piperni et al. (2013) that was used in an industrial context. More recently, Faïsse et al. (2022) also applied a bi-level strategy to an optimisation problem where both structural parameters and an active flutter suppression controller had to be sized concurrently. We describe our process in Figure 6.1.

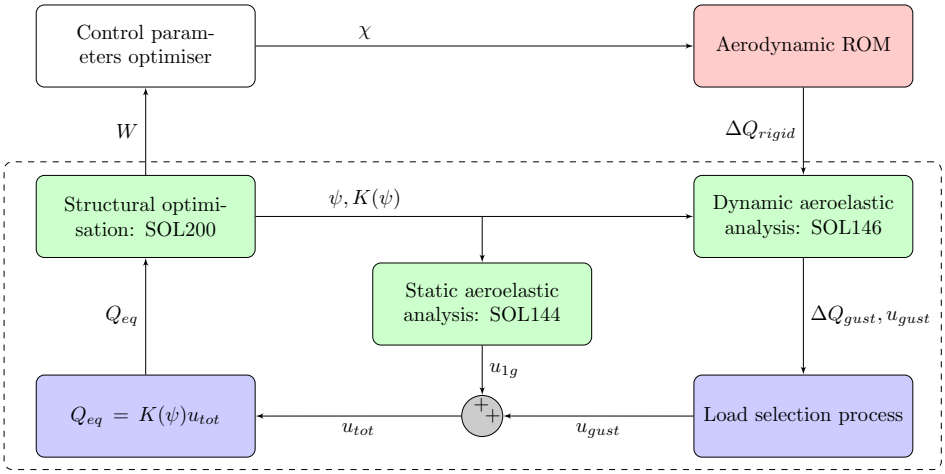

Figure 6.1: Optimisation loop with structural and control design parameters.

χ represents the active loads alleviation design parameters and ψ the structural design parameters. W is defined as the optimised weight from the structural sizing with SOL200 and is ultimately the objective to minimise. $K(\psi)$ is the stiffness matrix of the model and u the displacements of the wing under the aeroelastic loads. ΔQ represents the incremental loads from either the dynamic loads analysis or the aerodynamic ROM. The nested cost function relies on the Equivalent Static Load method (ESL) to account for gust load cases with active control. These are usually difficult to include in structural optimisation problems

due to their high computational cost. Such capability is not directly available in SOL200. Only a handful of aeroelastic sizing frameworks can compute gust loads sensitivities such as Airbus Lagrange (Schuhmacher et al., 2012) and TU Delft Proteus (Rajpal et al., 2019). Others like Stodieck et al. (2017) or Binder et al. (2021) use finite difference approximations to derive the gust response sensitivities required for gradient based optimisation. Instead, the ESL method formalised by Kang et al. (2001) does not require such information and relies only on the loads gradients derived from static loads representative of the stress and displacements of the dynamic gust loads. Equivalent static loads are derived as follows:

$$Q_{eq} = K(\psi)(u_{gust} + u_{1g}) \tag{6.1}$$

The sum of u_{gust} and u_{1g} corresponds to the incremental displacements due to gust loads added to the wing displacement at 1g. As part of the load selection process, a dynamic gust case can be "sliced" in multiple snapshots taken at the highest loads or displacements recorded during the simulation as done by Handojo (2020).

Skipping the gust sensitivities presents the advantage of simplifying the dynamic loads analysis as no sensitivity analysis needs to be performed outside of SOL200. Solano et al. (2022) show that when multiple gust cases are included in the optimisation problem, the ESL method can converge to a similar optimum as when using gust sensitivities. One of the ESL drawbacks identified in his study is the non-compliance of some constraints when using the ESL. This can however be corrected by increasing the number of loads snapshots (up to several hundred in the present thesis) to be used directly as static cases in SOL200. The method is also verified by Bordogna et al. (2020) by performing a compliance check of the optimised structure for the stress and buckling constraints under gust loads.

We use NASTRAN SOL144 and SOL146 for 1g steady loads and dynamic gust loads respectively. Additionally, we directly use SOL200 to compute steady aeroelastic loads and derive sensitivities for pull-up and push-over manoeuvres. SOL200 also computes automatically the sensitivities for the static load cases derived with the ESL method. For both SOL144 and SOL200 simulations, we apply the steady transonic aerodynamic corrections using the HSA already described and validated in Chapter 4. The control surface loads are introduced in the same way as described in Chapter 5 using non-linear unsteady aerodynamic ROM as input to the SOL146 solution. Likewise, the gust loads are also corrected for this model, using linearized CFD obtained on a rigid model, following the method described by Raveh (2010).

6.1.1 FEM MODEL

For the optimisation problem, we use the same test case already introduced in Chapter 3. We show the finite elements model in Figure 6.2. It is based on the uCRM geometry but meshed with a reduced element count to speed up analysis and hence optimisation run-time. It is comprised of about 1300 CQUAD4 and 50 CTRIA3 shell elements, which are used to model the wing skins, spars and ribs. The number of grid points is around 1500. CONM2 elements are used to add non-structural mass to the model, such as fuel loads, but also to account for the aircraft fuselage inertia. There are 45 design regions along the wingbox which each possesses a unique aluminium panel thickness. This FEM model is available under CC BY 4.0 Creative Commons license (Lancelot, 2021).

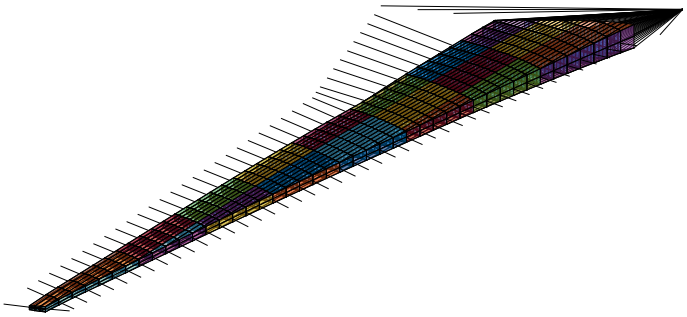

Figure 6.2: FEM model of the wingbox, based on the uCRM geometry. Tiles of colours indicate the different design regions and the black lines show the RBE2 and RBE3 elements used to improve the splining with the aerodynamic models.

The aerodynamic model is described in Figure 4.3. During dynamic simulation, the aircraft is only free in plunge. This is to emulate the use of a "perfect" control law which would suppress dynamic pitch motion caused by the gust encounter while not having to model the horizontal tail plane and the elevators.

6.1.2 OBJECTIVE AND CONSTRAINTS

The objective of the optimisation is to minimise the wing structural weight. Constraints are on the Von Mises stress in the aluminium panels (set to a limit of 250 Mpa) and on the panel buckling. The equations for the buckling are taken from Hürlimann (2010). A safety factor of 1.5 is added to both responses.

We have purposely not included constraints on the wing critical flutter speed to reduce the complexity of the optimisation problem. This allows us to more

easily derive the theoretical weight savings from active load alleviation and study the impact of aerodynamic fidelity on the results. The aileron effectiveness is implicitly tackled as we apply MLA. There, the structural optimiser must guarantee a sufficient wingbox torsional stiffness so that the control surfaces have enough authority to reduce the wing loads.

6.1.3 Load cases

The load cases used in the optimisation problem are listed below in Table 6.1:

Table 6.1: Load cases.

Case	Mass	Mach	q	Type
1	MZFW	0.85	16,500Pa	Pull-up: +2.5g
2	MZFW	0.85	16,500Pa	Push-down: -1g
3 to 14	MTOW	0.85	11,100Pa	1-cos gusts

The gust cases are computed according to the certification EASA CS25 (2016). The different gust lengths and amplitudes are shown below in Figure 6.3. The gusts are applied in both positive and negative vertical directions.

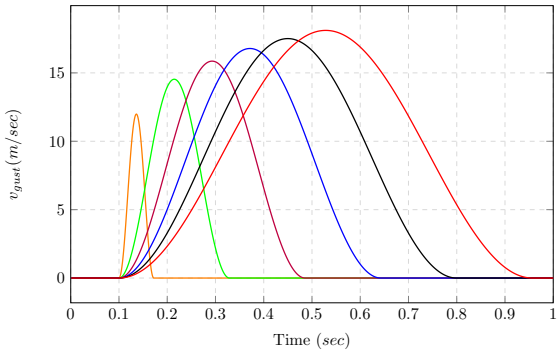

Figure 6.3: Discrete gust lengths and amplitudes.

6.1.4 Control optimisation

We include control in the optimisation with the scheme shown in Figure 6.4. Using this controller design means that the control deflections are only a function of the gust input and control parameters, and not of the aircraft response, as in a closed-loop system. The gust model also runs on SIMULINK, along with the control surface aerodynamic models already introduced in Chapter 5. We use a proportional gain controller that reacts to the incoming gust field and sends the

deflection command to the aileron and/or spoiler. A delay can be added as well. If set to 0 seconds, it means that the aileron and spoiler will deploy as soon as the gust hits the nose of the aircraft. A longer delay can be used to simulate actuators and control lag. A negative delay means that the gust is anticipated by the system. Although this is outside the scope of the thesis, such a system could be achieved using a LIDAR (Fezans et al., 2019).
Both control and gust aerodynamic contributions are then summed up and sent to NASTRAN SOL146 to get the aeroelastic response of the wing, as described in Chapter 5.

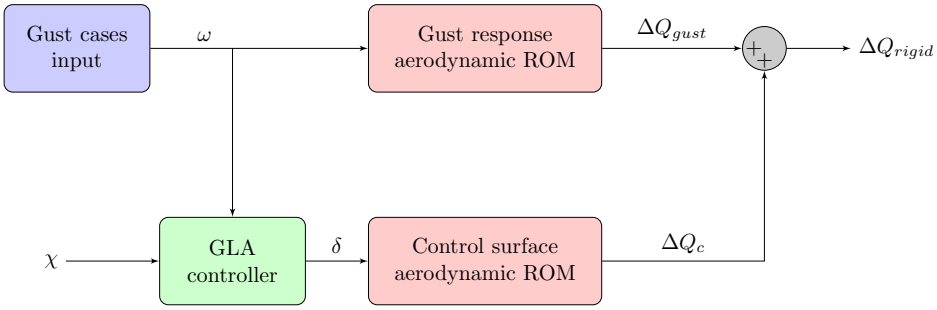

Figure 6.4: GLA system implemented with the rigid aerodynamic ROM.

A more detailed view of the GLA controller is given in Figure 6.5. On top of the aforementioned gain and delay, we can also adjust the maximum deflection rate and saturation. A deflection limit of +25 to -25 degrees is imposed on the aileron motion, and from 0 to +35 degrees on the spoiler. We also use a linear actuator model using with a fixed 20 rad/sec bandwidth and 0.5 damping ratio.

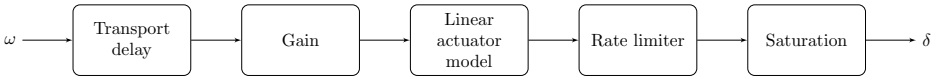

Figure 6.5: GLA control architecture.

As already described in Figure 6.1, the control optimisation relies on a structural optimisation loop nested within a random search optimisation algorithm. The latter is gradient-free but is only used to optimise the control parameters χ. For every set of χ, the wingbox is resized with static and dynamic loads. This method is not as fast as the use of gradients but is easier to implement. There is also no risk of getting stuck in a local optima and it is easy to parallelize, as each nested optimisation process can run independently of each other as illustrated in Figure 6.6.

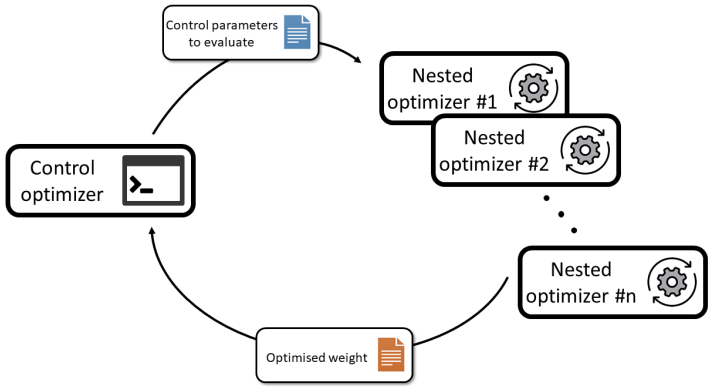

Figure 6.6: The nested optimisations used to compute the loads and perform the wing sizing are parallelized to evaluate multiple control parameters at the same time.

Additionally, to improve the convergence, we have an adaptive design space, which shrinks as the optimisation progresses as shown in Figure 6.7:

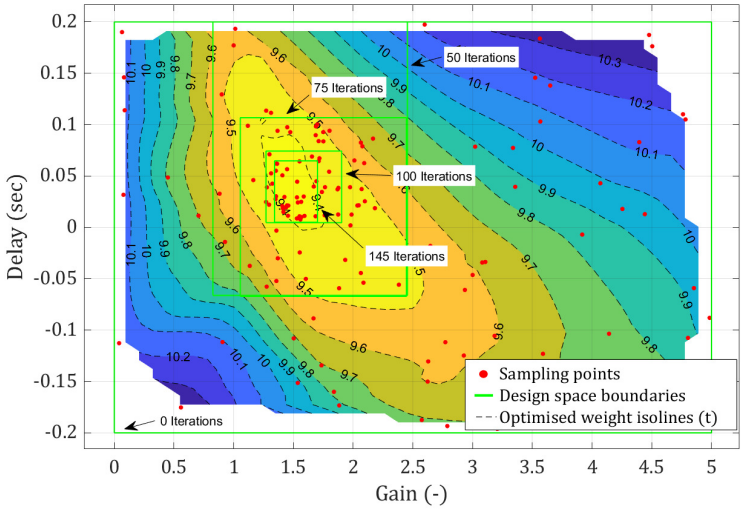

Figure 6.7: Optimisation overview of the optimal control parameters (aileron gain and delays) for the minimum wingbox weight.

In Figure 6.7, two control parameters are being concurrently optimised with the structural design parameters of the wingbox. Each sampling point equates to one nested structural optimisation. After an initial design exploration period, the

design space window starts to reduce once the first 50 nested optimisation results are obtained. The design space window is reduced by taking the 10 best designs in terms of optimised weight. The next control parameters to be evaluated from there on are only to be within the bounds of the most promising range of the control variables. The convergence of the objective function is shown in Figure 6.8. We show the weight convergence for two and four parameters: GLA with the aileron and GLA with aileron+spoiler respectively. Both optimisation problems converge to roughly the same weight (9.37t vs 9.36t) as the spoiler does not provide much help for GLA. The impact of the GLA and the efficacy of the spoiler are further investigated in Sections 6.3 and 6.4.

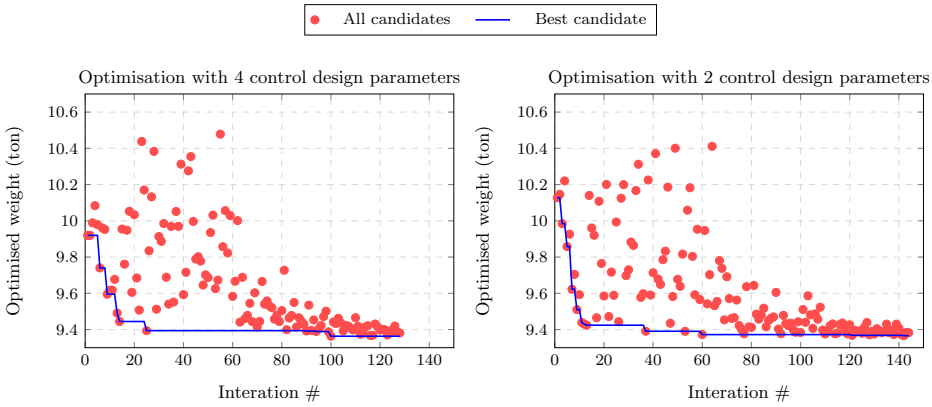

Figure 6.8: Convergence of the method for optimisations with 4 and 2 control parameters.

6.2 EFFECT OF THE MLA

MLA is generally thought to be less complex to implement than GLA as the logics of the load control system is directly dependent on the static load factor and not on the dynamic response of the wing due to a gust. We do not compare the effect of the aerodynamic fidelity of the MLA and manoeuvres loads on the optimised weight as this has been already done by Bordogna et al. (2020).
In Table 6.2 we show a weight comparison between various MLA settings. For the cases with MLA On, both aileron and spoiler are used. Additionally, an inboard spoiler is also deployed during the push-down manoeuvre to reduce the loads at the root. We also included cases without gusts, to assess their contribution to the aircraft weight. The gust cases (lengths and amplitudes) are presented in Figure 6.3.
From this table, we see that the gust adds between 600kg to 2200kg of weight to the wingbox based on the MLA setting. More importantly, even with the MLA used with the maximum deflection, the weight benefit is less than 100kg.

Table 6.2: Optimised wingbox weight.

MLA setting (deg)	Gust	Weight (ton)
±25	On	10.2293
±25	Off	8.0268
±15	On	10.2206
±15	Off	8.2328
±0	On	10.3064
±0	Off	9.7152

From the table, we first see that gusts have a significant influence on the optimised weight. It is definitively the driving sizing case in our current optimisation problem. In Figure 6.9, we show the resulting bending moment in the span-wise direction. We compare the loads from an optimisation run with MLA and another without. Both runs have gust case used in the sizing too. Even in the case with no MLA, we can see that the gust is creating higher loads on the outboard part of the wing. This observation has been shared in other research work such as Lancelot and De Breuker (2016), Lancelot and De Breuker (2019), Bordogna et al. (2020), and more recently Sinha et al. (2021). When the MLA is applied, however, the loads from the manoeuvre drop almost entirely below the gust load level.

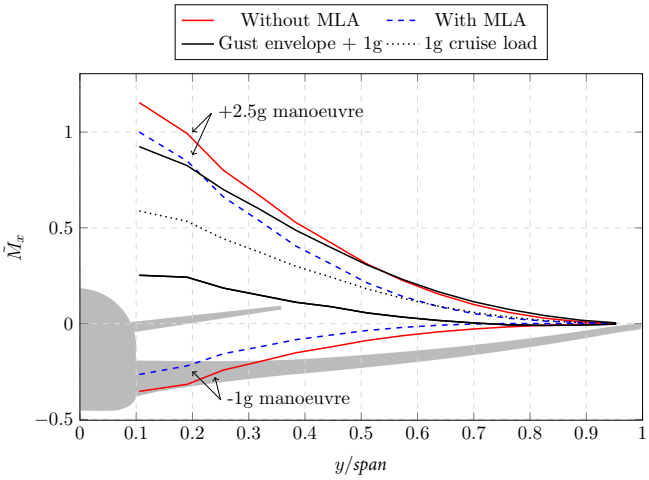

Figure 6.9: Results with MLA but no GLA. Gust cases are On and the MLA is set to ±15 degrees.

In Figure 6.10, we show the optimised wingbox for a scenario with gusts but no MLA. Most of the wing is sized for stress, meaning that the wing panel thickness is sufficient to avoid buckling failure with the current ribs/stringers arrangement. Buckling happens on panels inboard of the wing with low thickness but still experiencing high compression loads. The combined safety factor (the failure limits

in either strength or buckling) is close but below 1.0 on most of the wingbox. This shows that the wing is correctly sized by the optimiser. As is clear in Figure 6.9, the inboard part of the wing is sized by manoeuvres, while the remaining part is sized by the gust.

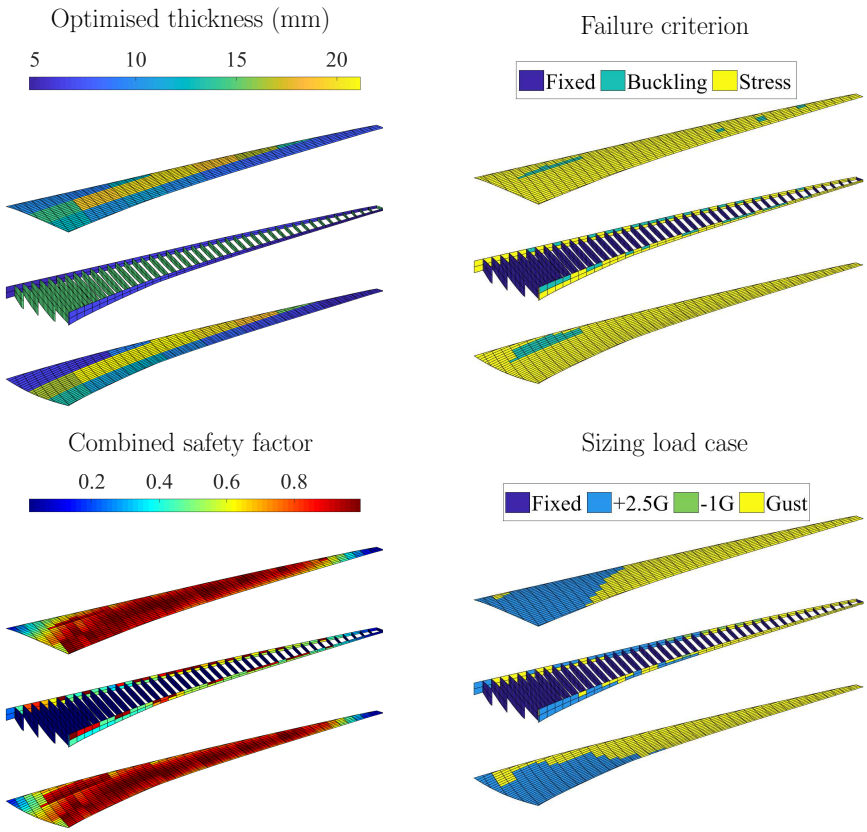

Figure 6.10: Results with no MLA and no GLA.

In Figure 6.11, we show the optimised results for the case with gusts and MLA. The gust cases are almost sizing everywhere. This gives further confirmation that in our optimisation problem, the gust cases are the most driving conditions for design, with or without MLA. The current methodology correctly sizes the wing thickness, and for such wing design, MLA alone is not sufficient to bring the weight down, therefore the use of GLA is required.

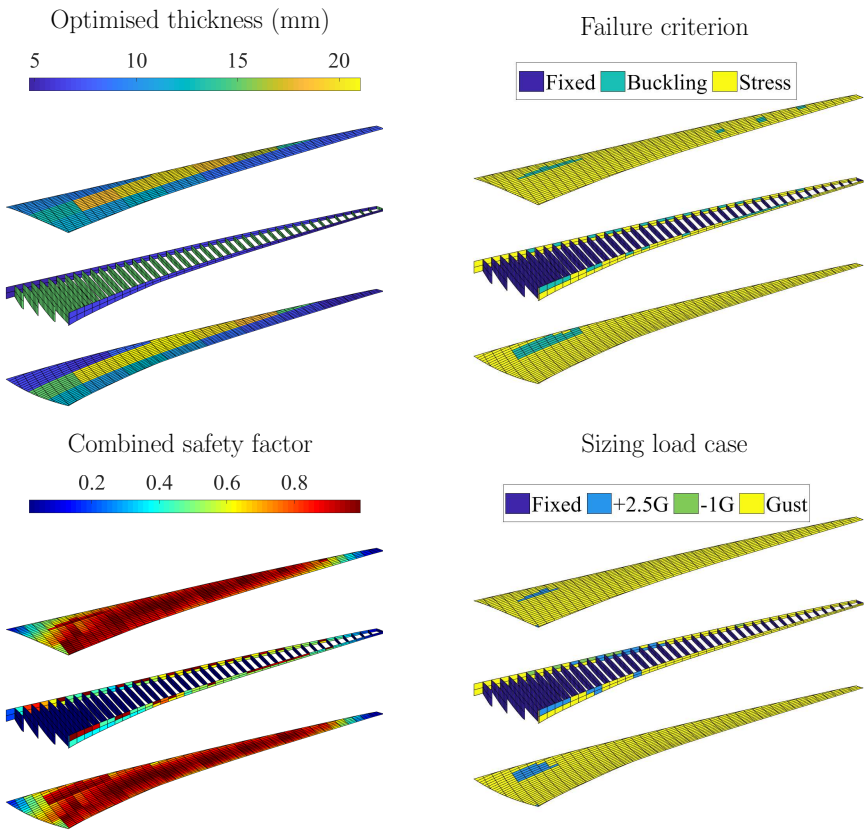

Figure 6.11: Results with MLA but no GLA.

6.3 AILERON EFFICACY FOR GLA

To reduce the number of parameters to investigate, the aileron is used as the primary means of direct lift control during gust encounters. The spoiler efficacy for GLA is investigated in Section 6.4. Here, we look at several aspects of using gust load alleviation methods in the wingbox sizing procedure:

a) What are the optimal design parameters for the controller?

b) To what extent does the aerodynamic fidelity of the control loads impact the optimised weight?

We partially answer both aspects with the optimisation results shown in Figure

6.12. The method followed to reach these optimum control and weight values is described in Section 6.1.4. We show the wingbox weight, gain and delay variations as a function of both the aileron maximum deflection rate and aerodynamic fidelity. Linear and non-linear models differ in the unsteady aerodynamic models generating the incremental loads due to the aileron deflection. Both models are compared in Chapter 3. The optimisation is performed with MLA active for the steady manoeuvres (aileron and outer+inner spoilers).

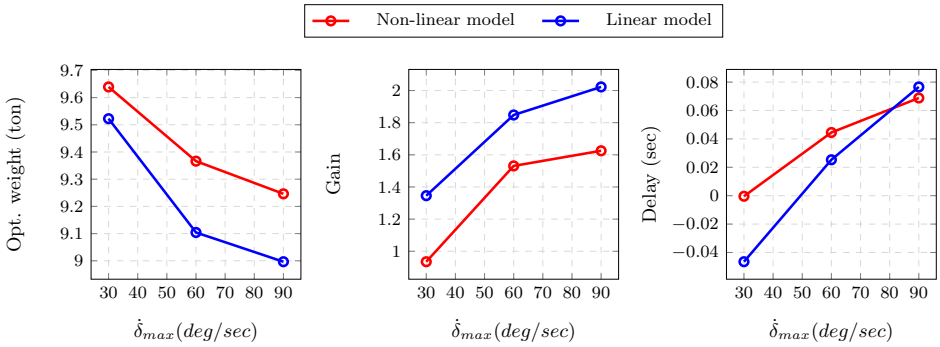

Figure 6.12: Objectives and optimum control parameters after the GLA optimisation. The GLA only relied on the aileron. All cases used MLA during steady manoeuvre.

We see that our optimisation process yields the expected outcome that a faster aileron produces a lower wing weight. A faster aileron deflection also allows for more delay between the gust detection and the GLA response. Nonetheless, these weight gains would have to be traded against potential weight penalties due to heavier actuators.

Secondly, a lower fidelity model using a linear approximation of the aileron control response, leads to over-optimistic weight benefits. The difference between both models increases with the deflection rate. This is likely because at lower rates, the potential weight benefit gets lower, and since the non-linearities in the aileron aerodynamic response are mostly at high deflection angles, a slower deflection rate means that the aileron does not get as far in the non-linear region as seen in Figure 6.13. Nonetheless, this figure also shows that the GLA yields a significant reduction for all the deflection rates in incremental root bending moments (up to 40%) and wing tip acceleration (up to 55%). Interestingly, these reductions do not provide any relief on the acceleration measured at the root of the wing. The subsequent oscillations however are of lower amplitudes which may still provide benefits for passenger comfort and handling qualities.

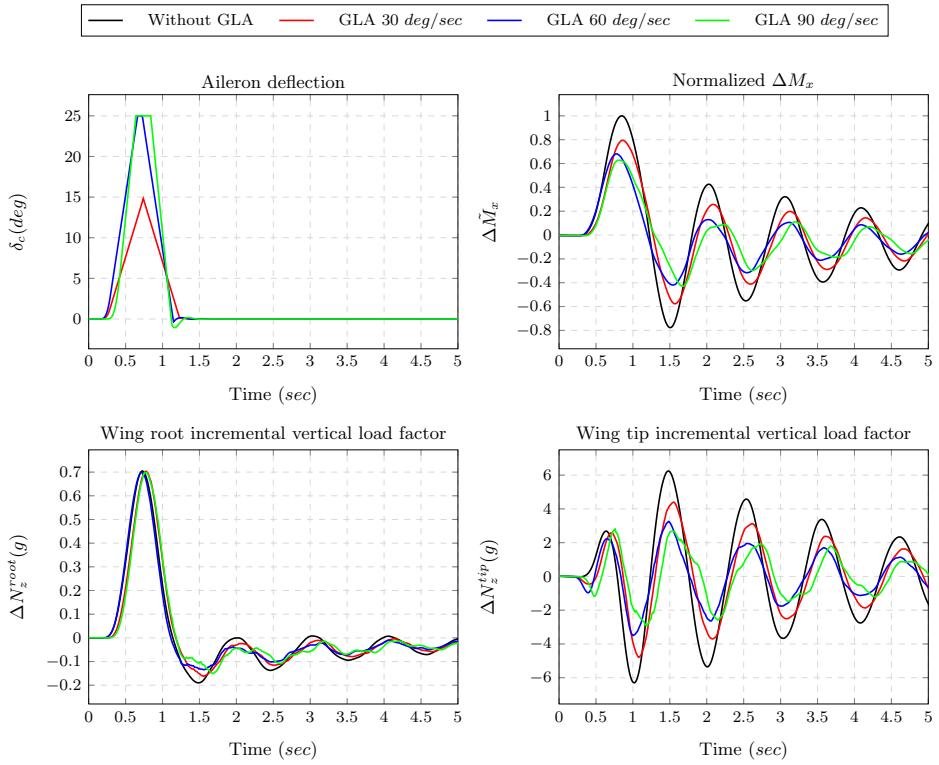

Figure 6.13: Aileron deflection and resulting loads and displacements on the wing after the control optimisation.

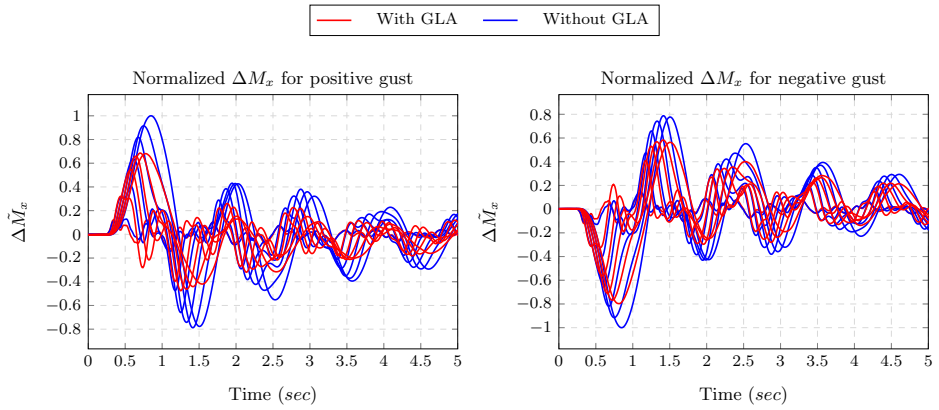

Figure 6.14: Incremental root bending for all gust cases with and without the GLA. The GLA uses the aileron at a deflection rate of 60deg/sec.

In Figure 6.14 we show the reduction in root bending loads for all 12 gust cases with a maximum deflection rate set to 60 deg/sec for the aileron. We can see the effect of the non-linear aerodynamic model used for the control surfaces aerodynamic modelling. For the positive gusts, negative aileron deflection is required for GLA, which makes it less sensitive to aerodynamic non-linearities and gives a higher reduction in root bending moments (up to 30%). In contrast, the reduction (down to 20%) is less significant with negative gusts which require positive aileron deflections.

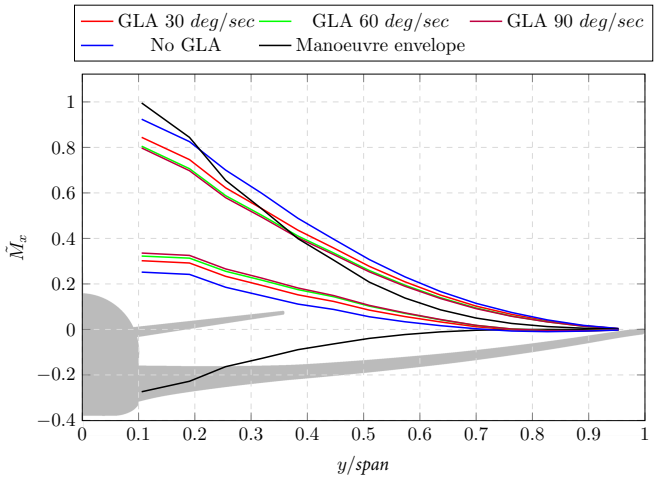

Figure 6.15: Loads with aileron GLA at different deflection rates. The MLA setting is set to ±15 degrees.

The use of GLA also changes the sizing loads along the wingspan. In Figure 6.15 we show that an aggressive GLA can make the manoeuvre (with MLA) more critical again for the first 1/3 of the wingspan. This observation is confirmed by looking at the optimisation results in Figure 6.17, where the manoeuvres are sizing again for some elements at the root. Of course, the overall weight and the overall panel thickness is reduced. This also increases the likelihood of buckling being the sizing failure criterion.

As already highlighted in Figure 6.12, we have seen an important effect of the aerodynamic fidelity on the optimised weight. In Figure 6.16, we show the spanwise loads difference between the linear and the non-linear aileron aerodynamic models. Most of the difference is in the middle portion of the wing, where the incremental gust load envelope is reduced with the linear aerodynamic aileron model. There is almost no difference in loads at the root, however this is not where the gust cases are the most sizing anyway.

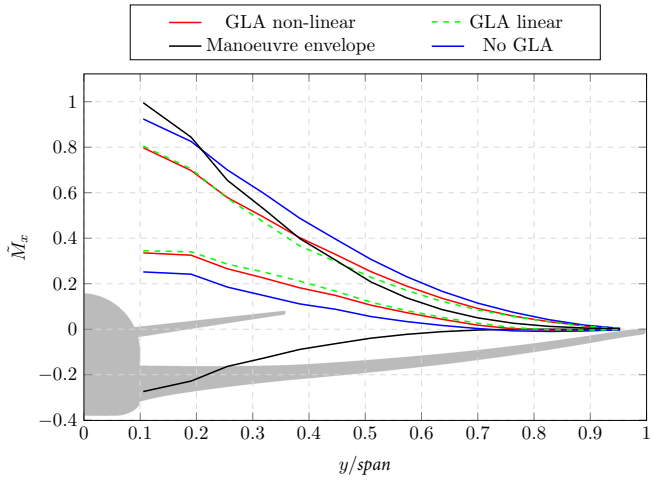

Figure 6.16: Loads with aileron GLA using both aerodynamic models. The maximum deflection rate is set to 60deg/sec. The MLA is set to ±15 degrees.

6.4 IS THE SPOILER USEFUL?

Finally, we look at the combined use of spoiler and aileron for the GLA function. In Table 6.3, we show a summary of the optimised weight with the aileron only, the spoiler only and both devices used together. All cases use MLA as well and the maximum control surface deflection rates are set to 60 deg/sec. We see that the spoiler has barely any effect on the weight reduction when combined with the aileron, while only achieving a 200kg reduction when used alone, compared to a case with no GLA.

Table 6.3: Optimised wingbox weight.

Device	Weight (ton)
Aileron and spoiler	9.3633
Aileron only	9.3663
Spoiler only	10.0183
No GLA	10.2206

In Figure 6.19, we see that the spoiler is only able to alleviate the positive incremental loads of the gust envelope. This is due to its kinematics which prevents such device to deflect downward. The combined effect of the spoiler and the aileron has only a marginal difference to the aileron GLA case.

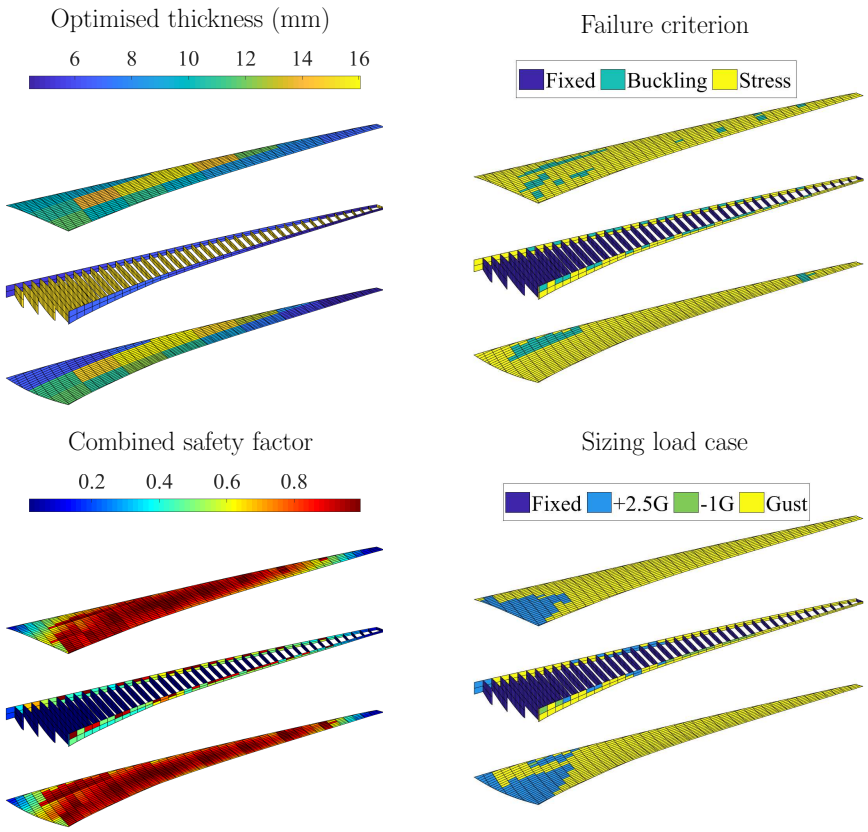

Figure 6.17: Optimisation results with the MLA and the GLA (aileron only, at 90deg/sec).

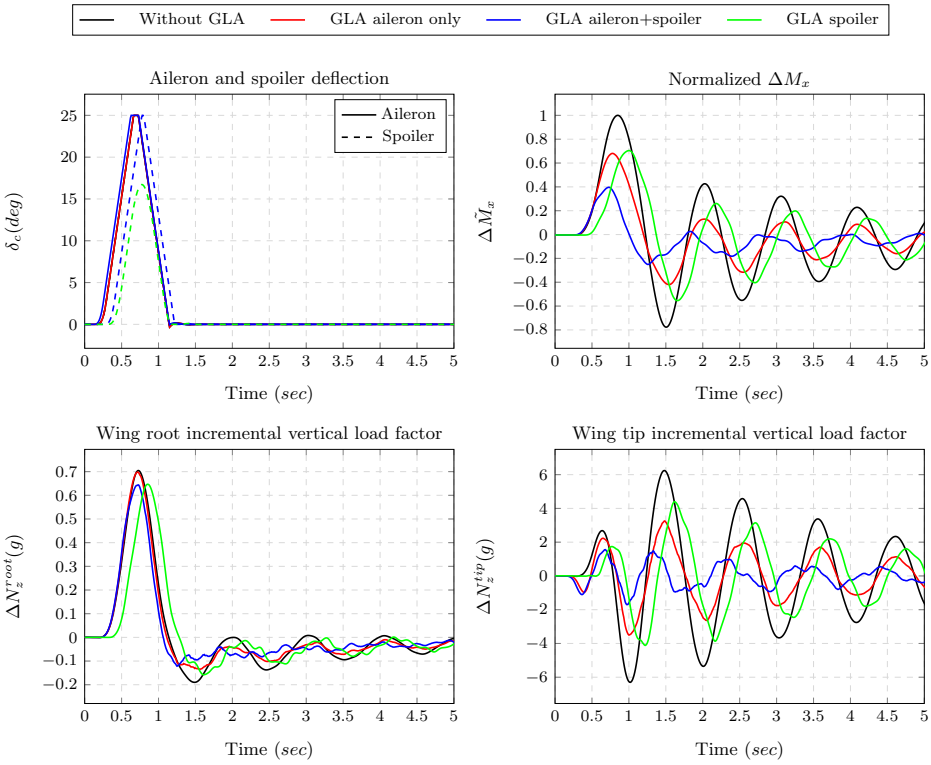

Figure 6.18: Aileron and spoiler deflections with the resulting loads and displacements on the wing.

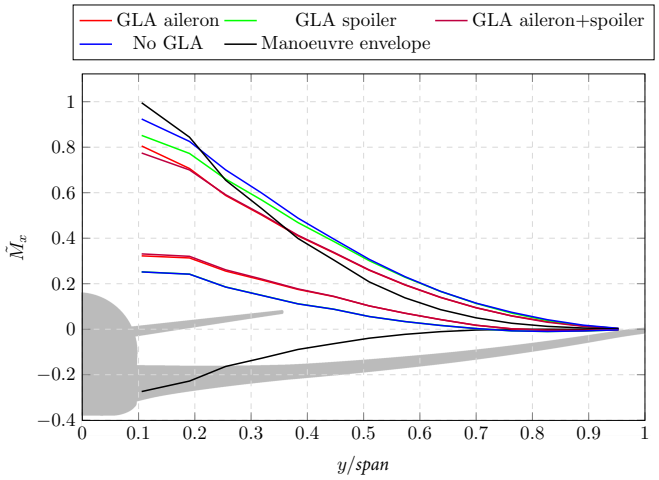

Figure 6.19: Loads with GLA rely on both the spoiler and the aileron, or either one movables. The MLA uses both control surfaces.

What is interesting, however, is that the spoiler, due to its more inboard location, has a much greater effect on the vertical load factor at the root, as seen in Figure 6.18. This also means that it puts it at a disadvantage compared to the aileron for reducing wingtip acceleration, or bending moment due to the lower moment arm. While a higher authority on the rigid vertical motion of the aircraft is less of a benefit for wing weight reduction, it can be helpful for passenger comfort and handling qualities. Additionally, more advance control laws could be used to make the spoiler more effective for GLA, as demonstrated by Binder et al. (2021).

6.5 CONCLUSION

In this chapter, we applied the non-linear aerodynamic models derived from Chapters 4 and 5 to a wingbox optimisation problem featuring MLA and GLA. Concurrent optimisation of the control and structural design variables was performed using a bi-level scheme which was parallelised to improve the rapidity of finding the optimum solution.
Different scenarios were evaluated with and without MLA and GLA. In our setup, gusts were mostly the sizing load cases for the wingbox and the usefulness of MLA was therefore reduced compared to GLA. We saw that a reduction in wingtip displacement correlated better with a decrease in structural weight than a reduction of the load factor at the wing root. Nonetheless, the MLA remained effective in reducing root bending loads during static manoeuvres, which still remained the sizing load cases for that portion of the wingbox. This emphasised the increased

complexity of the load case selection process when MLA and GLA are mixed in the structural optimisation.
We also investigated the impact aerodynamic fidelity had on the results. In our setup, we compared the use of linear and non-linear unsteady aerodynamic aileron models on the optimisation outcome. There, the linear model was giving overly optimistic results (250kg difference in structural weight), especially when fast aileron deflections ($\geq$ 60 deg/sec) were permitted. This is because the aileron could get faster and more often to large deflection angles, leading to a non-linear aerodynamic behaviour with a saturation of its control authority.
Finally, while more sophisticated control laws can be used to improve the GLA performance of both aileron and spoiler, it must be noted that in a real-life scenario, not all of the aileron or spoiler deflection "budget" would be allocated to MLA or GLA alone. The maximum incremental deflection angle achievable by both surfaces would be capped to allow flight control input to insure lateral controllability of the aircraft. This legitimatises the use of non-linear aerodynamic models to ensure an accurate representativity of the control surfaces authority at all deflection angles, whether it is to perform a roll or load alleviation or both at the same time.

7

Conclusion

The research question to answer in this thesis, as introduced in Chapter 1, is the following:

How can we predict aircraft control surfaces unsteady non-linear aerodynamic and aeroelastic responses, and how can we integrate this assessment into the early phases of airframe sizing?

This a highly multi-disciplinary problem, which encompasses aerodynamic and aeroelastic modelling, loads predictions, flight mechanics, aircraft geometric and analysis model generation (CAD, CFD and FEM meshes), structural sizing, actuators and control engineering. The scope of our research was determined to be the control surface transonic aerodynamic modelling, the load prediction with active and passive control and the resulting wingbox-sizing for one fixed aircraft configuration.
We still had to tackle several open questions related to the inclusion of the aerodynamic non-linear behaviour of the control surface responses since high-fidelity methods were too expensive for iterative aircraft design. Simulating aircraft moveables due to complex mesh deformation was an additional difficulty.
Finally, including aerodynamic corrections, static and dynamic loads and control design variables in the structural optimisation was the last challenge of this dissertation since we were relying on existing commercial software such as NASTRAN SOL200 to perform the wingbox optimisation.

In the next section, we discuss the results of each chapter and present the main takeaways of this thesis.

7.1 Discussion

In Chapter 2, we first introduced a 2D aeroelastic model relying on both CFD and analytical modelling. We showed that CFD identification gave us consistent results with the Theodorsen theory for the pitch and heave of an airfoil as all simulations were done in the low subsonic regime. Moreover, RANS-CFD allowed us to build a linear approximation of a spoiler response, which would have been difficult to estimate with a lower order method due to the inherently detached flow nature behind this type of control surface. After identifying the aerodynamic contributions required by the model (pitch, heave, gust and spoiler deflection and all the couplings), the system was solved with Simulink with the possibility of varying the gust input. The resulting fast aeroelastic model helped us look at passive load alleviation with the added non-linear behaviour required to deflect the spoiler with the right timing. We found an effective solution with the magnet and mechanical spring combination which nonetheless required a semi-active system to fully retract the spoiler. Furthermore, since spoilers are truly multi-functional devices (air brake and roll control on top of load control), active control would remain more practical for most applications.

In Chapter 3, we extended the transfer function methodology of Chapter 2 to transonic flow conditions with an aerodynamic non-linear response. This was a necessity since most airliners fly at this regime. One source of aerodynamic non-linearities at such speed is the interaction between the transonic shock and the control surface deflection. This creates a strong shift in the pressure distribution over the wing as the aileron is moving. Additionally, flow separation may occur behind the shock, which can reduce the surface effectiveness. Many approaches, such as non-linear auto-regressive models, exist to capture such behaviour but often require the full order simulation to work to generate the training data set. This can be complex as mesh motion around control surfaces is difficult to handle for the RANS-CFD solver. We showed that we could accurately capture unsteady non-linear aerodynamic responses with a combination of look-up tables and transfer functions, which are trained with only CFD steady simulation and unsteady CFD simulation with small disturbance. Our approach gave adequate predictions for a realistic range of dynamic deflection amplitude and frequencies and is generally better than unsteady linearized or quasi-steady approximation, for a minimum cost increase in model development.

In Chapter 4, we introduced steady aerodynamic corrections (manoeuvre and control surface loads) for static 3D aeroelastic problems. This is because coupled

FSI is still computationally too expensive for sizing a wing with high-fidelity analysis. Therefore, we implemented the Hybrid-Static Approach (HSA) which relies on decoupling rigid aerodynamic loads from the aeroelastic incremental loads. We compared this method to coupled FSI and it gave accurate results for wing angles of attack up to 4 degrees, which at Mach 0.85 can be considered already well within the non-linear aerodynamic region of the flight envelope. For higher angles of attack, the corrected loads were conservative. The HSA correction is quick to implement as it only relies on a limited number of rigid CFD simulations (only two for the manoeuvres loads in our case) and is therefore suitable for aircraft sizing problems, as the corrections do not have to be recalculated as the wing structure changes. Also, this approach is suitable for static control surface deflections, including the spoiler for which there is no panel method readily available. We also show that we could combine individual spoiler and aileron deflection databases to simulate the simultaneous deflections. Good precision was achieved when both the spoiler and aileron were up, while the accuracy of the prediction was degraded when only the spoiler was up and the aileron was down. The latter would be considered less operational in normal aircraft operation. Finally, the investigations of this chapter also highlighted the positive side of aeroelasticity and wing flexibility, as it can reduce the flow nonlinearities on the wing.

In Chapter 5, we looked at dynamic control surface deflections on a flexible wing. We had already shown in Chapter 4 that a hybrid approach was a suitable way to increase the fidelity of steady aeroelastic predictions and that it was possible to model unsteady nonlinear control surface aerodynamic responses with rapid models in Chapter 3. To simulate the aeroelastic response of a wing due to dynamic control surface motion, we combined both approaches. The process remained non-intrusive and black-box commercial codes can be used. A spoiler and an aileron were tested on a flexible CRM wing. We used a dynamic FSI framework to run the comparison, as proper wind tunnel data was very scarce. The comparison was made for the incremental lift, moment and tip deflection as the wing experienced dynamic control surfaces rotation. We got results in the 5% to 10% error range in most of the cases which we consider adequate for the purpose of these models. Our model predicted accurately the loss of control effectiveness as we change the wing stiffness to softer properties. The comparison also highlighted the issue with the FSI modelling, which was very expensive to run, and could not handle control surface deflections beyond ± 10 degrees. Therefore, we had to resort to a piece-wise comparison against our model for large spoiler deflections.

In Chapter 6 we assessed the impact of aerodynamic fidelity and control parameters on the wingbox structural sizing. First, we had to include dynamic loads and control into the optimiser. For this, we relied on a multi-level approach, with a nested gradient-based optimiser inside a gradient-free random search for the control design variables. The random search convergence was supported by an adaptive design space window, which would shrink as the optimisation progressed

and could be parallelised easily. The gust loads were included through the ESL approach.

Once the framework was in place, we looked at three aspects:

a) How does increasing the aileron deflection speed for GLA improve the structural weight reduction?

b) How does aerodynamic modelling of the aileron used for GLA impact the optimised weight?

c) Do an aileron and a spoiler perform equally well at GLA?

For the comparison, we had the same MLA set-up (combined static aileron and spoilers deflection) with the same static aerodynamic corrections for the manoeuvre cases relying on the HSA method presented in Chapter 3.

For a) we saw that the weight improves with faster aileron deflection. However, it is not certain that the weight benefit is worth considering as faster actuators will be heavier. The lack of available data on actuator mass makes the trade-off difficult, but we can still conclude that we should be cautious when trying to oversize control surfaces in the hope to save structural weight. A multidisciplinary approach should be followed when sizing the actuators. Additionally, taking more sizing cases into account, such as flutter, roll authority, hard landing or control surface failure may limit further the weight benefits of having GLA with very fast actuation.

For b) we saw that the use of the mixed fidelity control surface loads derived in Chapter 5 led to higher wing loads during gust encounters. This is expected, as aerodynamic non-linearity around the aileron generally tends to decrease the incremental loads from the control surface deflection and therefore limits the GLA capability. This may be, however, an opportunity to reduce safety margins in the preliminary design phase.

In c) we looked at the use of a spoiler for GLA applications. Spoilers, because they are generally located closer to the root, have a lower moment arm and therefore create less bending load relief. This has a direct influence on the sizing of the wingbox. Additionally, because they can only deflect up, this means that they are less efficient to reduce the wing gust loads. A benefit of spoilers, however, is their higher authority on the fuselage motion, and therefore they are better suited than outboard ailerons to control the aircraft acceleration at the center of gravity. We expect flaperons (type of control surface combining aileron flaps function mostly found on Boeing's large commercial jets) to provide the same benefits. This means that based on the objectives of the GLA, such as improving

the passanger comfort or decreasing structural stress, different control surfaces could be used.

7.2 Recommendations and future work

This thesis covers multiple topics, from aerodynamic identification to structural sizing. Potential gaps and improvements to the methods used are highlighted in this section.

Regarding the control surface loads prediction methodology, coupling between the aircraft AoA and the control surfaces incremental lift could be added. Industrial publications suggest potential aerodynamic control reversal around the spoiler in transonic flow at high angles of attack (Bertrand, 2008; Tinoco, 2008). The methodology presented in this thesis should allow it with only the added cost of additional CFD analysis to enrich the control surface aerodynamic databases. AoA effects on gust loads could also be added. CFD computations of the detached flow behind the spoiler or the aileron may also help in gaining accuracy by using more elaborated turbulence models or large-eddy simulations. Additionally, more validations of the aileron and spoiler unsteady aerodynamic models must be performed with wind tunnel results when available.

On the structural optimisation itself, the use of composite materials instead of aluminium may provide additional tailoring options. The use of additional structural design constraints and load cases during the sizing could help refine some of the conclusions on the weight benefits of GLA and the importance of the aerodynamic fidelity. Notably, including fatigue would be particularly relevant when using active load alleviation which is, in the industry today, one of the few possible ways the GLA can contribute to a weight reduction on the structure. Along with additional load cases, failure scenarios of one or several load alleviation systems on the aircraft may also be included in the sizing process to determine a safe MLA/GLA budget.

Finally, the overall process would also gain in using surrogate modelling to improve the global control optimisation strategy and allow more design variables. This way, more advanced control laws could be used to leverage the use of the spoiler for instance. Different wing layouts and control surfaces would also greatly improve the overall trade-off but this also requires tools to automate the model generation for both the FEM and the CFD modelling.

BIBLIOGRAPHY

Albano, E. and Rodden, W. P. (1969). "A doublet-lattice method for calculating lift distributions on oscillating surfaces in subsonic flows." *AIAA Journal*, vol. 7, no. 2, pp. 279–285. doi:10.2514/3.5086. URL https://doi.org/10.2514/3.5086.

Ansys (2009a). "Ansys fluent 12.0 theory guide - 3.3.1 dynamic mesh update methods". https://www.afs.enea.it/project/neptunius/docs/fluent/html/th/node40.htm.

Ansys (2009b). "Ansys fluent 12.0 theory guide - 4.5.2 shear-stress transport (sst) - model". https://www.afs.enea.it/project/neptunius/docs/fluent/html/th/node67.htm.

Baars, W., Stearman, R., and Tinney, C. (2010). "A review on the impact of icing on aircraft stability and control." *ASDJournal*, vol. 2, pp. 35–52. URL https://www.asdjournal.org/index.php/ASD/article/download/7/Baars_ASDJ2010.pdf.

Beckert, A. and Wendland, H. (2001). "Multivariate interpolation for fluid-structure-interaction problems using radial basis functions". *Aerospace Science and Technology*. doi:10.1016/S1270-9638(00)01087-7. URL https://www.sciencedirect.com/science/article/pii/S1270963800010877.

Begnini, G. R., Spode, C., Pantaleão, A. V., Neto, B. G., Marcório, G. O., Pedras, M. H., and Bones, C. A. (2016). "A comparison of CFD and AIC-based methods for unsteady aerodynamics and flutter computations of the AePW-2 wing model". In *34th AIAA Applied Aerodynamics Conference*. ISBN 9781624104374. doi:10.2514/6.2016-3123. URL https://arc.aiaa.org/doi/10.2514/6.2016-3123.

Bekemeyer, P., Thormann, R., and Timme, S. (2019). "Investigation into gust load alleviation using computational fluid dynamics". In *18th International Forum on Aeroelasticity and Structural Dynamics*. https://livrepository.liverpool.ac.uk/3046290/1/IFASD-2019-068.pdf.

Belesiotis-Kataras, P. and Timme, S. (2018). "Numerical Study of Incipient Transonic Shock Buffet on Large Civil Aircraft Wings". In *2018 Applied Aerodynamics Conference*, July, pp. 1–12. URL https://livrepository.liverpool.ac.uk/3023587.

Berci, M., Mascetti, S., and Incognito, A. (2010). "GUST RESPONSE OF A TYPICAL SECTION VIA CFD AND analytical solutions". *Eccomas Cfd 2010*, , no. June, pp. 14–17. URL https://www.flow3d.com/wp-content/uploads/2014/08/Gust-Response-of-a-Typical-Section-Via-CFD-and-Analytical-Solution.pdf.

Bertram, A., Bekemeyer, P., and Held, M. (2021). "Fusing Distributed Aerodynamic Data Using Bayesian Gappy Proper Orthogonal Decomposition". doi:10.2514/6.2021-2602. URL https://arc.aiaa.org/doi/abs/10.2514/6.2021-2602.

Bertrand, X. (2008). *Modélisation aérodynamique des surfaces de contrôle de la voilure d'un avion de transport*. Phd thesis, Toulouse, ISAE. https://depozit.isae.fr/theses/2008/2008_Bertrand_Xavier.pdf.

Biannic, J., Hardier, G., Roos, C., Seren, C., and Verdier, L. (2016). "Surrogate Models for Aircraft Flight Control: Some Off-Line and Embedded Applications". *Aerospace Lab*, , no. 12, pp. pages 1–21. doi:10.12762/2016.AL12-14. URL https://hal.science/hal-01515765.

Binder, S., Wildschek, A., and De Breuker, R. (2021). "The interaction between active aeroelastic control and structural tailoring in aeroservoelastic wing design". *Aerospace Science and Technology*, vol. 110, p. 106516. doi:https://doi.org/10.1016/j.ast.2021.106516. URL http://www.sciencedirect.com/science/article/pii/S1270963821000286.

Blanc, F., Roux, F.-X., Jouhaud, J.-C., and Boussuge, J.-F. (2009). "Numerical methods for control surfaces aerodynamics with flexibility effects". In *IFASD 2009 - International Forum on Aeroelasticity and Structural Dynamics*. URL https://www.cerfacs.fr/~cfdbib/repository/TR_CFD_09_54.pdf.

Boely, N., Botez, R., and Kouba, G. (2009). "Identification of an f/a-18 nonlinear model between control and structural deflections". In *47th AIAA Aerospace Sciences Meeting including The New Horizons Forum and Aerospace Exposition*. doi:10.2514/6.2009-426. URL https://arc.aiaa.org/doi/abs/10.2514/6.2009-426.

Bordogna, M. T., Lancelot, P., Bettebghor, D., and De Breuker, R. (2020). "Static and dynamic aeroelastic tailoring with composite blending and manoeuvre load alleviation". *Structural and Multidisciplinary Optimization*, vol. 61, no. 5, pp.

2193–2216. doi:10.1007/s00158-019-02446-w. URL https://doi.org/10.1007/s00158-019-02446-w.

Bosco, E., Lucchetti, A., Trapier, S., di Vincenzo, F. G., Gourdain, N., and Morlier, J. (2016). "Nonlinear transient fluid/structure interaction approach using surrogate models: Industrial application to aircraft fairing vibration excited by engine jet flow". *15th Dynamics Specialists Conference*. doi:10.2514/6.2016-2049. URL https://arc.aiaa.org/doi/abs/10.2514/6.2016-2049.

Brooks, T. R., Kenway, G. K. W., and Martins, J. R. R. A. (2018). "Benchmark aerostructural models for the study of transonic aircraft wings". *AIAA Journal*, vol. 56, no. 7, pp. 2840–2855. doi:10.2514/1.J056603. https://arc.aiaa.org/doi/10.2514/1.J056603.

Brunton, S. L. and Rowley, C. W. (2013). "Empirical state-space representations for Theodorsen's lift model". *Journal of Fluids and Structures*, vol. 38, pp. 174–186. doi:10.1016/j.jfluidstructs.2012.10.005. URL http://dx.doi.org/10.1016/j.jfluidstructs.2012.10.005.

Bussemaker, J. (2018). "Wing Optimization with Active Load Control: Integrating Maneuver Load Control and Gust Load Alleviation in Wing Structural Optimization of Large Transport Aircraft". URL http://resolver.tudelft.nl/uuid:099604d8-c056-471c-b003-e31605523074.

Castells Marin, P. (2020). *Modelling and simulation of gust and atmospheric turbulence effects on flexible aircraft flight dynamics*. Phd thesis, University of Toulouse. URL https://oatao.univ-toulouse.fr/27676/1/Castells_Pau.pdf.

Castrichini, A., Hodigere Siddaramaiah, V., Calderon, D. E., Cooper, J. E., Wilson, T., and Lemmens, Y. (2016). "Nonlinear folding wing tips for gust loads alleviation". In *Journal of Aircraft*. doi:10.2514/1.C033474. URL https://arc.aiaa.org/doi/10.2514/1.C033474.

Chyczewski, T. S., Dubiel, M., McDaniel, D. R., Foster, M., Niestroy, M. A., Klausmeyer, S. M., Silva, W. A., Vicroy, D. D., Hummer, C., Thomas, W., and Green, B. E. (2020). "A position on current stability and control prediction capabilities and a path forward". In *AIAA Aviation 2020 Forum*. American Institute of Aeronautics and Astronautics. doi:10.2514/6.2020-2678. https://arc.aiaa.org/doi/pdf/10.2514/6.2020-2678.

Crovato, A., Almeida, H. S., Vio, G., Silva, G. H., Prado, A. P., Breviglieri, C., Guner, H., Cabral, P. H., Boman, R., Terrapon, V. E., and Dimitriadis, G. (2020). "Effect of levels of fidelity on steady aerodynamic and static aeroelastic computations". *Aerospace*. doi:10.3390/aerospace7040042. URL https://www.mdpi.com/2226-4310/7/4/42.

CS25 (2016). "Certification Specifications and Acceptable Means of Compliance for Large Aeroplanes". Tech. rep. URL https://www.easa.europa.eu/en/certification-specifications/cs-25-large-aeroplanes.

Deck, S., Gand, F., Brunet, V., and Khelil, S. B. (2014). "High-fidelity simulations of unsteady civil aircraft aerodynamics: Stakes and perspectives. Application of zonal detached eddy simulation". *Philosophical Transactions of the Royal Society A: Mathematical, Physical and Engineering Sciences*, vol. 372, no. 2022. doi:10.1098/rsta.2013.0325. URL https://royalsocietypublishing.org/doi/10.1098/rsta.2013.0325.

Delannoy, S. (2007). "A380 roll kinematics design". In *IFAC Proceedings Volumes (IFAC-PapersOnline)*. ISBN 9783902661241. doi:10.3182/20070625-5-fr-2916.00019. URL https://www.sciencedirect.com/science/article/pii/S1474667015332250.

Dequand, S., Geeraert, A., and Mortchelewicz, G. (2019). "Innovative tail configuration: Numerical vs wind tunnel test data". In *International Forum on Aeroelasticity and Structural Dynamics 2019, IFASD 2019*. URL https://hal.science/hal-02351334/document.

Dillinger, J. (2014). "Static Aeroelastic Optimization of Composite Wings with Variable Stiffness Laminates". URL http://repository.tudelft.nl/view/ir/uuid{%}3A20484651-fd5d-49f2-9c56-355bc680f2b7/.

Disney, T. E. (1977). "C-5a active load alleviation system". *Journal of Spacecraft and Rockets*, vol. 14, no. 2, pp. 81–86. doi:10.2514/3.57164. URL https://doi.org/10.2514/3.57164.

Faïsse, E., Vernay, R., Vetrano, F., Morlier, J., and Alazard, D. (2022). *Aeroservoelastic wing sizing using integrated structural and control (co-design) optimization*. doi:10.2514/6.2022-2243. URL https://arc.aiaa.org/doi/abs/10.2514/6.2022-2243.

Fezans, N., Joos, H.-D., and Deiler, C. (2019). "Gust load alleviation for a long-range aircraft with and without anticipation". *CEAS Aeronautical Journal*. doi:10.1007/s13272-019-00362-9. URL https://link.springer.com/article/10.1007/s13272-019-00362-9.

Fillola, G. (2006). *Étude expérimentale et simulations numériques d'écoulements autour des surfaces mobiles de voilure*. Phd thesis, Toulouse, ENSAE. https://depozit.isae.fr/theses/2006/2006_Fillola_Guillaume.pdf.

Gand, F. (2013). "Zonal detached eddy simulation of a civil aircraft with a deflected spoiler". *AIAA Journal*, vol. 51, no. 3, pp. 697–706. doi:10.2514/1.J052106. https://arc.aiaa.org/doi/10.2514/1.J052106.

Geisbauer, S. and Löser, T. (2017). "Towards the investigation of unsteady spoiler aerodynamics". In *35th AIAA Applied Aerodynamics Conference, 2017*. ISBN 9781624105012. doi:10.2514/6.2017-4229. URL https://arc.aiaa.org/doi/10.2514/6.2017-4229.

Ghoreyshi, M. and Cummings, R. M. (2014). "Unsteady aerodynamic modeling of aircraft control surfaces by indicial response methods". *AIAA Journal*, vol. 52, no. 12, pp. 2683–2700. doi:10.2514/1.J052946. https://arc.aiaa.org/doi/10.2514/1.J052946.

Giannelis, N. F., Levinski, O., and Vio, G. A. (2018). "Influence of Mach number and angle of attack on the two-dimensional transonic buffet phenomenon". *Aerospace Science and Technology*. doi:10.1016/j.ast.2018.03.045. URL https://www.sciencedirect.com/science/article/pii/S1270963817319302.

Goggin, P. (1992). "A general gust and maneuver load analysis method to account for the effects of active control saturation and nonlinear aerodynamics". In *Dynamics Specialists Conference*. American Institute of Aeronautics and Astronautics. doi:10.2514/6.1992-2126. https://arc.aiaa.org/doi/abs/10.2514/6.1992-2126.

GPIAAF (2020). "Aileron cables reversal during maintenance actions and consequent loss of control in flight - safety investigation report". URL http://www.gpiaa.gov.pt/wwwbase/wwwinclude/ficheiro.aspx?tipo=0&id=10652&ambiente=WebSiteMenu.

Guo, S., De Los Monteros, J. E., and Liu, Y. (2015). "Gust alleviation of a large aircraft with a passive twist wingtip". *Aerospace*, vol. 2, no. 2, pp. 135–154. doi:10.3390/aerospace2020135. URL http://www.mdpi.com/2226-4310/2/2/135.

Haas, A. E. and Verschoyle, T. (1928). *Introduction to theoretical physics ... by Arthur Haas ... translated ... by T. Verschoyle*. Constable company ltd London, 2nd ed.

Halder, R., Damodaran, M., and Khoo, B. C. (2020). "Signal interpolation augmented linear nonintrusive reduced-order model for aeroelastic applications". *AIAA Journal*, vol. 58, no. 1, pp. 426–444. doi:10.2514/1.j058529. https://doi.org/10.2514/1.J058529.

Handojo, V. (2020). *Contribution to load alleviation in aircraft pre-design and its influence on structural mass and fatigue*. Doctoral thesis, Technische Universität Berlin, Berlin. doi:10.14279/depositonce-10986. URL http://dx.doi.org/10.14279/depositonce-10986.

Handojo, V., Lancelot, P., and De Breuker, R. (2018). "Implementation of Active and Passive Load Alleviation Methods on a Generic mid-Range Aircraft Configuration". In *2018 Multidisciplinary Analysis and Optimization Conference*. American Institute of Aeronautics and Astronautics. ISBN 978-1-62410-550-0. doi:10.2514/6.2018-3573. URL https://arc.aiaa.org/doi/10.2514/6.2018-3573.

Hiller, B. R., Frink, N. T., Silva, W. A., and Mavris, D. N. (2020). "Aeroelastic indicial response reduced-order modeling for flexible flight vehicles". *Journal of Aircraft*, pp. 1–22. doi:10.2514/1.c035646. https://doi.org/10.2514/1.C035646.

Hoblit, F. M. (1988). *Gust loads on aircraft concepts and applications*. AIAA education series. American Institute of Aeronautics and Astronautics, Washington, D.C. ISBN 1-60086-188-1.

Huang, R., Liu, H., Yang, Z., Zhao, Y., and Hu, H. (2018). "Nonlinear reduced-order models for transonic aeroelastic and aeroservoelastic problems". *AIAA Journal*, vol. 56, no. 9, pp. 3718–3731. doi:10.2514/1.J056760. https://arc.aiaa.org/doi/10.2514/1.J056760.

Huebner, A. and Reimer, L. (2019). "Gust encounter simulations of a generic transport aircraft and analysis of load alleviation potentials by control surface deflections using a rans-cfd-based multidisciplinary simulation environment". In *AIAA Aviation 2019 Forum*. American Institute of Aeronautics and Astronautics. doi:10.2514/6.2019-3198. https://arc.aiaa.org/doi/pdf/10.2514/6.2019-3198.

Hürlimann, F. (2010). "Mass Estimation of Transport Aircraft Wingbox Structures with a CAD/CAE-Based Multidisciplinary Process". doi:10.3929/ethz-a-006361295. URL https://doi.org/10.3929/ethz-a-006361295.

Huvelin, F., Girodroux Lavigne, P., and Blondeau, C. (2013). "High fidelity numerical simulations for gust response analysis". In *15th International Forum on Aeroelasticity and Structural Dynamics*.

Huvelin, F., Lepage, A., and Dequand, S. (2019). "Experimental and numerical investigations of a 2d aeroelastic airfoil encountering a gust in transonic conditions". *CEAS Aeronautical Journal*. doi:10.1007/s13272-018-00358-x. URL https://link.springer.com/article/10.1007/s13272-018-00358-x.

Johnson, E. H. and Rodden, W. P. (1994). "Msc nastran version 68 aeroelastic analysis user's guide". *MSC Software Aeroelastic Guide*.

Jovanov, K. (2019). "High-Fidelity Load and Gradient Corrections for Static Aeroelastic Tailoring of Composite Wings". doi:10.4233/uuid:14b55d5e-586a-4641-8990-55a397674db8. URL https://doi.org/10.4233/uuid:14b55d5e-586a-4641-8990-55a397674db8.

Kang, B. S., Choi, W. S., and Park, G. J. (2001). "Structural optimization under equivalent static loads transformed from dynamic loads based on displacement". *Computers and Structures*. doi:10.1016/S0045-7949(00)00127-9. URL https://www.sciencedirect.com/science/article/pii/S0045794900001279.

Klimmek, T. (2014). "Development of a structural model of the crm configuration for aeroelastic and loads analysis". *Journal of Aeroelasticity and Structural Dynamics*, vol. 3, no. 2, pp. 31–49. doi:10.3293/asdj.2014.27. https://www.asdjournal.org/index.php/ASD/article/viewFile/27/Klimmek_ASDJ2014.pdf.

Krag, B., Rohlf, D., and Wuennenberg, H. (1980). "OLGA, a gust alleviation system for improvement of passenger comfort of general aviation aircraft."

Kuder, I. K., Arrieta, A. F., Rist, M., and Ermanni, P. (2016). "Aeroelastic response of a selectively compliant morphing aerofoil featuring integrated variable stiffness bi-stable laminates". In *Journal of Intelligent Material Systems and Structures*. doi:10.1177/1045389X15620038. URL https://journals.sagepub.com/doi/10.1177/1045389X15620038.

Lancelot, P. (2021). "pcrm9 aeroelastic aircraft wing model for nastran". doi:10.4121/16834387.v1. URL https://data.4tu.nl/articles/dataset/pCRM9_aeroelastic_aircraft_wing_model_for_NASTRAN/16834387/1.

Lancelot, P. and De Breuker, R. (2016). "Aeroelastic tailoring for gust load alleviation". *11th ASMO UK/ISSMO/NOED2016 International Conference of Numerical Optimisation Methods for Engineering Design*. URL https://repository.tudelft.nl/islandora/object/uuid{%}3A4798d555-69ca-472a-9bd4-9d050fd71c90?collection=research.

Lancelot, P. and De Breuker, R. (2023). "Video supporting the paper: Unsteady non-linear control surface modelling for aeroservoelastic applications". doi:10.4121/20390781-69BE-4454-90BE-CBFD85F6F897.V1. URL https://data.4tu.nl/datasets/20390781-69be-4454-90be-cbfd85f6f897/1.

Lancelot, P. M., Sodja, J., Werter, N. P., and De Breuker, R. (2017). "Design and testing of a low subsonic wind tunnel gust generator". *Advances in Aircraft and Spacecraft Science*. doi:10.12989/aas.2017.4.2.125. URL http://www.techno-press.org/fulltext/j_aas/aas4_2/aas0402003.pdf.

Lancelot, P. M. G. J. and De Breuker, R. (2019). "Transonic flight and movable load modelling for wing-box preliminary sizing". In *18th International Forum on Aeroelasticity and Structural Dynamics*. http://resolver.tudelft.nl/uuid:305d8d69-c069-480d-a674-f650316d8935.

Leishman, J. G. (2000). *Principles of Helicopter Aerodynamics*. Cambridge University Press. URL https://www.cambridge.org/fr/academic/subjects/engineering/aerospace-engineering/principles-helicopter-aerodynamics-2nd-edition-1?format=HB&isbn=9781107013353.

Lepage, A., Huvelin, F., and Le Bihan, D. (2016). "Experimental investigation and control of gust load response in transonic flow". Tech. rep. URL https://hal.science/hal-01400270.

Liu, L., Padthe, A. K., Friedmann, P. P., Quon, E., and Smith, M. J. (2011). "Unsteady aerodynamics of an airfoil/flap combination on a helicopter rotor using computational fluid dynamics and approximate methods". *Journal of the American Helicopter Society*, vol. 56, p. 32003. doi:10.4050/JAHS.56.032003. https://www.ingentaconnect.com/content/ahs/jahs/2011/00000056/00000003/art00004.

Livne, E. (1999). "Integrated aeroservoelastic optimization: status and direction". *Journal of Aircraft*. doi:10.2514/2.2419. URL https://arc.aiaa.org/doi/10.2514/2.2419.

Mamelle, H., Revalor, Y., Hasholder, J. M., Vallee, J. J., and Garrigues, E. (2013). "A new methodology for the estimation of structural load level due to complex unsteady aerodynamic excitation". In *IFASD 2013 - International Forum on Aeroelasticity and Structural Dynamics*.

Martins, J. R. R. A. and Ning, A. (2021). *Engineering Design Optimization*. Cambridge University Press. doi:10.1017/9781108980647. URL https://www.cambridge.org/highereducation/books/engineering-design-optimization/B1B23D00AF79E45502C4649A0E43135B#overview.

MathWorks (2020a). "Find k-nearest neighbors using input data - MATLAB knnsearch". URL https://www.mathworks.com/help/stats/knnsearch.html.

MathWorks (2020b). "Simulink - Simulation and Model-Based Design - MATLAB & Simulink". https://nl.mathworks.com/products/simulink.html.

MathWorks (2020c). "Transfer function estimation - matlab tfest". https://nl.mathworks.com/help/ident/ref/tfest.html.

Moulin, B. and Karpel, M. (2007). "Gust loads alleviation using special control surfaces". *Journal of Aircraft*. doi:10.2514/1.19876. URL https://arc.aiaa.org/doi/10.2514/1.19876.

MSC Software Corporation (2012a). "MSC SimCompanion - MSC Nastran 2012 Design Sensitivity and Optimization User's Guide". URL https://simcompanion.mscsoftware.com/infocenter/index?page=content{&}id=DOC10014.

MSC Software Corporation (2012b). "MSC SimCompanion - MSC Nastran 2012 Linear Static Analysis User's Guide". URL https://simcompanion.mscsoftware.com/infocenter/index?page=content{&}id=DOC10003.

MSC Software Corporation (2019). "Msc nastran quick reference guide". https://simcompanion.mscsoftware.com/infocenter/index?page=content&id=DOC9106.

Piñeiro Rielo, D. (2019). *Development of a Fluid-Structure Interaction simulation algorithm for the analysis of the static and dynamic*. Master's thesis, Universidade de Vigo (Spain) - Delft University of Technology (The Netherlands).

Piperni, P., DeBlois, A., and Henderson, R. (2013). "Development of a multilevel multidisciplinary-optimization capability for an industrial environment". *AIAA Journal*. doi:10.2514/1.J052180. URL https://arc.aiaa.org/doi/abs/10.2514/1.J052180?journalCode=aiaaj.

Pohl, J. E., Radespiel, R., Herrmann, B., Brunton, S. L., and Semaan, R. (2022). "Gust mitigation through closed-loop control. i. trailing-edge flap response". *Phys. Rev. Fluids*, vol. 7, p. 024705. doi:10.1103/PhysRevFluids.7.024705. URL https://link.aps.org/doi/10.1103/PhysRevFluids.7.024705.

Prachař, A., Hospodář, P., and Vrchota, P. (2018). "Gust alleviation of aeroelastic aircraft using cfd simulation". *Transportation Research Procedia*, vol. 29, pp. 366–375. doi:10.1016/j.trpro.2018.02.033. http://www.sciencedirect.com/science/article/pii/S2352146518300371.

Pusch, M., Knoblach, A., and Kier, T. (2019). "Integrated optimization of control surface layout for gust load alleviation". *CEAS Aeronautical Journal*, vol. 1, p. 3. doi:10.1007/s13272-019-00367-4. https://link.springer.com/article/10.1007/s13272-019-00367-4.

Rajpal, D., Gillebaart, E., and De Breuker, R. (2019). "Preliminary aeroelastic design of composite wings subjected to critical gust loads". *Aerospace Science and Technology*. doi:10.1016/j.ast.2018.11.051. URL https://www.sciencedirect.com/science/article/pii/S1270963818303948.

Ramsey, H. D. and Lewolt, J. G. (1979). "Design maneuver loads for an airplane with an active control system". In *20th Structures, Structural Dynamics, and Materials Conference*. American Institute of Aeronautics and Astronautics. doi:10.2514/6.1979-738. https://arc.aiaa.org/doi/10.2514/6.1979-738.

Raveh, D. (2010). "Cfd-based gust response analysis of free elastic aircraft". *Journal of Aeroelasticity and Structural Dynamics*, vol. 2, no. 1. doi:10.3293/asdj.v2i1.3. https://www.asdjournal.org/index.php/ASD/article/view/3.

Regan, C. D. and Jutte, C. V. (2012). "Survey of Applications of Active Control Technology for Gust Alleviation and New Challenges for Lighter-weight Aircraft". NASA Report. URL http://ntrs.nasa.gov/search.jsp?R=20120013450.

Reimer, L., Heinrich, R., and Ritter, M. (2019). "Towards higher-precision maneuver and gust loads computations of aircraft: Status of related features in the cfd-based multidisciplinary simulation environment flowsimulator". In *New Results in Numerical and Experimental Fluid Mechanics XII*, pp. 597–607. Springer International Publishing. ISBN 978-3-030-25253-3. https://link.springer.com/chapter/10.1007/978-3-030-25253-3_57.

Ricci, S., Castellani, M., and Romanelli, G. (2013). "Multi-fidelity design of aeroelastic wing tip devices". *Proceedings of the Institution of Mechanical Engineers, Part G: Journal of Aerospace Engineering*. doi:10.1177/0954410012459603. URL https://journals.sagepub.com/doi/abs/10.1177/0954410012459603?journalCode=piga.

Ricci, S., De Gaspari, A., Fonte, F., Riccobene, L., Toffol, F., Mantegazza, P., Karpel, M., Roizner, F., Wiberman, R., Weiss, M., Cooper, J. E., Howcroft, C., Calderon, D., and Adden, S. (2017). "Design and Wind Tunnel Test Validation of Gust Load Alleviation Systems". doi:10.2514/6.2017-1818. URL http://arc.aiaa.org.

Riso, C., Sanghi, D., and Cesnik, C. E. S. (2020). "Parametric roll maneuverability analysis of a high-aspect-ratio-wing civil transport aircraft". In *AIAA Scitech Forum*. American Institute of Aeronautics and Astronautics. https://arc.aiaa.org/doi/10.2514/6.2020-1191.

Ritter, M. and Roeser, M. S. (2020). "Cfd-based multi-axis maneuver simulation for system identification of flexible transport aircraft". In *AIAA Scitech Forum*. doi:10.2514/6.2020-2125. https://arc.aiaa.org/doi/abs/10.2514/6.2020-2125.

Schewe, G. and Mai, H. (2018). "Influence of flexibility on the steady aeroelastic behavior of a swept wing in transonic flow". *Journal of Fluids*

and Structures. doi:10.1016/j.jfluidstructs.2018.04.021. URL https://www.sciencedirect.com/science/article/pii/S0889974617308484.

Schuhmacher, G., Daoud, F., Petersson, Ö., and Wagner, M. (2012). "Multidisciplinary airframe design optimisation". In *28th Congress of the International Council of the Aeronautical Sciences 2012, ICAS 2012*. ISBN 9781622767540. URL https://www.icas.org/ICAS_ARCHIVE/ICAS2012/PAPERS/994.PDF.

Seidler, R. B., Marten, S., Widhalm, M., and Wild, J. (2020). "Efficient prediction of aerodynamic control surface responses using the linear frequency domain". *AIAA Journal*, vol. 58, no. 5, pp. 1964–1975. doi:10.2514/1.J058840. https://arc.aiaa.org/doi/10.2514/1.J058840.

Sensburg, O., Becker, J., Lusebrink, H., and Weiss, F. (1982). "Gust load alleviation on airbus a300". In *13th Congress of International Council of the Aeronautical Sciences (ICAS)*. http://www.icas.org/ICAS_ARCHIVE/ICAS1982/ICAS-82-2.1.1.pdf.

Sinha, K., Klimmek, T., Schulze, M., and Handojo, V. (2021). "Loads analysis and structural optimization of a high aspect ratio, composite wing aircraft". *CEAS Aeronautical Journal*, vol. 1, p. 3. doi:10.1007/s13272-021-00494-x. URL https://doi.org/10.1007/s13272-021-00494-x.

Sodja, J., Werter, N. P. M., and De Breuker, R. (2021). "Aeroelastic Demonstrator Wing Design for Maneuver Load Alleviation Under Cruise Shape Constraint". *Journal of Aircraft*. doi:10.2514/1.c035955. URL https://arc.aiaa.org/doi/10.2514/1.C035955.

Solano, D., Sarojini, D., Rajaram, D., and Mavris, D. N. (2022). "Adjoint-based analysis and optimization of beam-like structures subjected to dynamic loads". *Structural and Multidisciplinary Optimization*, vol. 65, no. 2, p. 52. doi:10.1007/s00158-021-03141-5. URL https://doi.org/10.1007/s00158-021-03141-5.

Stanford, B. K. (2020). "Optimal Aircraft Control Surface Layouts for Maneuver and Gust Load Alleviation". American Institute of Aeronautics and Astronautics. doi:10.2514/6.2020-0448. URL https://arc.aiaa.org/doi/10.2514/6.2020-0448.

Stodieck, O., Cooper, J. E., Weaver, P. M., and Kealy, P. (2017). "Aeroelastic tailoring of a representative wing box using tow-steered composites". *AIAA Journal*. doi:10.2514/1.J055364. URL https://arc.aiaa.org/doi/10.2514/1.J055364.

Theodorsen, T. (1935). "General theory of aerodynamic instability and the mechanism of flutter". Tech. rep., NACA. URL http://www.tree-o-life.org/ARO202/naca-report-496.pdf.

Tinoco, E. N. (2008). "Validation and minimizing CFD uncertainty for commercial aircraft applications". In *Collection of Technical Papers - AIAA Applied Aerodynamics Conference*. doi:10.2514/6.2008-6902. URL https://arc.aiaa.org/doi/abs/10.2514/6.2008-6902.

Vincenzo, F. G. D. and Castrichini, A. (2013). "Msc nastran hybrid static aeroelasticity integrated, accurate static aeroelastic analysis with cfd data". Tech. rep.

Vos, R. and Farokhi, S. (2015). *Introduction to Transonic Aerodynamics*, vol. 110 of *Fluid Mechanics and Its Applications*. Springer Netherlands, Dordrecht. ISBN 978-94-017-9746-7. doi:10.1007/978-94-017-9747-4. URL http://link.springer.com/10.1007/978-94-017-9747-4.

Voß, A. (2019). "Comparison between VLM and CFD Maneuver Loads Calculation at the Example of a Flying Wing Configuration". *Journal of Aeroelasticity and Structural Dynamics*, vol. 7, no. 1. doi:10.3293/ASDJ.V7I1.52. URL https://www.asdjournal.org/index.php/ASD/article/view/52.

Waite, J. M., Stanford, B. K., Silva, W. A., and Bartels, R. E. (2019). "Reduced order modeling for transonic aeroservoelastic control law development". In *AIAA Scitech Forum*. doi:10.2514/6.2019-1022. https://arc.aiaa.org/doi/pdf/10.2514/6.2019-1022.

Weisshaar, T. A. (1995). *Aircraft Aeroelastic Design and Analysis*.

Wentz, W. H., Seetharam, H. C., and Calhoun, J. T. (1975). "Wind tunnel and flight development of spoilers for general aviation aircraft". In *National Business Aircraft Meeting and Engineering Display*. SAE International. doi:https://doi.org/10.4271/750523. URL https://doi.org/10.4271/750523.

Wiart, L. and Carrier, G. (2012). "Accounting for wing flexibility in the aerodynamic calculation of transport aircraft using equivalent beam model". In *13th AIAA/ISSMO Multidisciplinary Analysis and Optimization Conference*. ISBN 9781600869549. doi:10.2514/6.2010-9135. https://arc.aiaa.org/doi/10.2514/6.2010-9135.

Wildschek, A. (2015). "Concurrent Optimization of a Feed-Forward Gust Loads Controller and Minimization of Wing Box Structural Mass on an Aircraft with Active Winglets". In *16th AIAA/ISSMO Multidisciplinary Analysis and Optimization Conference*. American Institute of Aeronautics and Astronautics, Reston, Virginia. ISBN 978-1-62410-368-1. doi:10.2514/6.2015-2490. URL http://arc.aiaa.org/doi/10.2514/6.2015-2490.

Wilkinson, W., Lines, T., and Yu, N. (1996). "Navier-stokes calculations for massively separated flows". In *14th Applied Aerodynamics Conference*. doi:10.2514/6.1996-2383. https://arc.aiaa.org/doi/abs/10.2514/6.1996-2383.

Xu, C. and Yeung, W. W. H. (1999). "Unsteady aerodynamic characteristics of airfoil with moving spoilers". *Journal of Aircraft*, vol. 36, no. 3, pp. 530–540. doi:10.2514/2.2488. URL https://doi.org/10.2514/2.2488.

Xu, J. and Kroo, I. (2014). "Aircraft Design with Active Load Alleviation and Natural Laminar Flow". *Journal of Aircraft*, vol. 51, no. 5, pp. 1532–1545. doi:10.2514/1.C032402. URL http://dx.doi.org/10.2514/1.C032402.

List of Publications

Journal Papers:

Lancelot, P., De Breuker, R. (2021). "Unsteady Non-linear Control Surface Modelling for Aeroservoelastic Applications". *Journal of Aeroelasticity and Structural Dynamics*.

Bordogna, M.T., Lancelot, P., Bettebghor, D., De Breuker, R. (2020). "Static and dynamic aeroelastic tailoring with composite blending and manoeuvre load alleviation". *Struct Multidisc Optim* 61.

Lancelot, P., Sodja, J., Werter, N., De Breuker, R. (2017). "Design and testing of a low subsonic wind tunnel gust generator". *Advances in aircraft and spacecraft science* 4(2):125-144.

Macquart, T., Bordogna, M.T., Lancelot, P., De Breuker, R. (2015). "Derivation and application of blending constraints in lamination parameter space for composite optimisation". *Composite Structures* 135.

Conference Papers:

Lancelot, P., De Breuker, R. (2019). "Transonic flight and movable load modelling for wing-box preliminary sizing". In *18th International Forum on Aeroelasticity and Structural Dynamics, Savannah, GA, USA.*

Handojo, V., Lancelot, P., De Breuker, R. (2018). "Implementation of active and passive load alleviation methods on a generic mid-range aircraft configuration". In *Multidisciplinary Analysis and Optimization Conference, Atlanta, GA, USA.*

Lancelot, P., Sodja, J., De Breuker, R. (2017). "Investigation of the unsteady flow over a wing under gust excitation". In *17th International Forum on Aeroelasticity and Structural Dynamics, Como, Italy.*

Lancelot, P., De Breuker, R. (2016). "Passively actuated spoiler for gust load alleviation". In *International Conference on Adaptive Structure and Technologies, Lake George, NY, USA.*

Lancelot, P., De Breuker, R. (2016). "Aeroelastic tailoring for gust load alleviation". In *11th ASMO UK/ISSMO/NOED International Conference of Numerical Optimisation Methods for Engineering Design, Technische Universität München, Germany.*

Datasets:

Lancelot, P., De Breuker, R. (2023). "Video supporting the paper: Unsteady Non-linear Control Surface Modelling for Aeroservoelastic Applications" https://doi.org/10.4121/20390781-69be-4454-90be-cbfd85f6f897.v1

Lancelot, P. (2021). "pCRM9 aeroelastic aircraft wing model for NASTRAN" https://doi.org/10.4121/16834387.v1

BIOGRAPHICAL NOTE

Paul Lancelot started his mechanical engineering studies in 2009 in Tours, France. During his degree, he spent a year at the University of Western Ontario, Canada, where he studied flight mechanics and composites structure design, among other topics. He also participated in the 2013 SAE Aero Design competition held in Fort-Worth, Texas. Back in France, he did a two month internship on granular flow at the Rennes Physics Institute. Paul moved to The Netherlands in 2014 for his final year internship at TU Delft.

The internship was on the development of a wind tunnel gust generator, to experimentally replicate the atmospheric conditions experienced by aircraft and study the impact of turbulences on the wings. While later focusing on more numerical aspects of aeroelasticity, Paul remained involved with the gust generator by supporting several other wind tunnel experiments lead by his colleagues.

After completing his internship and gaining his Mechnical Enginner degree from Tours, Paul took the opportunity offered by his supervisor to continue working at TU Delft on aeroelastic optimisation, within the AMEDEO EU Marie Curie program. He then started to work on the ReLOAD Clean Sky 2 project in late 2015 on passive and active load alleviation, and in parallel begun his PhD.

After the completion of ReLOAD, Paul embarked on MANTA, another EU project, where Paul also performed loads and aeroelastic simulations on novel concepts of aircraft control surfaces.

Upon the completion of the bulk of his PhD work, Paul moved to Toulouse, France, early 2021 to work in the aerospace industry. He first worked at Capgemini within the handling qualities team for the Airbus A321neo XLR program as well as with the aerodynamic department. In September 2022, he joined Aura Aero to work on aeroelasticity topics for new aerobatic and hybrid-electric passenger airplanes.

Besides aviation and aeroelasticity, Paul enjoys travelling, volleyball, photography, urbanism, rapid transit, trains and spending time with his wife, Katie.